Applying Computational Systems Serology to Unravel the Heterogeneity of Antibody-Mediated Immunity in Infectious and Autoimmune Diseases

by

Suzanne K. Shoffner-Beck

A dissertation submitted in partial fulfillment
of the requirements for the degree of
Doctor of Philosophy
(Biomedical Engineering)
in the University of Michigan
2024

Doctoral Committee:

Associate Professor Kelly B. Arnold, Chair
Associate Professor Sriram Chandrasekaran
Professor J. Michelle Kahlenberg
Professor Deepak Nagrath

Suzanne K. Shoffner-Beck

suzshoff@umich.edu

ORCID iD: 0000-0003-0010-6318

© Suzanne K. Shoffner-Beck 2024

Dedication

This dissertation is dedicated to my husband and my family for their unwavering love and support.

Acknowledgements

I want to thank:

- My committee, for supporting me and providing unique insight and feedback
- Dr. Kelly Arnold, for seeing me through my growth as a researcher and a person
- Dr. Michelle Kahlenberg, for providing me with career inspiration and opportunities to pursue research in autoimmunity and dermatology
- Dr. Amy Chung and Dr. Martin Killian for helping me stick to my timeline while organizing Zoom meetings in absurd times in 3 different time zones.
- My husband, David, for supporting me unconditionally, motivating me to be the best I can be, and for serving as my personal, on-demand MATLAB concierge
- My mom, the master proofreader and a constant source of support, and my dad, for his optimism and email forwards of any research news slightly related to medicine
- Dr. Lukela, for fueling my purpose and reminding me of why I embarked on this journey
- Christina, Kat, Melissa, and Katy for being the reason I joined the lab and great teammates
- Robby, for keeping me sane and for being our lab's in-house financial advisor
- Kade, for making me feel old and being a true MATLAB workhorse and Sina, for joining us on the BMES dance floor
- Freddie and Schnitzel, for countless snuggles and meditative fetch sessions
- My friends, for bringing so much joy and meaning to my life

Table of Contents

Dedication ii

Acknowledgements iii

List of Tables ix

List of Figures x

List of Appendices xiii

Abstract xiv

Chapter 1 Introduction 1

1.1 Fc Receptors and antibody-mediated effector functions 2

1.2 Data-driven and theory-driven approaches in systems serology 3

1.3 Coronavirus Infectious Disease 2019 (COVID-19) and SARS-CoV-2 pathology 5

1.4 Sjogren's syndrome pathology 6

1.5 Human Immunodeficiency Virus (HIV) pathology 7

1.6 Structure of Thesis 9

Chapter 2 Systems Serology Detects Functionally Distinct Coronavirus Antibody Features in Children and Elderly 11

2.1 Authors and Contributions 11

2.2 Abstract 13

2.3 Introduction 13

2.4 Results 15

2.4.1 Distinct systems serology signatures in children versus elderly 15

2.4.2 Primed Ab responses to CoVs increase with repeated hCoV exposures 19
2.4.3 Immune maturation drives mature CoV Ab responses 20
2.4.4 HLA class II alleles influence CoV Ab signatures in healthy individuals 22
2.4.5 Distinct Fc Ab signature in COVID-19 patients 24
2.4.6 Qualitative and quantitative differences of IgM in children 27
2.4.7 Distinct Ab features between children and elderly COVID-19 patients 29
2.5 Discussion 32
2.6 Methods 36
2.6.1 Study participants and sample collection 36
2.6.2 Deglycosylation of Escherichia coli-expressed NP 37
2.6.3 Coupling of carboxylated beads 38
2.6.4 Luminex bead-based multiplex assay 38
2.6.5 Enzyme-linked immunosorbent assay (ELISA) 40
2.6.6 Antibody avidity assay 41
2.6.7 Neutralization antibody assay 41
2.6.8 Cell-based antibody Fc effector assays 41
2.6.9 Statistical analysis 42
2.6.10 Data normalization 43
2.6.11 Feature selection using Elastic Net/PLSR and Elastic Net/PLSDA 44
2.6.12 PCA 45
2.6.13 PLSDA 45
2.6.14 PLSR 46
2.6.15 Hierarchical clustering 47
2.6.16 Software 47
Chapter 3 Systems Serology Identifies Novel Autoantibody Signatures for Sjögren's Syndrome Diagnosis 48

3.1 Authors and Contributions 48

3.2 Abstract 50

3.3 Introduction 51

3.4 Results 54

3.4.1 IgG and FcγR autoantibody signatures distinguish between healthy individuals and those with Sjögren's syndrome 54

3.4.2 Unique autoantibody responses between non-Sjögren's sicca syndrome and Sjögren's syndrome differentiate these individuals from healthy controls 57

3.4.3 N-linked glycosylation profiling reveals variations in IgG glycans associated with Sjögren's syndrome 59

3.4.4 Cell-based phagocytosis assay suggests autoantibody-associated FcγR binding is linked to elevated autoantigen-specific phagocytosis in Sjögren's syndrome 61

3.4.5 Seronegative SjS patients can be differentiated from healthy controls based on an autoantibody signature driven by non-classical antigens 62

3.5 Discussion 64

3.6 Methods 69

3.6.1 Study participants and sample collection 69

3.6.2 Customized Sjögren's syndrome bead-based multiplex assay 70

3.6.3 Data normalization 71

3.6.4 Statistical analyses: 72

3.6.5 IgG antibody purification 72

3.6.6 IgG N-linked glycosylation profiling: 72

3.6.7 Bead-based THP-1 antibody-dependent phagocytosis assay 72

3.6.8 Feature selection and data-driven methods 73

3.6.9 Receiver operating characteristic (ROC) curves 73

3.7 Acknowledgements 73

Chapter 4 Decoupling Antibody Levels from Fc Effector Functions: An Ordinary Differential Equation Framework Challenges the 'More is Better' Assumption for Polyfunctionality 74

4.1 Authors and Contributions 74
4.2 Abstract 74
4.3 Introduction 75
4.3.1 Antibody and Fc Receptor responses in HIV infection and vaccination 76
4.3.2 HIV transmission and immune responses across different tissues 77
4.3.3 A new framework for a multiple FcR model to explore competition and polyfunctionality 78
4.4 Results 80
4.4.1 A sensitivity analysis highlights importance of IgG1- and IgG3-related parameters 80
4.4.2 The model reveals mechanisms that underpin individual heterogeneity in ADCP and ADCC responses depending on IgG1 and IgG3 concentrations 82
4.4.3 Host genetics influence optimization of effector functions 86
4.4.4 Model illustrates the potential for vastly different Fc responses in mucosal tissues 88
4.5 Discussion 90
4.6 Methods 92
4.6.1 Computational methods 92
4.6.2 Experimental methods 96
Chapter 5 Conclusions and Discussion 99
5.1 Scientific contributions 99
5.1.1 Elucidating heterogeneity across diseases 99
5.1.2 Developing diagnostic tools 100
5.1.3 Guiding vaccination and therapeutic interventions 101
5.2 Limitations 102
5.2.1 Early pandemic constraints 102
5.2.2 Lack of validation cohort 103

5.2.3 Limitations of the multiplex assay and ODE model 103
5.3 Future directions 105
5.3.1 New theory-driven model applications: COVID-19 infection and vaccination 105
5.3.2 Linking antibody neutralization and other Fc effector functions 106
5.3.3 Diagnosing autoimmune disease 107
5.4 Overall conclusions 108
Appendices 109
Bibliography 133

List of Tables

Table 3-1: Cohort demographics..... 70

Supplementary Table B-1: Sjogren's related autoantigens, their known functions and the reported clinical manifestations in the respective seropositive patients 114

Supplementary Table C-1: Affinity parameters for two FcR ODE model 126

Supplementary Table C-2: Concentration parameters for two FcR ODE model 126

List of Figures

Figure 1-1: Overview of the immunity balance. 2

Figure 1-2: Variability within Fc activation system 3

Figure 1-3: Systems serology modeling approaches. 4

Figure 2-1: Cohort information and setup of the custom CoV multiplex. 17

Figure 2-2: Vastly different SARS-CoV-2 serological signatures between healthy children and elderly 19

Figure 2-3: Healthy children and elderly have differing correlation networks. 22

Figure 2-4: Healthy versus COVID-19 serological signatures. 25

Figure 2-5: Receptor binding domain Abs in healthy versus COVID-19 patients. 29

Figure 2-6: COVID-19 Ab responses in COVID-19-positive children and elderly. 32

Figure 3-1: Schematic of bead-based multiplex assay..... 54

Figure 3-2: Serologic signature identified for Sjögren's (SjS) patients..... 55

Figure 3-3: Sjögrens versus healthy..... 57

Figure 3-4: PLSDA of healthy controls vs. non-Sjogren sicca patients vs. Sjögren's patients... 59

Figure 3-5: Cell-based phagocytosis assays and glycans. 61

Figure 3-6: Healthy vs. Seronegative Sjögren's patients. 64

Figure 4-1: Model Schematic 80

Figure 4-2: 1D sensitivity analysis of two-FcR model using in vivo blood parameters 82

Figure 4-3: 2D Sensitivity Analysis and relationship between IgG1 and IgG3. 84

Figure 4-4: Simulation of the impact of antibody boosting in RV144 vaccinee data on FcR complex formation. 85

Figure 4-5: Simulating FcR complex formation across different polymorphisms combinations 87

Figure 4-6: Fc receptor functions across different tissues. 89

Supplementary Figure A-1: SARS-CoV-2 serological signatures differ between healthy children, adults, and elderly 109

Supplementary Figure A-2: HLA class II alleles influence Ab signatures..... 110

Supplementary Figure A-3: Multiplex Assay setup and optimization 111

Supplementary Figure A-4: SARS2 Ab titrations 112

Supplementary Figure A-5: Accuracy of feature selection between COVID+ Children and Elderly model..... 113

Supplementary Figure B-1: Univariate analysis across groups for Ro52 (a) and La (b) specific responses (healthy control, non-SjS sicca syndrome, and all Sjogren's syndrome). Significant differences denoted with asterisks..... 121

Supplementary Figure B-2: a) Comparison of cross validation errors for the models plotted in Figure 3d. ROC curve showing sensitivity and specificity for the classical antigen PLSDA model, our seven-feature signature Healthy vs. Sjogrens PLSDA model, and multiplex positivity. 122

Supplementary Figure B-3: a) Glycosylation profiles from Figure 5a plotted by individuals across the different disease groups. b) Sialylation profiling showed no significant differences between groups 122

Supplementary Figure B-4: Univariate analysis across groups for Ro60 (a), Ro52 (b) and La (c) specific responses (healthy control, non-SjS sicca syndrome, and Sjogren's syndrome subdivided into seropositive and seronegative SjS). Significant differences denoted with asterisks..... 123

Supplementary Figure B-5: a) Hierarchical clustering for seronegative vs. healthy model from Figure 6. b) Comparison of cross validation errors for the PLSDA models plotted in Figure 6d. 124

Supplementary Figure B-6: Comparison of cross validation accuracy for our chosen PLSDA models to 100 randomly generated signatures with the same number of features. Significance denoted by asterisks. 124

Supplementary Figure C-1: Global sensitivity analysis using in vivo blood parameters as baseline values 125

Supplementary Figure C-2: 1D Sensitivity analysis across blood and mucosal tissues..... 127

Supplementary Figure C-3: Genetic polymorphisms across tissues. 127

Supplementary Figure D-1: I GET DRY Cohort data months from symptom onset and ESSDAI severity index by active (moderate/severe) vs. inactive (mild) disease status. Asterisks indicate level of significance. 129

Supplementary Figure D-2: Univariate analysis of Ro60 responses across healthy donors, non-Sjogren's patients, and Sjogren's patients (inactive or mild versus active or moderate/severe disease). 130

Supplementary Figure D-3: Univariate analysis of Ro52 responses across healthy donors, non-Sjogren's patients, and Sjogren's patients (inactive or mild versus active or moderate/severe disease). 130

Supplementary Figure D-4: Mild Sjogren's versus moderate and severe Sjogren's PLSDA scores (a) and Elastic-net-selected LV1 loadings (b). 131

Supplementary Figure D-5: Cell-based phagocytosis assays based on antigen-specific disease activity for A) Ro60, B) Ro52, or C) La. 131

Supplementary Figure D-6: IgG glycosylation profiling by disease activity 132

List of Appendices

Appendix A: Supplement to Systems Serology Detects Functionally Distinct Coronavirus Antibody Features in Children and Elderly 109

Appendix B: Supplement to Systems Serology Identifies Novel Autoantibody Signatures for Sjögren's Syndrome Diagnosis 114

Appendix C: Supplement to Decoupling Antibody Levels from Fc Effector Functions: An Ordinary Differential Equation Framework Challenges the 'More is Better' Assumption for Polyfunctionality 125

Appendix D: Unpublished Data 128

D.1 Serological signatures that explain heterogeneity in disease severity in Sjogren's syndrome 128

Abstract

Antibodies are a vital part of the immune system that provide protection against infectious diseases, but they have also been implicated in the development of autoimmune disease. While the fragment antigen-binding (Fab) domain of the antibody plays an important role in neutralization, the fragment crystallizable (Fc) region of the antibody binds to Fc receptors on innate immune cells to activate cellular effector functions, including antibody-dependent cellular toxicity (ADCC) and antibody-dependent cellular phagocytosis (ADCP). These functions are important for protection in infectious disease, but overactivation can lead to autoimmunity. Many different antibody and Fc receptor features contribute to these processes and thus it is difficult to unravel the role of each in ADCC and ADCP. As an additional layer of complexity, these features are highly variable across individuals, depending on personalized genetic and environmental factors. Newly developed systems serology approaches offer the opportunity to gain unique quantitative insight into these complex systems in both infectious and autoimmune diseases. In this work, we use systems serology to study the role of Fc effector functions in an autoimmune disease (Sjogren's syndrome) and in two different infectious diseases (SARS-CoV-2 and HIV). We show how these approaches can identify novel biomarkers, enable better understanding of disease heterogeneity, and provide new insights that may guide the development of diagnostic tools and therapeutic strategies.

Using data-driven systems serology approaches in Sjogren's syndrome, an autoimmune disease that causes dry mouth and dry eye, we found antibody/FcR signatures involving FcγRIIa and FcγRIIIa responses to classical antigens (such as Ro and La) were elevated in Sjogren's patients. We also found that non-classical antigen signatures were elevated in non-Sjogren's Sicca patients, as well as seronegative Sjogren's patients who had lower levels of classical antibody responses. Overall, this suggests a new mechanism whereby FcR activation via both classical and non-classical autoantigen binding could play a role in disease pathogenesis. These results provide important insight into biomarkers that could be used for diagnosis. In SARS-CoV-2, we were able

to identify cross-reactive SARS-CoV-2 antibody signatures that distinguished between pre-pandemic healthy children and elderly, providing the novel insight that elderly had more cross-reactive responses to human coronaviruses, while children had more targeted, SARS-CoV-2-specific responses. Furthermore, data-driven approaches identified an antibody signature that distinguished between a small sample size of COVID-19 infected individuals and healthy controls, driven by elevated FcγRIIIa responses. These results provided some of the first evidence to help understand differences in disease severity in younger children versus older adults early in the COVID-19 pandemic. Lastly, we employed mechanistic ordinary differential equation (ODE) models to gain insight into Fc effector function in HIV. A new model with two different FcR types was able to help us explore the complex dynamics between FcγRIIa and FcγRIIIa activation, depending on complex balances of antibody subclass concentrations and binding affinity related to host genetic background. The model revealed optimal combinations of IgG1 and IgG3 concentrations for maximizing ADCP and ADCC respectively. Surprisingly, the model also revealed a new mechanism whereby increases in IgG3 could decrease ADCP. Simulations specific to different tissues indicated that that host genetics (Fc receptor polymorphisms) may influence responses in the blood but are not expected to contribute to differences in mucosal tissues. Overall, these approaches provide new knowledge that could help guide future vaccines and therapeutic interventions, specific to desirable Fc effector functions.

Chapter 1 Introduction

Antibodies (Abs) are a vital component of the immune response, required for protection against infection from foreign pathogens, but failure to distinguish between "self" and "non-self" antigens can lead to autoimmune disease.[1] The immune system defends against infectious diseases and even has the ability to eliminate pathogenic cancer cells. These processes are activated by protein and chemical compounds called antigens that are present in foreign cells and recognized by Abs. In autoimmune disease, innocuous antigens can mimic true invaders causing overstimulation of the immune system resulting in inappropriate immune response and/or allergies. In order to better understand this complex balance of appropriate immune responses (**Figure 1-1**), computational systems biology approaches ("systems serology") have been applied. These systems serology approaches enable quantitative evaluation of the relationship between Ab features and immunological function.[2] Depending on the type of data and prior knowledge available, systems serology approaches offer the ability to: 1) use high-throughput data to infer new relationships between antibody features that classify disease states ("data-driven approaches"); and 2) gain new insight into quantitative mechanistic relationships ("theory-driven approaches") that drive immune behavior. Together these approaches enable an understanding of Ab signatures that differentiate disease state and give quantitative mechanistic insight into how these feature differences translate to function. In this study, we will apply data- and theory-driven systems serology approaches to infectious diseases and an autoimmune disease to give new insight into disease pathogenesis and to identify new quantitative mechanisms associated with immune

function. In particular, we will use these approaches to study the role of antibody-mediated Fc effector functions.

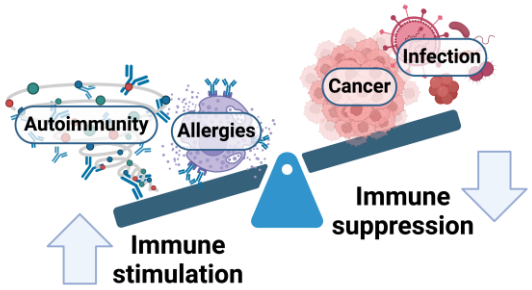


Figure 1-1: Overview of the immunity balance.

Too little immune response can lead to infection and cancer while immune overstimulation can cause autoimmunity and allergies.

1.1 Fc Receptors and antibody-mediated effector functions

Abs generally provide protection against infection by "neutralizing" or tightly binding to pathogens via the Fab portion of the antibody, but can also activate the innate immune system (via the Fc portion of the antibody) to induce cellular functions including antibody-dependent cellular phagocytosis (ADCP) and antibody-dependent cellular cytotoxicity (ADCC) via cellular Fc receptors.[3] These functions are enacted when antibodies bind antigen and then form immune complexes (antibody IgG dimers bound to antigen), in turn to bind different types of Fc receptors, namely the Fc gamma receptor, with FcRIIa being primarily found on monocytes for phagocytosis and FcRIII found mainly on natural killer (NK) cells to secrete cytotoxic factors.[4] FcR receptor polymorphisms have been identified, which can affect the binding affinity of IgG to the FcR. For example, FcRIIa-H has a higher affinity for IgG than FcRIIa-R and FcRIIIa-V has a higher affinity than the FcRIIIa-F polymorphism. Individuals can be homozygous or heterozygous for these polymorphisms, further complicating the system. There are multiple points within the system where heterogeneity can occur, as shown in **Figure 1-2**. This leads to a complex system that suits

itself well to systems serology approaches, which combine high-throughput experimental methods with computational methods to evaluate a system with complexity and high variability.

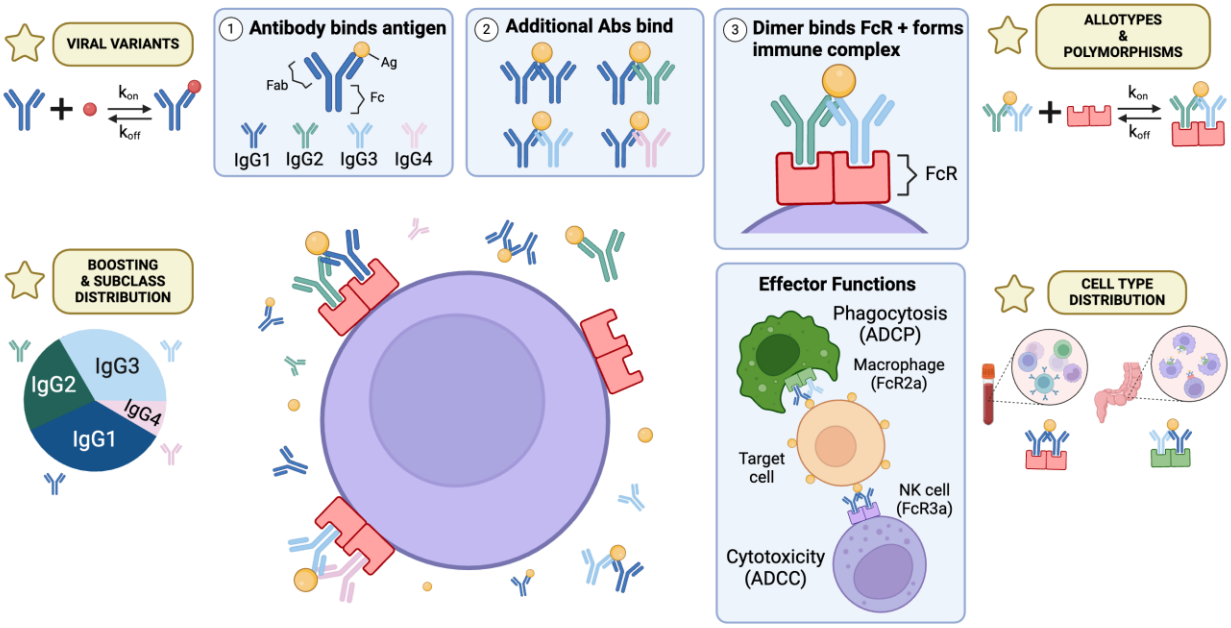


Figure 1-2: Variability within Fc activation system

Stepwise Fc receptor activation from binding of antibody to antigen, to the binding of FcRs on immune cells to intiate cellular effector functions. Potential areas for variability within the system labeled with stars.

1.2 Data-driven and theory-driven approaches in systems serology

Systems serology encompasses both data-driven (or machine learning) techniques and theory-driven (or mechanistic) techniques.[5–15] Determining which type of model to use depends on several factors. Data-driven modeling is useful when analyzing high dimensional datasets without clear underlying principles because classification and clustering models can help provide meaningful insights with knowledge of mechanism. Unsupervised machine learning techniques are a great initial option for analysis because they are unbiased without providing knowledge about which class the data belongs to. These techniques are most useful for diseases like COVID-19 or Sjogren's, in which patterns have been observed, but not much is yet known about the underlying

mechanisms of disease. Theory-driven models are more useful when there is some knowledge about the rules governing a system and simulations are desired to explore complex systems. They are especially useful when data-driven techniques have already identified patterns and principles, and the goal is to perform hypothesis testing or simulated interventions. Mechanistic mathematical models can be especially useful when in vivo or clinical testing is difficult or impossible. Theory-driven models of a disease such as HIV, which has a plethora of available research, allow us to take the information we know and test different circumstances to gain more information about the system. In this work, we will use both methods depending on the research question of interest: in COVID and Sjogren's, we would like to find patterns in the data using data-driven techniques, and in HIV, we will perform hypothetical simulations based on physiologically relevant parameters in a theory-driven mathematical model. In order to understand the current state of knowledge on these diseases, first a brief summary of the pathology of each condition will be discussed.

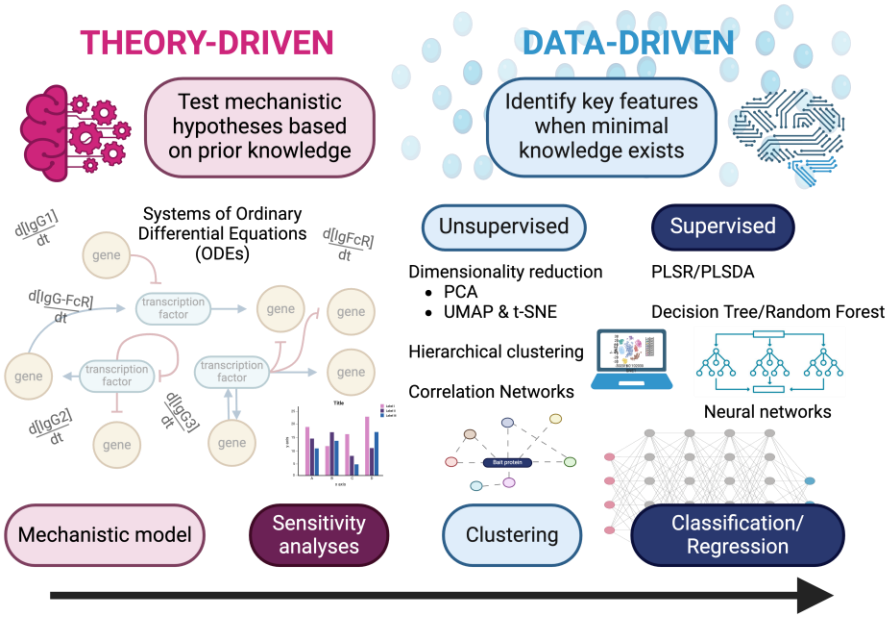


Figure 1-3: Systems serology modeling approaches.

High-throughput experimental assays measure functional data which can be used for theory-driven modeling when mechanisms are known and data-driven modeling when little is known about a complex system.

1.3 Coronavirus Infectious Disease 2019 (COVID-19) and SARS-CoV-2 pathology

Coronavirus disease 2019 (COVID-19) is an infectious disease caused by the severe acute respiratory syndrome coronavirus 2 (SARS-CoV-2) that has caused global disease burden and mortality as well as unprecedented social and economic disruption.[16] At the time of this study, the body of research for COVID-19 was rapidly growing, and yet it was still unknown how cross-reactive antibody responses and Fc receptor activation contributed to a wide range of disease severity. Although risk factors for severe illness included comorbidities (such as cardiovascular disease, diabetes mellitus, lung disease, kidney disease, obesity, and cigarette smoking) and blood type,[17] the largest differences in disease severity were observed with age. Children more commonly have asymptomatic or mild disease and fewer incidences of severe outcomes. This trend was even more prominent when comparing case fatality among young children and elderly individuals; at the peak of the pandemic in January 2021, there were 70 weekly deaths due to COVID-19 per 100,000 elderly individuals and only 0.01 weekly deaths due to COVID-19 per 100,000 individuals ages 0-5.[18] It still remains largely unknown what other factors contribute to the heterogeneity of disease severity and what mechanisms are primarily responsible for the clear difference in disease severity between pediatric and elderly populations.[17] One theory was that older adults had repeated exposures to human coronaviruses (a common cold) and therefore had existing cross-reactive Abs and created a skewed, off-target response.[10] There are still many gaps in our knowledge about coronavirus cross-reactivity and antibody responses. A better understanding of antibody responses and Fc receptor activation will be essential for continuing to monitor waning natural and vaccine-induced immunity and coverage of variants. Given the minimal information known at the start of the pandemic, a data-driven systems serology approach

was most appropriate to address these questions by identifying signatures of key antibody features that could describe differences between groups.

1.4 Sjogren's syndrome pathology

While antibody responses are generally thought to be important to maximize in infectious diseases like COVID-19 (except in rare cases, such as antibody-dependent enhancement), in autoimmune disease, pathogenic autoantibody responses can result in tissue destruction. Sjogren's syndrome is an example of an autoimmune disease of the exocrine glands that causes dry eyes and mouth, leading to significant patient discomfort and decreased quality of life.[19] While many studies have associated individual autoantibodies with Sjogren's syndrome, causing them to be used as part of diagnosis, the pathogenesis, role of Fc receptor activation, and clinical relevance of the autoantibodies are not fully understood. The pathogenesis is thought to be a multistep process, beginning with an environmental trigger, such as viral infection, in a genetically predisposed person.[20] Autoreactive B cell clones then generate autoantibodies, which cause chronic inflammation of the lacrimal and salivary glands.[21] Many different autoantibodies have been identified, with anti-Ro/SSA and anti-La/SSB present in 60-80% of patients.[22] These Abs, along with non- specific antinuclear antibodies (ANA) can be used to aid with diagnosis. There is no single diagnostic test for Sjogren's, although there are widely accepted criteria for diagnosis. The American College of Rheumatology/European Alliance of Associations for Rheumatology (ACR/EULAR) criteria are most widely used and utilize a weighted scoring system.[23,24] The score includes salivary gland sialadenitis (3), anti-Ro/SSA positivity (3), the ocular staining score (1), Schirmer (eye dryness) test (1), and salivary flow rate (1), with a summed score of greater or equal to 4 to qualify for diagnosis. Diagnosing disease in patients who are seronegative (do not test positive for Ro or La Abs) remains a challenge. Treatment is also difficult and is generally aimed

at reducing symptoms, although those with moderate and severe involvement can require systemic immunosuppressants.[25] The exact mechanism is not yet fully understood, and while Fc receptor variants have been identified in association with other autoimmune diseases, the role of Fc receptor activation in Sjogren's syndrome remains unclear.[26] Due to the limited knowledge of mechanisms playing a role in disease, data-driven techniques are preferred for identifying key sets of antibody signatures that can distinguish between healthy controls and Sjogren's patients, as well as between healthy controls and seronegative Sjogren's patients.

1.5 Human Immunodeficiency Virus (HIV) pathology

Much like COVID-19, HIV is an antigenically variable virus that can mutate rapidly to evade the immune system. HIV is a sexually transmitted infection that can also be transmitted through the blood or breastmilk. The virus destroys T-cells, thereby weakening the immune system and increasing the risk of opportunistic infections. Acute HIV infection often presents similarly to other viral infections like Epstein Barr Virus (mononucleosis), with fever, sore throat, and lymphadenopathy. Chronic infection without treatment can lead to Acquired Immunodeficiency Syndrome (AIDS) when the T-cell count decreases below 200. Antiretroviral therapy (ART) is highly effective if taken properly, but prevention remains an important approach to control the spread of disease, especially in asymptomatic individuals. Pre-exposure prophylaxis is up to 92% effective,[27] but access can be prohibitory. There has been one clinical vaccine trial (RV144) which showed significant efficacy against infection (60%), but follow-up studies have had mixed results in the mechanism behind this result.[28–30] It is thought that broadly neutralizing Abs are less effective in viruses that mutate rapidly because of the need for tight antigen-antibody bonding for neutralization to occur. Previous work using data-driven systems serology analysis has revealed

that RV144 was thought to increase ADCC responses, and increased levels of IgG1 and IgG3 led to higher Fc effector functions.[8]

While data-driven systems serology approaches have been valuable for identifying associations between groups regarding Ab levels and FcR activation, the remaining challenge is that these models do not consider the driving mechanisms behind the associations. A mechanistic ordinary differential equation model provides the added value of integrating knowledge of IgGs and Fc receptor activation and has the capability to run targeted simulations to explore the mechanistic reasoning behind the disease pathogenesis. Furthermore, mechanistic models are useful for exploring parts of the system that would be difficult to test experimentally or clinically, due to the ability to easily simulate interventions via hypothesis-driven modeling.

Recent work from our lab has highlighted the value of these mechanistic models for exploring personalized differences in antibody and Fc receptor features contribute to variation in FcR activation after HIV vaccination. Lemke et. al (2021) created an ordinary differential equation- (ODE-) based model to determine how personalized variability in IgG subclass concentrations and binding affinities influenced IgG-FcgRIIIa complex formation.[9] They validated the model with samples from the Human Immunodeficiency Virus (HIV) RV144 vaccine trial, which induced Fc effector responses rather than neutralizing antibodies. They found that IgG1 affinity to FcRIIIa is the most important parameter for FcR activation and that there was an IgG1 boosting plateau at which further boosting would not increase FcR activation in certain individuals. One limitation of this model, however, was that it only included one FcR type, FcRIIIa. In reality, there are multiple FcRs present which compete with each other for IgG binding. Our model structure, will better be able to consider multiple FcR types present, and the resulting competition

between substrates and receptors which ultimately affects the balance between Fc effector functions.

1.6 Structure of Thesis

A systems biology approach will help address the gaps in our understanding of how antibody responses and FcR function contribute to heterogeneity of disease in COVID-19, Sjogren's syndrome, and HIV and will allow us to gain a deeper understanding of complex antibody responses. A key uniting feature to these aims is a collaborative multidisciplinary team that allows for experimental and computational techniques to be used in parallel to provide new systems-level insight into diseases. In this work, we will use both data-driven and theory-driven systems serology approaches to address gaps in knowledge about antibody responses in infectious and autoimmune diseases, in particular COVID-19, Sjogren's syndrome, and HIV. Data-driven approaches will allow us to look for sets of antibody signatures that can differentiate between disease groups or disease severity in diseases with less knowledge about pathogenesis, such as COVID-19 and Sjogren's syndrome. For HIV, a mechanistic theory-driven that builds on insight from previous data-driven models (such as Lemke et al. (2021)[9]) will allow us to better understand the relative importance of multiple parallel the Ab features and their mechanistic contribution to heterogeneity in FcR functions across individuals. The thesis is organized via the following specific aims:

Aim 1 (Chapter 2) will utilize data-driven modeling to identify antibody signatures that are associated with disease heterogeneity in COVID-19. **Aim 1a** will evaluate the differences in coronavirus cross-reactivity between healthy children, adults, and elderly using pre-pandemic plasma samples. Aim 1b will examine the differences between coronavirus antibody signatures in individuals with COVID-19 vs. age-matched healthy individuals. **Aim 1c** will look at the

differences between antibody signatures in mild vs. severe COVID-19 disease. Results will give insight into the relationship between key antibody features that differ based on age and disease severity. This work is published in Nature Communications.[10]

Aim 2 (Chapter 3) will use data-driven approaches to identify antibody signatures associated with Sjogren's syndrome, an autoimmune disease. **Aim 2a** will examine the differences between healthy controls and patients with Sjogren's syndrome. **Aim 2b** will investigate the differences between healthy controls and non-Sjogren's Sicca patients, as well as between healthy controls and seronegative Sjogren's patients. Results will identify networks of antibody features associated with Sjogren's syndrome and disease severity. This work is currently in submission.

Aim 3 (Chapter 4) will build on an existing ODE model to unravel mechanisms driving FcR activation in HIV infection and vaccination. In this aim, we will apply an ordinary differential equation (ODE) model with two types of Fc receptors and evaluate the activation of effector functions such as antibody-dependent cellular cytotoxicity (ADCC) and antibody-dependent cellular phagocytosis (ADCC) through binding of various IgG subclasses and autoantigen. This will help identify how differences in Ab concentration in individuals drive differences in Fc effector functions. Results can be used to understand how therapeutic interventions that modify antibody concentrations may have a variable impact on Fc effector functions across individuals.

Chapter 2 Systems Serology Detects Functionally Distinct Coronavirus Antibody Features in Children and Elderly

2.1 Authors and Contributions

Kevin J. Selva[1]*, Carolien E. van de Sandt[1,2]*, Melissa M. Lemke[3]*, Christina Y. Lee[3]*, Suzanne K. Shoffner[3]*, Brendon Y. Chua[1], Samantha K. Davis[1], Thi H. O. Nguyen[1], Louise C. Rowntree[1], Luca Hensen[1], Marios Koutsakos[1], Chinn Yi Wong[1], Francesca Mordant[1], David C. Jackson[1], Katie L. Flanagan[4,5,6,7], Jane Crowe[8], Shidan Tosif[9,10,11], Melanie Neeland[9,11], Philip Sutton[9,11], Paul Licciardi[9,11], Nigel W Crawford[9,12], Allen C. Cheng[13,14], Denise L. Doolan[15], Fatima Amanat[16,17], Florian Krammer[16], Keith Chappell[18], Naphak Modhiran[18], Daniel Watterson[18], Paul Young[18], Wen Shi Lee[1], Bruce D. Wines[19,20,21], P. Mark Hogarth[19,20,21], Robyn Esterbauer[1, 22], Hannah G. Kelly[1,22] , Hyon-Xhi Tan[1,22], Jennifer A. Juno[1], Adam K. Wheatley[1,22], Stephen J. Kent[1,22, 23], Kelly B. Arnold[3], Katherine Kedzierska[1+], Amy W. Chung[1+]

*These authors contributed equally. [+]These authors supervised the work.

[1]Department of Microbiology and Immunology, Peter Doherty Institute for Infection and Immunity, The University of Melbourne, Victoria, Australia [2]Department of Hematopoiesis, Sanquin Research and Landsteiner Laboratory, Amsterdam UMC, University of Amsterdam, Amsterdam, Netherlands [3]Department of Biomedical Engineering, University of Michigan, Michigan, USA [4]Department of Infectious Diseases and Tasmanian Vaccine Trial Centre, Launceston General Hospital, Launceston, Tasmania, Australia [5]School of Health Sciences and School of Medicine, University of Tasmania, Launceston, Tasmania, Australia [6]Department of

Immunology and Pathology, Monash University, Commercial Road, Melbourne, Victoria, Australia [7]School of Health and Biomedical Science, RMIT University, Melbourne, Victoria, Australia [8]Deepdene Surgery, Deepdene, Victoria, Australia [9]Infection and Immunity, Murdoch Children's Research Institute, Melbourne, Victoria, Australia [10]Department of General Medicine, Royal Children's Hospital Melbourne, Melbourne, Victoria, Australia [11]Department of Paediatrics, The University of Melbourne, Victoria, Australia [12]Royal Children's Hospital Melbourne, Immunisation Service, Melbourne, Victoria, Australia [13]School of Public Health and Preventive Medicine, Monash University, Melbourne, Victoria, Australia [14]Infection Prevention and Healthcare Epidemiology Unit, Alfred Health, Melbourne, Victoria, Australia [15]Centre for Molecular Therapeutics, Australian Institute of Tropical Health & Medicine, James Cook University, Cairns, Queensland, Australia [16] Department of Microbiology, Icahn School of Medicine at Mount Sinai, New York, New York, USA [17]Graduate School of Biomedical Sciences, Icahn School of Medicine at Mount Sinai, New York, NY, USA [18]School of Chemistry and Molecular Bioscience, University of Queensland, Brisbane, Queensland, Australia [19]Immune Therapies Group, Burnet Institute, Melbourne, Victoria, Australia [20]University of Melbourne, Clinical Pathology, Vic, Australia [21]Department of Immunology and Pathology, Central Clinical School, Monash University, Australia [22]ARC Centre of Excellence in Convergent Bio-Nano Science and Technology, University of Melbourne, Melbourne, Victoria, Australia [23]Melbourne Sexual Health Centre, Infectious Diseases Department, Alfred Health, Central Clinical School, Monash University, Melbourne, Victoria, Australia

This work is published in Nature Communications.[10]

2.2 Abstract

The hallmarks of COVID-19 are higher pathogenicity and mortality in the elderly compared to children. Examining baseline SARS-CoV-2 cross-reactive immunological responses, induced by circulating human coronaviruses (hCoVs), is needed to understand such divergent clinical outcomes. Here we show analysis of coronavirus antibody responses of pre-pandemic healthy children (n = 89), adults (n = 98), elderly (n = 57), and COVID-19 patients (n = 50) by systems serology. Moderate levels of cross-reactive, but non-neutralizing, SARS-CoV-2 Abs are detected in pre-pandemic healthy individuals. SARS-CoV-2 antigen-specific Fcγ receptor binding accurately distinguishes COVID-19 patients from healthy individuals, suggesting that SARS-CoV-2 infection induces qualitative changes to antibody Fc, enhancing Fcγ receptor engagement. Higher cross-reactive SARS-CoV-2 IgA and IgG are observed in healthy elderly, while healthy children display elevated SARS-CoV-2 IgM, suggesting that children have fewer hCoV exposures, resulting in less-experienced but more polyreactive humoral immunity. Age-dependent analysis of COVID-19 patients, confirms elevated class-switched Abs in elderly, while children have stronger Fc responses which we demonstrate are functionally different. These insights will inform COVID-19 vaccination strategies, improved serological diagnostics and therapeutics.

2.3 Introduction

Since the first reported coronavirus disease 2019 (COVID-19) patient in December 2019,[31] the severe acute respiratory syndrome coronavirus 2 (SARS-CoV-2) has become a global pandemic, infecting millions of individuals worldwide.[32] Though the majority of COVID-19 patients experience mild symptoms, approximately 20% of cases have more severe disease outcomes involving hospitalization or intensive care treatment, especially in those with

underlying co-morbidities such as diabetes and cardiovascular disease.[33] Furthermore, COVID-19-related morbidity and mortality is significantly higher in the elderly population and almost absent in school-aged children.[34] A disproportional outcome in disease severity with increasing age is not unique to the SARS-CoV-2 pandemic and has been observed during previous influenza pandemics.[35] Understanding whether baseline pre-existing immunological responses, induced by previous exposure to seasonal coronaviruses, contribute to such differences may provide important insights into the divergent clinical outcomes between children and elderly.

Antibodies (Abs) are a vital component of the immune response with demonstrated importance in the control of most viral pathogens. However, their ability to respond to new pathogens can be largely affected by age. In influenza studies, elderly donors have increased levels of IgG and IgA antibodies directed to a broad range of historic influenza viral strains, but have decreased ability to generate de novo antibodies towards novel influenza viruses.[36] In comparison, children seem to benefit from more promiscuous antibody responses, better equipped to deal with novel viruses in general.[37] Apart from playing a key role in virus neutralization, Abs also have the capacity to engage Fc Receptors (FcRs) or complement to induce a range of Fc-effector functions, including Ab-dependent cellular cytotoxicity (ADCC), Ab-dependent cellular phagocytosis (ADCP) and Ab-dependent complement activation (ADCA)[6] among others. Abs eliciting Fc-mediated functions are not limited to targeting just neutralizing viral epitopes, such as the SARS-CoV-2 receptor binding domain (RBD), but may instead utilize any available epitope derived from viral proteins[6]. Indeed, non-neutralizing Abs have been shown to be protective against various virus infections by mediating Fc-effector functions.[38,39] A previous SARS-CoV (also called SARS-CoV-1) study associated ADCP with viral clearance[40]; individuals expressing a higher affinity FcγRIIa (CD32a)-H131 polymorphism,

associated with enhanced Fc functions, had better disease outcomes.[41,42] A recent study from Schäfer et al. also demonstrated that the loss of Fc-effector function in mice models significantly impaired the potency of several protective anti-SARS-CoV-2 antibodies in vivo. However, Fc functional Abs may also enhance infection or pathology through Ab-dependent enhancement (ADE), previously observed in some SARS-CoV-1 animal vaccine and in vitro studies.[43,44] ADE has the potential to turn mild infections into life-threatening conditions, as exemplified by dengue virus infections, in which non-neutralizing cross-reacting antibodies can exacerbate disease progression.[45] Although cross-reactive antibodies to SARS-CoV-2 antigens, such as the nucleoprotein (NP) and spike 2 (S2), have been detected in uninfected individuals, it is not understood whether ADE could contribute to poorer disease outcome amongst COVID-19 patients, particularly amongst the elderly.[46] Given the alarming rise in COVID-19 deaths, particularly amongst the elderly, it is imperative to profile the impact of age on CoV antibodies. Here, we present evidence of markedly different Ab signatures between pre-pandemic healthy children and elderly samples. We further contrast the pre-pandemic antibody signatures observed in healthy individuals with those of COVID-19-infected patients, children and elderly, to provide a broader context for the implications of these systems serology signatures for disease outcome and future vaccine development strategies.

2.4 Results

2.4.1 Distinct systems serology signatures in children versus elderly

In-depth characterization of cross-reactive SARS-CoV-2 Ab responses in healthy children compared to healthy elderly is needed to understand whether pre-existing human coronavirus (hCoV)-mediated Ab immunity potentially contributes to COVID-19 disease outcome. We designed a cross-reactive CoV multiplex array, including SARS-CoV-2, SARS-

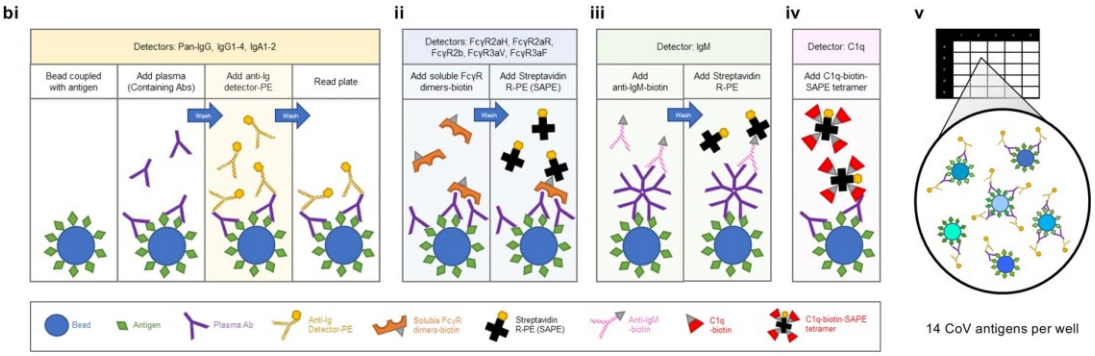
CoV-1, MERS-CoV and hCoV (229E, HKU1, NL63) spike (S) and NP antigens (**Figure 2-1**). We assessed CoV-antigen-specific detector levels of isotypes (IgG, IgA, IgM) and subclasses (IgG1, IgG2, IgG3, IgG4, IgA1, IgA2), along with C1q binding (a predictor of ADCA via the classical pathway) and FcγRIIa (CD32a), FcγRIIb (CD32b) and FcγRIIIa (CD16a) soluble dimer engagement (recombinant dimers which mimic FcγR engagement at the immunological synapse and had been previously shown to correlate with a range of Fc-effector functions)[47] (**Figure 2-1b**). A composite dataset of baseline CoV Ab features (14 CoV antigens × 14 detectors, thus 196 Ab features) was generated for the plasma of 89 children, 98 adults and 57 elderly individuals (**Figure 2-1c**).

To begin, we compared CoV Ab responses between children and elderly. Accounting for multiple comparisons, we identified that 58 of the 196 (29.6%) antibody features were significantly different between the two age groups (all $p < 0.00037$; **Figure 2-2a**). Children (orange) were characterized by elevated IgM Ab responses targeting a range of CoV antigens, including several SARS-CoV-2 antigens (S, NP and RBD). Furthermore, SARS-CoV-2 spike-specific Abs engaged the high-affinity FcγRIIa-H131 soluble dimers, previously associated with better disease outcome against SARS-CoV-1.[41] FcγRIIa (CD32a) is found on phagocytes such as macrophages, neutrophils and dendritic cells (DCs) and mediates Ab-dependent functions such as ADCP among others.[47] In contrast, the antibody response in healthy elderly individuals (dark blue) was characterized predominantly by IgA and IgG antibodies directed against a range of CoV antigens, including SARS-CoV-2 S and RBD. In particular, hCoV-specific Abs were found to engage soluble FcγRIIIa dimers. FcγRIIIa (CD16a) can be found on NK cells and phagocytes such as monocytes and macrophages, and mediates Ab-dependent functions such as ADCC and ADCP.[47,48]

a

Pathogen	Protein	Acronym	Vol coupled / 12.5 x 10^6 beads	Source	Cat #	Expression	Tag	Accession #	Amino Acid
SARS-CoV-2	Spike 1	SARS2 S1	100µg	Sino Biological	40591-V08H	HEK293	His	YP_009724390.1	Val16-Arg685
SARS-CoV-2	Spike 2	SARS2 S2	100µg	Sino Biological	40590-V08B	Insect	His	YP_009724390.1	Ser686-Pro1213
SARS-CoV	Spike	SARS1 S	100µg	Sino Biological	40150-V08B1	Insect	His	AAX16192.1	Met1-Arg667
HCoV-229E	Spike	HCoV 229E S	100µg	Sino Biological	40601-V08H	HEK293	His	APT69883.1	Cys16-Asn536
HCoV-HKU1	Spike	HCoV HKU1 S	100µg	Sino Biological	40021-V08H	HEK293	His	YP_173238.1	Met1-Arg760
SARS-CoV-2	Receptor Binding Domain	SARS2 RBD	49.7µg	Florian Krammer		HEK293	His	MN908947.3	Arg319-Phe541
SARS-CoV-2	Trimeric S	SARS2 Trimer	100µg	Adam Wheatley		HEK293	His	YP_009724389.1	Met1-Lys1208
SARS-CoV-2	SClamp	SARS2 SClamp	100µg	UQ‡					
MERS-CoV	SClamp	MERS SClamp	100µg	UQ‡					
SARS-CoV-2	Nucleoprotein	SARS2 NP	100µg	Sino Biological	40588-V08B	Insect	His	YP_009724397.2	Met1-Ala419
SARS-CoV	Nucleoprotein	SARS1 NP	100µg	Sino Biological	40143-V08B	Insect	His	NP_828858.1	Met1-Ala422
MERS-CoV	Nucleoprotein	MERS NP	100µg	Sino Biological	40068-V08B	Insect	His	AFS88943.1	Met1-Asp413
HCoV-229E	Nucleoprotein	HCoV 229E NP	40µg	Prospec-Tany	SARS-001	E. Coli	His	Q1HVQ0	Ile39-Asn389
HCoV-NL63	Nucleoprotein	HCoV NL63 NP	40µg	Prospec-Tany	SARS-003	E. Coli	His	ABE73423	Gln221-Gln340
C. Tetani*	Tetanus Toxin*	Tetanus	100µg	Sigma	T3194				
Influenza A H1N1* (A/Cali/07/2009)	Hemagglutinin*	H1Cal2009	100µg	Sino Biological	11085-V08H	HEK293	His	ACP44189.1	Met 1-Gln 529

* Tetanus toxin and influenza hemagglutinin were used as positive controls
‡ UQ = University of Queensland



ci

Demographics healthy age groups and COVID19 patients

Group	Total #	Age mean (range)	Birth year mean (range)	Sex # (%) Male	Sex # (%) Female	Year sample obtained mean (range)
Children	89	8 (1.5-19)	2011 (1999-2018)	47 (52.8)	42 (47.2)	2019 (2019-2020)
Adults	98	37 (22-63)†	1980 (1950-1997)†	52 (53.1)†	46 (46.9^)	2018 (2009-2020)
Elderly	57	76 (65-92)	1939 (1923-1954)	14 (24.6)	43 (75.4)	2016 (2012-2020)
COVID19	50*	47 (1-76)	1978 (1944-2020)	28 (56.0)	22 (44.0)	April 2020 (Feb-Sep)

* 3 of 50 donors had two consecutive time points
† one donor unknown

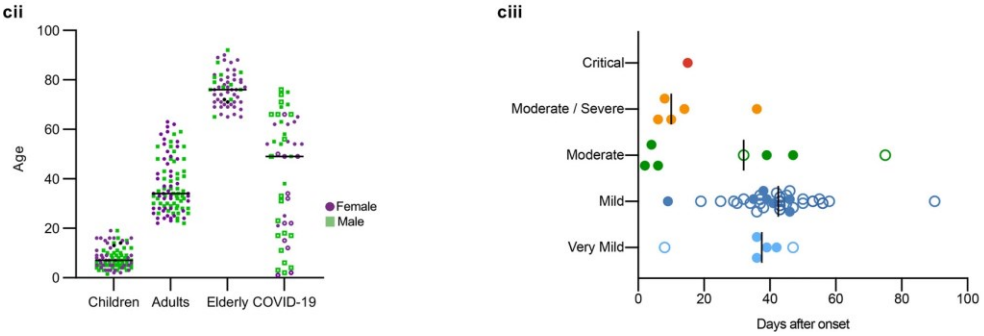


Figure 2-1: Cohort information and setup of the custom CoV multiplex.

a) Details of antigens included in the assay. **b)** Overview of bead-based multiplex assay. Assay setup for detectors Pan-IgG, IgG1-4, IgA1-2 (**b**-i), FcγR2aH, FcγR2aR, FcγR2b, FcγR3aV, FcγR3aF (**b**-ii), IgM (**b**-iii) and C1q (**b**-iv). FcγR2aH and FcγR3aV are the high-affinity variants of the dimers, while FcγR2aR and FcγR3aF are the respective

low-affinity dimer variants. (**b**-v) Beads coupled to respective CoV antigens are added together into wells of a 384-well plate for multiplexing. **c)** Overview of the demographics in the healthy donors per age group and COVID-19 patients.

Vastly different CoV serological signatures between children and elderly were also observed when analysing the same data using systems serology[8] (**Figure 2-2b,c**). To identify the minimal signature of Ab features that best distinguished children from elderly, we performed feature selection (Elastic-Net) followed by a supervised multidimensional clustering analysis (partial least squares discriminant analysis, PLSDA; **Figure 2-2b**). Fifteen Ab features selected by Elastic-Net accurately discriminated between children and elderly (99.1% calibration, 98.6% cross-validation accuracy), with significant separation of children and elderly PLSDA scores across the first latent variable (LV1) on the *x*-axis ($p < 0.0001$, $t = 21.60$) (**Figure 2-2c**). These data reiterated that children have elevated cross-reactive IgM responses to a range of CoV antigens, including SARS-CoV-2 Abs that engaged FcγRIIa-H131 soluble dimers, which were also detected in the multiple comparison analysis (**Figure 2-2a**). Furthermore, this analysis supported that elderly had elevated IgA and IgG to a variety of CoV antigens, including an IgA1 response to SARS-CoV2 RBD and an IgG2 response to SARS-CoV2 NP. Similar trends were also observed when we visualized the data through unsupervised hierarchical clustering (**Supplementary Figure A-1a**).

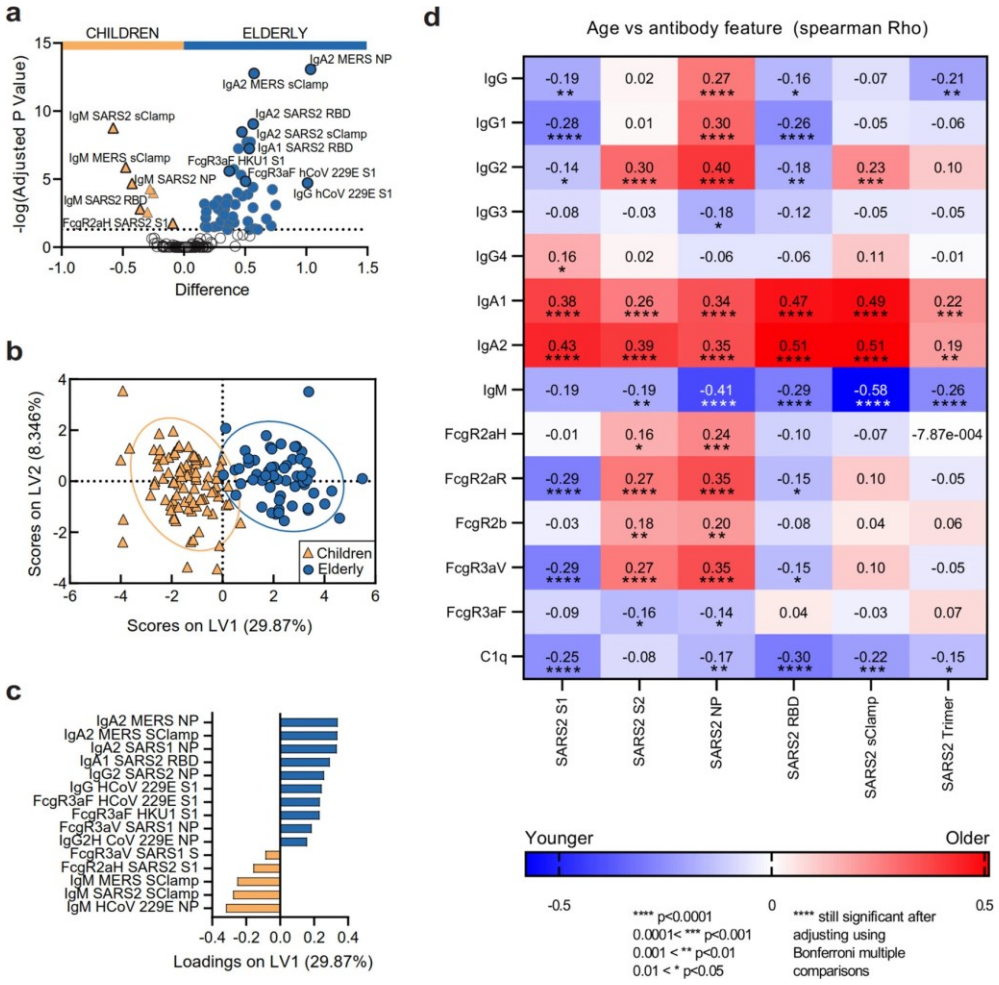


Figure 2-2: Vastly different SARS-CoV-2 serological signatures between healthy children and elderly

a) Volcano plot of healthy children (orange) versus elderly (dark blue), open circles are not significantly different between two groups. Data were z-scored prior to analysis. **b)** PCA of all 196 Ab features for healthy children, adults (light-blue square) and elderly. PLSDA scores **(c)** and loadings plots **(d).** Two-tailed Spearman correlation was performed to associate age with the strength of Ab features against the six SARS-CoV-2 antigens. Multiplex assays were repeated in duplicates

2.4.2 Primed Ab responses to CoVs increase with repeated hCoV exposures

A recent study by Edridge et al. confirmed that seasonal hCoVs can repeatedly infect individuals of all ages,[49] hence the differences between more immature CoV-specific IgM signatures in children and the more mature, class-switched CoV-specific IgA and IgG signatures observed in elderly were likely due to decades of repeated prior exposures to circulating hCoVs

in the elderly population. To explore this hypothesis, we investigated whether these differences were gradually introduced in an aging population. A cohort of pre-pandemic healthy adults (ages 22–63) was added to the analysis, together with our children and elderly cohorts. Age was rank-correlated (Spearman's) with the strength of Ab responses picked up by the 14 multiplex detectors against the six SARS-CoV-2 antigens (**Figure 2-2d**). While age once again clearly segregated IgM and IgA responses, we also noticed that Ab responses towards SARS-CoV-2 S2 and NP were largely associated with increasing age. As both S2 and NP[50] are more conserved regions across CoV strains, this observation supports our hypothesis that repeated exposure to circulating hCoV could be driving pre-existing immunity and cross-reactive responses in the elderly. Multivariate regression analysis (partial least square regression, PLSR) and unsupervised hierarchical clustering performed on the combined cohort, also showed similar associations between CoV Ab responses and age (**Supplementary Figure A-1b-d**).

2.4.3 Immune maturation drives mature CoV Ab responses

To interrogate Ab functionality and cross-reactivity between antigens of selected CoV signatures, we conducted a correlation network analysis, focusing upon significant correlations of the 15 Ab features selected by Elastic-Net. The children's network demonstrates how a range of SARS-CoV-2 S2 Ab features correlate significantly with various features related to SARS-CoV-1 S (**Figure 2-3a**, top left), while features relating to SARS-CoV-2 S1 cluster independently (**Figure 2-3a**, bottom left). This is in line with our previous observations where cross-reactivity of SARS-CoV-2 S1 signatures trended differently from that of S2, possibly due to S2 being more conserved across CoV species.[51] SARS-CoV-2 FcγRIIa was associated with the higher affinity polymorphism-H131 (SARS2 S1 FcgR2aH in **Figure 2-3a**, bottom left) dimer binding against S1, which also correlated strongly with multiple other SARS-CoV-2 Fc

responses against S1, including FcγRIIb (FcgR2b), C1q and binding to FcγRIIIa-V158 (the higher affinity FcγRIIIa polymorphism, FcgR3aV) dimers. These larger networks suggest that children might have better capacity to engage a range of Fc-effector functions targeting the SARS-CoV-2 S. Separately correlated IgM networks of SARS-CoV-2 antigens together with other CoVs (**Figure 2-3a**, right) suggest that the IgM-dominated immature immune system in children might be more responsive towards SARS-CoV-2 antigens and may be polyreactive in nature, thus might be more rapidly activated upon SARS-CoV-2 infection.[37]

The elderly predominantly had hCoV-driven cross-functional Ab signatures to S protein (**Figure 2-3b**, top). Interestingly, while the networks were complex, and driven by both Fc-effector functions and C1q, they were species-specific with a lack in overlap between the networks for either circulating hCoV 229E or hCoV HKU1, unlike the more polyreactive networks observed in the children. These findings further support the notion of pre-conceived immunity in the elderly primed by prior exposures to circulating hCoV drive more focused specificity. Expanding upon our prior observation of matured class-switched cross-reactive antibodies in the elderly, a network of IgA1 and IgA2 responses were formed between SARS2 RBD and S. Similarly, networks involving IgG2 and FcγRIIa-H131 (FcgR2aH) or IgA to CoV antigens were observed (**Figure 2-3b**, bottom). However, notably, these networks were largely species-specific with minimal overlap, suggesting a more rigid immune response present in the elderly, directed towards prior hCoV-exposed antigens. Altogether, the network analyses suggest that children have less exposure to CoV antigens but may have a more adaptable humoral immune responses, both in antigen recognition and Fc responses, targeted towards SARS-CoV-2 compared to elderly. Furthermore, the overall response in children is likely to benefit from the broad polyfunctionality of the SARS-CoV-2 antibody repertoire, which may offer them greater

non-neutralizing protection through FcγR engagement than the elderly following initial SARS-CoV-2 exposure, in line with the theory proposed by Carsetti et al.[37]

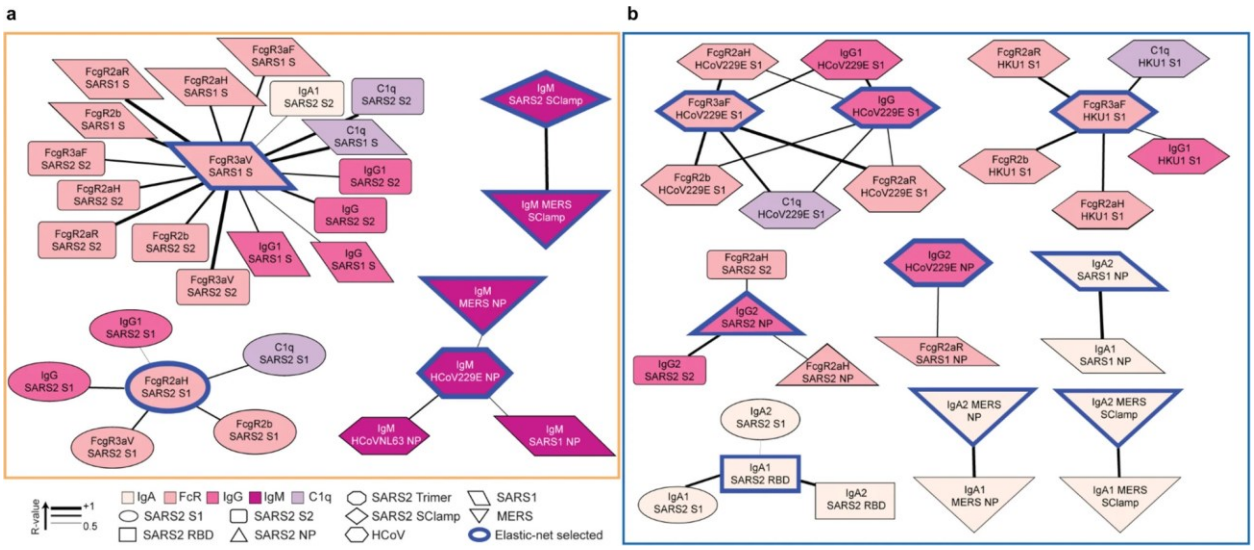


Figure 2-3: Healthy children and elderly have differing correlation networks.

Correlation network analyses for healthy children **(a)** and elderly **(b)** identify features associated with the Elastic-Net-selected features (blue outline). Coded by Ab feature type (colour), antigen (shape) and correlation coefficient (line thickness).

2.4.4 HLA class II alleles influence CoV Ab signatures in healthy individuals

Establishment of an effective humoral immune response after infection and/or vaccination depends on the generation of affinity-matured long-lived plasma cells and memory B cells, and is correlated with effective activation of T follicular helper (T_{FH}) cells.[52] T_{FH} cells are activated by presentation of viral epitopes presented by HLA class II alleles on antigen presenting cells, such as DCs. However, a broad array of HLA class II alleles expressed in humans could affect the activation of T_{FH} cells and thus likely to differentially shape the humoral immune responses. Moreover, several studies demonstrate that variations in HLA class II alleles were associated with susceptibility or resistance to several infectious diseases including MERS-CoV[53,54] and with vaccine-induced Ab responses.[55] Hence, we investigated whether HLA class II alleles could

affect CoV Ab signatures observed in healthy individuals, which would improve our understanding of the role of HLA class II alleles in shaping the Ab response upon SARS-CoV-2 infection. We analysed the antibody signatures of healthy individuals for whom HLA class II allele information was available (children $n = 84$, adults $n = 17$ and elderly $n = 10$; **Supplementary Figure A-2**). Data for all healthy donors were pooled since subsets for adult and elderly donors were too small to analyse individually. HLA distributions per age group can be found in **Supplementary Figure A-2**. To determine whether HLA class II alleles contributed to differences in Ab predisposition, we conducted Elastic-Net and PLSDA to distinguish Ab responses between the two most frequently observed HLA-DQB1, -DRB1, or -DPB1 alleles in our cohort (**Supplementary Figure A-2a, d, g**). Intriguingly, HLA-DQB1*03:01 and HLA-DQB1*06:02 were associated with distinct Ab features (**Supplementary Figure A-2b, c**; calibration 86.4%, and 82.6% cross-validation accuracy), and to a minor extent between HLA-DRB1*07:01 and HLA-DRB1*15:01 (**Supplementary Figure A-2e, f**; calibration 79.1%, and 76.3% cross-validation accuracy), and HLA-DPB1*04:01 and HLA-DPB1*02:01 (82.3% calibration and 72.2% cross-validation accuracy; **Supplementary Figure A-2h, i**). Discriminating features included both Ab isotypes and FcR engagement for both hCoV, SARS-CoV1 and 2, and MERS antigens. The driving HLA class II allele behind the differences observed between HLA-DQB1*03:01 and HLA-DQB1*06:02, and HLA-DRB1*07:01 and HLA-DRB1*15:01 remains elusive as HLA-DQB1*06:02 and HLA-DRB1*15:01 are strongly co-expressed in our cohort (93.9% of all HLA-DQB1*06:02 donors also expressed HLA-DRB1*15:01; 27.6% of all HLA-typed donors expressed both HLA-DQB1*06:02 and HLA-DRB1*15:01). Nevertheless, these results suggest that HLA class II alleles, in combination with prior hCoV exposures, can contribute to differences in Ab predispositions in our healthy donor

cohort. Hence, HLA class II alleles could contribute to shaping the SARS-CoV-2 Ab response upon infection or vaccination, possibly resulting in differences in SARS-CoV2-specific Ab titres and/or FcR engagements across individuals.

2.4.5 Distinct Fc Ab signature in COVID-19 patients

A cohort of 19 SARS-CoV-2 PCR-positive patients (**Figure 2-1c-iii** (closed symbols)) were screened for SARS-CoV-2 antigen-specific serological profiles (**Supplementary Figure A-3** and **Supplementary Figure A-4**). An individual who was SARS-CoV-2-exposed but remained SARS-CoV-2 PCR-negative was also assessed (Donor D1). Elevated SARS-CoV-2-specific Ab responses in COVID-19 patients relative to healthy or the exposed but PCR-negative individual were observed across multiple titrations (**Supplementary Figure A-4**). In particular, we found that in the majority of COVID-19 patients, the SARS-CoV-2 antigen-specific Abs bound to FcγRIIIa-V158 and FcγRIIa-H131 soluble dimers at high levels, even at 1:800 plasma titrations, suggesting that besides potential neutralizing activity, alternative antibody-mediated activity such as ADCC and ADCP are likely to contribute to viral clearance.[47,48,56]

As the global focus shifts towards serological testing as a strategy for population surveillance to inform government policies, there is an urgent need to distinguish unique Ab profiles in COVID-19 patients to improve the sensitivity and specificity of these tests.[57] Therefore, we next explored if we could detect distinct serological patterns of SARS-CoV-2 antigen-specific Ab features among the various isotypes (IgG, IgA or IgM) that would distinguish our small COVID-19 cohort from healthy individuals (including D1). Through the use of hierarchical clustering, we observed that majority of COVID-19-positive individuals induced high SARS-CoV-2-specific IgM responses, especially to spike antigens, while modest levels of cross-reactive SARS-CoV-2-specific IgM, mainly directed against SARS-CoV-2 NP,

were also detected within the healthy individuals, particularly amongst the children (**Figure 2-4a**). Similarly, modest SARS-CoV-2-specific IgA (**Figure 2-4b**) and IgG (**Figure 2-4c**) were observed in healthy, predominantly adult and elderly individuals, though less frequently than IgM, with cross-reactive IgG responses observed at the lowest frequencies of all isotypes (**Figure 2-4c**). Overall, modest levels of SARS-CoV-2 cross-reactive Abs in healthy donors resulted in poor clustering of COVID-19 patients from healthy individuals when a single isotype was assessed, even though multiple SARS-CoV-2 antigens were included. These results suggest that reported low levels of false positives in current serological diagnostics tests could be due to pre-existing levels of cross-reactive Abs that lead to similar serological signatures as observed in SARS-CoV-2-infected individuals when only the quantity of antigen-specific Abs is assessed.

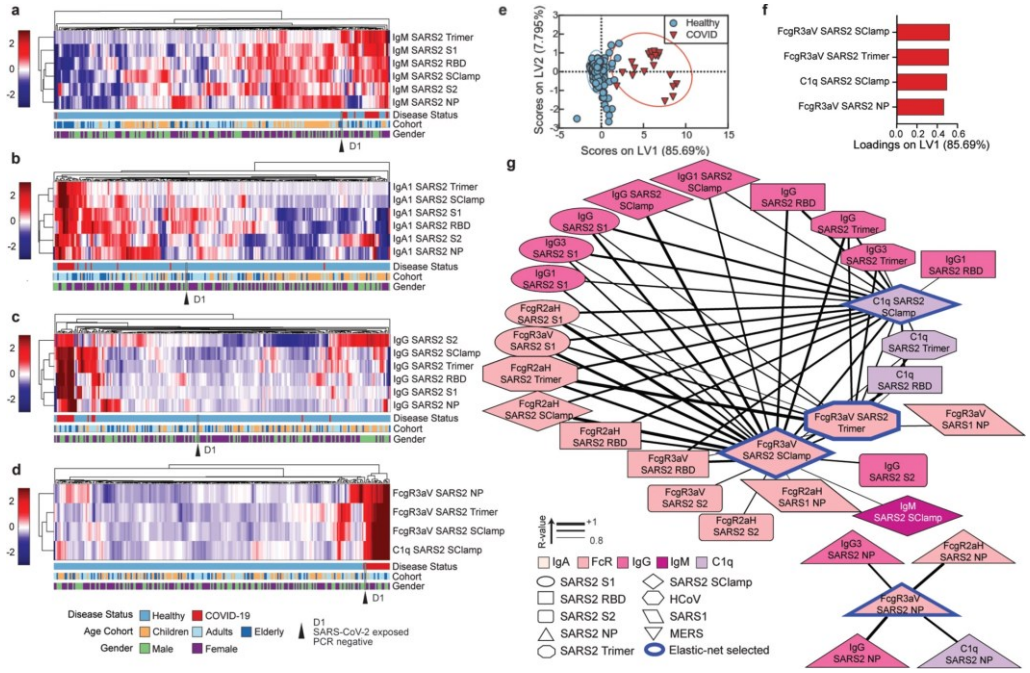


Figure 2-4: Healthy versus COVID-19 serological signatures.

Hierarchical clustering of all SARS-CoV-2 antigens for IgM **(a)**, IgA1 **(b)** and IgG **(c)**. Levels are coloured from low (dark blue) to high (dark red). Hierarchical clustering **(d)** and PLSDA model scores **(e)** and loadings **(f)** were performed using the four-feature Elastic-Net-selected SARS-CoV-2 antigen signature (98.51% calibration accuracy, 98.51% cross-validation accuracy). Variance explained by each LV is in parentheses. **(g)** Correlation network analysis for COVID-19 patients was performed to identify features significantly associated with the Elastic-Net-selected features (blue outline). Coded by Ab feature type (colour), antigen (shape) and correlation coefficient (line thickness). Data were z-scored prior to analysis. Multiplex assays were repeated in duplicates.

To identify the minimum Ab signature that best distinguishes the COVID-19 patients from healthy individuals, feature selection was used and identified four SARS-CoV-2 Ab variables that differentiated the two groups (**Figure 2-4d-f**), targeting three different SARS-CoV-2 antigens, S trimer, fold on stabilized spike ectodomain, 2P mutation,[58] NP, and Sclamp (molecular clamp stabilized spike ectodomain). Intriguingly, antigen-specific engagement of FcγRIIIa-V158 and C1q, but not IgG, was selected. This suggests that SARS-CoV-2 infection potentially induces antigen-specific Ab with distinct Fc qualities, e.g. Fc glycosylation changes, enhancing binding of FcγRIIIa-V158 and C1q,[8,48] unlike pre-existing cross-reactive SARS-CoV-2 Abs observed in our healthy donor cohort. In contrast to previous unsupervised hierarchical clustering for IgA, IgM and IgG (**Figure 2-4a-c**) to multiple SARS-CoV-2 antigens, these four SARS-CoV-2 Ab features had distinct patterns in COVID-19 patients, which led to the clustering of COVID-19 patients together with a single exception, this notably being the healthy, exposed, SARS-CoV-2 PCR-negative individual (**Figure 2-4d**). Strikingly, a supervised PLSDA model of these four features, all associated with COVID-19 patients, could significantly distinguish COVID-19 patients from healthy individuals on LV1 (**Figure 2-4e-f**; *x*-axis, $p < 0.0001$, $t = 34.80$; 98.51% calibration accuracy, 98.51% cross-validation accuracy). Collectively, these results suggest that future COVID-19 serological diagnostic tests could be improved by assessing the Fc quality of antigen-specific Abs in addition to Ab quantity.

To specifically define these four SARS-CoV-2 Ab features, we conducted a correlation network of Ab responses in the COVID-19-positive individuals (**Figure 2-4g**). High levels of correlation were observed between all SARS-CoV-2 spike antigens: S1, S2, RBD, S trimer and Sclamp; while NP antigen-specific Ab features created a separate network. Antigen-specific

IgG1 and IgG3, which are the most highly functional IgG subclasses[59] were highly correlated with FcγR and C1q antigen-specific Ab engagement, demonstrating they may be the key mediators of these Fc-effector functions. These results suggest that COVID-19 patients develop a strong SARS-CoV-2-specific Ab response over the course of their infection, eliciting both neutralizing and non-neutralizing functions.

2.4.6 Qualitative and quantitative differences of IgM in children

Neutralizing Ab responses targeting the RBD have been observed in the majority of convalescent COVID-19 serum sample, which has been associated with control of SARS-CoV-2.[60] All baseline pre-pandemic samples were tested via a virus microneutralization (VN) assay,[61] and not surprisingly, neutralizing antibody titres were solely detected in COVID-19 patients. However, examining both the quantity and quality of pre-existing RBD may provide insights towards the development of these responses. Baseline RBD isotype-specific levels between healthy children, adults, elderly and COVID-19 patient plasma samples were assessed via multiplex-assay and validated with published ELISA methods[62] (**Figure 2-5**). ELISA data confirmed our earlier observations that children induced elevated IgM (**Figure 2-5a**) while elderly had higher RBD-specific IgA1 responses as measured by multiplex and trended with ELISA IgA results (**Figure 2-5b**), while no differences in IgG were observed among the healthy donors (**Figure 2-5c**). The absence of significant differences between age groups in the ELISA can be accounted for by the fact that we only tested a fraction of the healthy donors and that the multiplex is in general more sensitive.

Since Ab neutralization quality and potency is often correlated with Ab avidity, we conducted a urea disassociation assay on a subset of children, elderly and COVID-19 plasma samples (**Figure 2-5a-iv, b-iv**). Avidity of RBD-specific IgM from children and elderly was

significantly weaker than COVID-19 patients ($p = 0.0059$ and $p = 0.0006$, respectively). Interestingly, children's IgM responses span a large and slightly higher range of avidities (median 60.88; IQR 49.37–79.8) as compared to the elderly (median 50.73; IQR 43.83–71.55). No differences in IgA avidity were found between children (median 62.22; IQR 56.37–70.99), elderly (median 63.08; IQR 34.84–76.46) and COVID-19 patients (median 64.77; IQR 32.63–81.78). The avidity assay was not conducted for IgG, due to lack of resolution for healthy individuals in the ELISA. Altogether, our data suggest that, compared to the elderly, children may have increased potential to mount a higher quality of antibody responses originating from the high binding avidity IgM population which is less commonly observed in the elderly. This may offer them greater development of non-neutralizing protection through FcR engagement than the elderly following initial SARS-CoV-2 exposure, in line with the theory proposed by Carsetti et al.[37]

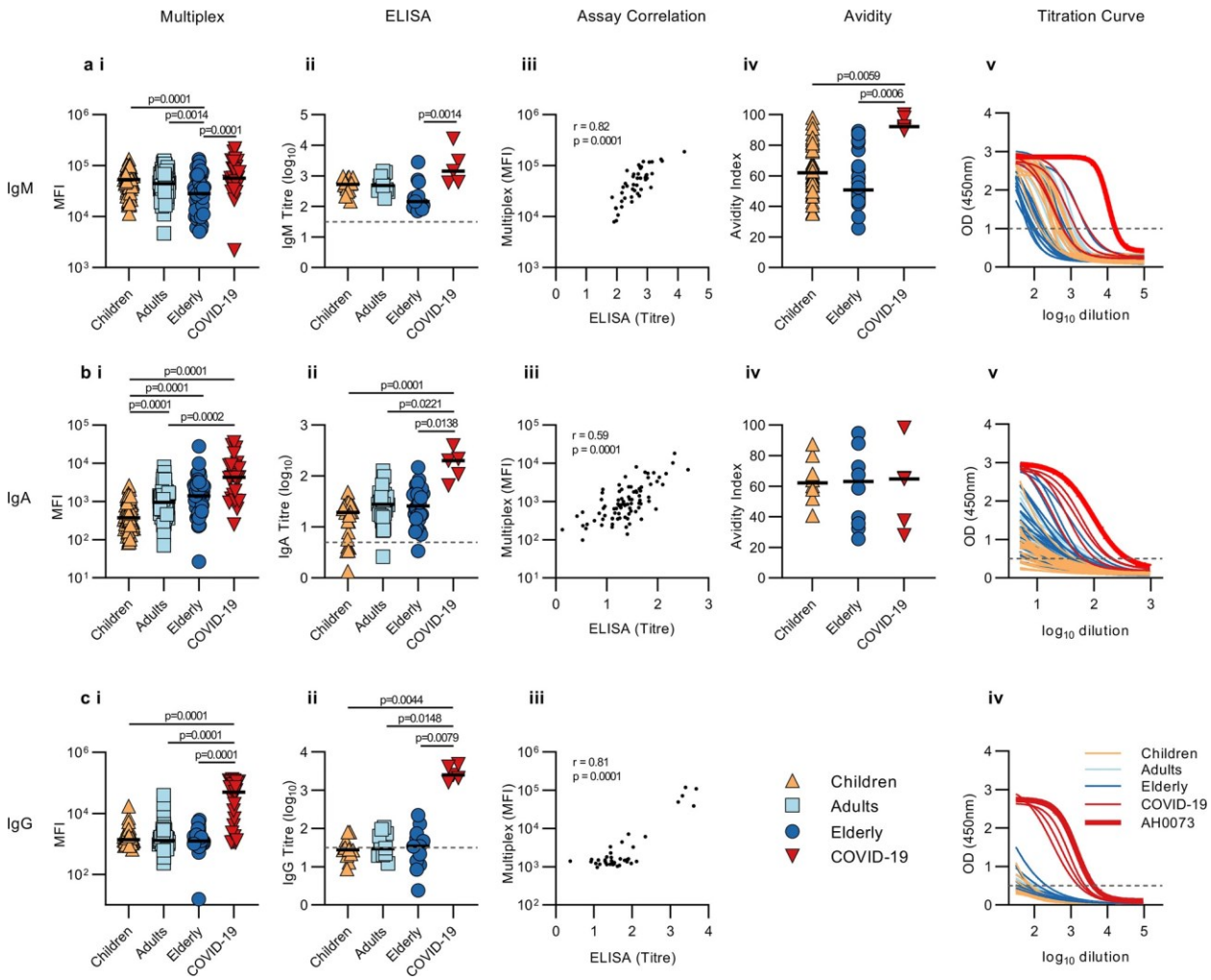


Figure 2-5: Receptor binding domain Abs in healthy versus COVID-19 patients.

Multiplex MFI data for IgM **(a-i)**, IgA **(b-i)** and IgG **(c-i)**; ELISA endpoint titres for IgM **(a-ii)**, IgA **(b-ii)** and IgG **(c-ii)**; and their respective correlations **(a–c iii)**. Avidity index following urea dissociation for IgM **(a-iv)** and IgA **(b-iv)**. Children (orange), adults (light blue), elderly (dark blue) and COVID-19 patients (red). Bar indicates the median response of each group. Statistical significance was determined using one-way ANOVA (Kruskal-Wallis with Dunn's multiple comparisons), exact p-values were provided. Serial dilutions of plasma from healthy children (n = 14) (orange), 12 adults (n = 12) (light blue), 14 elderly (n = 14) (dark blue) and 5 COVID-19 patients (red) tested in IgM **(a-v)**, IgA **(b-v)** and IgG **(c-iv)** ELISA. Bold red line represents COVID-19 patient AH0073 who was used as a positive control in all multiplex and ELISA plates. Dashed lines represent cut-offs (15% of positive control for IgA and IgG; 30% for IgM) used to interpolate endpoint titres by non-linear regression analysis. ELISA and multiplex assays were repeated in duplicates.

2.4.7 Distinct Ab features between children and elderly COVID-19 patients

In line with a recent study,[49] we observed that repetitive infections with seasonal hCoVs have shaped the humoral immune responses in elderly to a more mature and class-switched CoV-specific IgA and IgG response. This is in contrast to the less-experienced antibody signatures

observed in children, which potentially could impact the functionality of the humoral immune response following SARS-CoV-2 exposure. Hereto, we investigated differences in age-specific Ab features among COVID-19 patients. To this end, we included additional COVID-19 patients (**Figure 2-1d-ii-iii**; open symbols) to even out distribution across a range of age groups. No significant differences in virus neutralization were observed between the different age groups, indicating that additional immune functions, beyond neutralization may contribute to recovery.

To focus in on the particular serological differences between COVID-19 children and elderly, we performed a COVID-19-specific systems analysis on both cohorts. Using supervised feature selection followed by multivariate regression analysis, we were able to identify age-dependent Ab signatures in this distinct COVID-19 patient cohort (**Figure 2-6a, b**). We detected that SARS-CoV-2-specific IgA and IgG features were associated with increasing age, especially to both S2[51] and NP,[50] which could be a result of cross-reactivity driven by prior exposure to hCoV antigens.

In contrast, SARS-CoV-2-specific functional responses, especially both polymorphisms of FcγRIIa and FcγRIIb to Spike 1 and RBD were associated with COVID-19 cohort children. These data were verified using unsupervised hierarchical clustering in which similar trends were observed (**Figure 2-6c**). To confirm the accuracy of the selected features (**Supplementary Figure A-5a**), we compared the cross-validation (CV) accuracy of our selected model with randomly selected antibody features, observing significantly higher accuracy ($p = 0.006$) with our model (**Supplementary Figure A-5b**). Engagement of FcγRIIa is commonly associated with antibody-mediated phagocytosis. Significant univariate differences between Spike 1-specific antibody engagement for both FcγRIIa polymorphisms were observed (FcγRIIaR, $p = 0.0332$; **Figure 2-6d** and FcγRIIaF, $p = 0.0387$; **Figure 2-6e**), despite the small sample size. To further

validate that children have enhanced FcγRIIa-mediated antibody functions, we utilized THP-1 monocyte cell line, which express high levels of FcγRIIa and very low levels of FcγRIIIa,[63] to assess for antibody-mediated Fc-effector functions. Children tended to have elevated THP-1 cell-based Fc-mediated uptake of spike-coated beads ($p = 0.1277$, children: median 12.35; IQR 11.09–14.92; elderly: median 10.96; IQR 6.17–13.43; **Figure 2-6f**). Similarly, when using cells transfected with Spike trimer and mOrange as targets, we observed similar trends ($p = 0.0684$, children: median 22.34; IQR 14.55–28.71; elderly: median 14.17, IQR 7.16–21.47; **Figure 2-6g**). Importantly, both cell-based Fc-effector assays highly correlated with each other and to SARS2 S1 FcγRIIa (**Figure 2-6h**). Overall, these findings, albeit done on a small cohort, support our hypothesis that differences in Ab signatures between children and elderly, primed by their prior exposure(s) to circulating hCoV, may contribute to their differential clinical outcomes to COVID-19, where children benefit from their less-experienced immune status prior to SARS-CoV-2 infection, which provides them with the ability to exert a more functional antibody response against SARS-CoV-2.

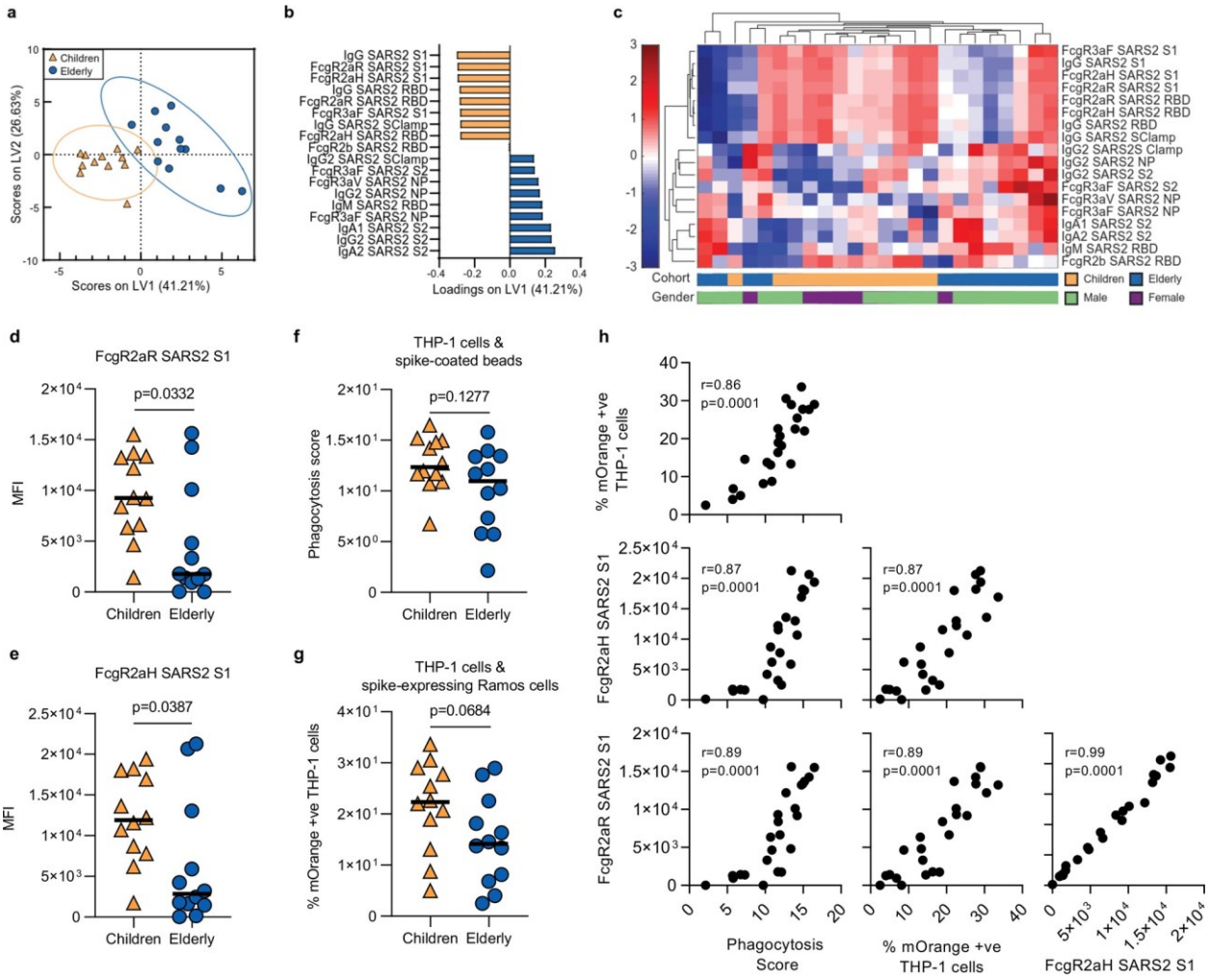


Figure 2-6: COVID-19 Ab responses in COVID-19-positive children and elderly.

PLSDA scores **(a)** and loadings **(b)** plots for the children (n = 12) (orange) and elderly (n = 12) (dark blue) with an Elastic-Net-selected 18-feature signature (100.00% calibration accuracy, 91.37% cross-validation accuracy). Hierarchical clustering was performed using the 18-feature signature for the children and elderly cohorts **(c)**. S1-specific antibody engagement of FcγRIIaR **(d)** and FcγRIIaR **(e)** were amongst the strongest features in the PLSDA loadings plot **(b)** and are significantly elevated in children. THP-1 monocyte cell line antibody-mediated uptake of spike-coated bead assay **(f)** and spike-expressing target cell assay **(g)**. Statistical significance was calculated using the two-tailed Mann-Whitney U test and exact p-values were reported. S1-specific antibody engagement of FcγRIIaR, FcγRIIaR and the two THP-1 SARS-CoV2 spike Fc effector assays highly correlate with each other, as measured by two-tailed Spearman correlation **(h)**. Multiplex assays were repeated in duplicates.

2.5 Discussion

Using systems serology, we observed distinct coronavirus serological signatures in healthy children compared to elderly. Children had elevated CoV-specific IgM signatures,

whereas elderly had more mature, class-switched CoV-specific IgA and IgG, indicating that multiple rounds of infections and/or exposures over several decades might be needed to develop fully experienced CoV humoral immune response. Intriguingly, similarly to the current SARS-CoV-2 pandemic, school-aged children have shown better clinical outcomes during past influenza pandemic outbreaks[35] and can induce more potent, broadly neutralizing Ab responses upon HIV infection.[64] It is plausible that upon infection with SARS-CoV-2, the elderly may preferentially induce skewed Ab responses targeting prior cross-reactive hCoV antigens and as observed in this study, COVID-19-positive elderly induced elevated IgG and IgA antibodies to the more cross-reactive antigens of SARS-CoV2 including S2 and NP, compared to children. Recent Ab repertoire study from a single adult COVID-19 subject observed a larger proportion of non-neutralizing Abs that displayed high levels of somatic hypermutation which cross-react with hCoV, which the authors suggest indicate pre-existing memory B cells by prior hCoV.[65] In addition, recent studies have observed boosting of hCoV antibody responses, especially OC43 upon SARS-CoV2 infection.[66–68] As such, upon exposure to SARS-CoV-2 in elderly individuals, the influence of pre-existing memory responses in combination with potentially slower activation of the memory B cell response in general,[37] may contribute to them inducing a less effective antibody response.

In contrast, children, who have less-experienced humoral immunity to hCoV, may mount a more targeted immune response towards antigens from SARS-CoV-2, such that FcyRIIa-mediated responses and IgG features targeted against SARS2-CoV-2 S1 and RBD dominated the antibody response in SARS-CoV2-infected children. In line with this observation, we also demonstrate that COVID-19 children responded better than the elderly using two different antibody-mediated functional assays. These results need to be repeated within larger cohort

studies; however, these findings give an indication that children may benefit from early Fc-mediated viral clearance and induce more targeted and Fc functional immunity against SARS-CoV-2 antigens in comparison to elderly.

Interestingly, no differences in the in vitro virus neutralization were observed between the different age groups of COVID-19 patients, which indicates that additional immune functions, possibly exerted by the FcR or complement could contribute to the divergent age-related clinical outcomes. Of note, a recent study comparing neutralizing monoclonal Abs observed that Fc capacity was essential for enhancing protection against SARS-CoV-2 in vivo mouse models, which were not detected via in vitro neutralization assays, as all the currently described neutralization assays lack Fc functions.[42] This highlights the necessity to examine both neutralizing and non-neutralizing responses of Abs in future studies.

Our assay used recombinant FcyR dimers to assess the CoV serological profiles of our healthy donors and COVID-19 patients for additional functions beyond viral neutralization. Recombinant FcyR dimers have previously been demonstrated to be an excellent surrogate system to mimic FcγR engagement at the immunological synapse and was shown to correlate with a range of in vitro cellular Fc effector assays including ADCC and ADCP.[48,69] Similarly, we observed that SARS-CoV2 FcyR dimer engagement strongly correlated with two different cellular Fc effector assays. FcγR dimers have also been used to assess Fc-effector functions against a range of infectious disease pathogens including HIV,[70,71] influenza[72,73] and malaria.[74] Similarly, C1q binding has been correlated with in vitro Ab-dependent complement deposition (ADCD) assays[75] and have been used to assess ADCD against HIV,[76] Ebola[77] and malaria.[78]

We observed distinct SARS-CoV-2 Fc Ab signatures associated with enhanced engagement of the high-affinity FcγRIIIa-V158 dimer and C1q, distinguishing COVID-19

patients from healthy controls. Ab Fc binding to FcγR can be modulated by multiple structural, genetic and post-translational modifications, including Fc glycosylation.[79,80] Fc-effector functions, while beneficial against many pathogens,[8,56,81,82] can also enhance infection and pathogenesis in other infectious diseases, including dengue, where disease severity is associated with afucosylated IgG1 that enhances FcγRIIIa affinity.[83] This is also observed with other respiratory diseases including tuberculosis, where greater overall inflammation, including inflammatory Fc glycosylation is associated with poorer disease outcomes.[82,84] IgG with reduced fucosylation has been detected in COVID-19 patients and further implicated with COVID-19 progression, with the critically ill showing aggravated afucosylated-IgG responses against spike, while mild cases displayed higher levels of fucosylation of spike-specific IgG.[85,86] It is important for future larger SARS-CoV-2 serological studies to assess not only quantitative changes in Ab titres, but also qualitative differences in FcR engagements between patients with mild and severe disease, whereas in our study the majority of patients had mild-to-moderate COVID-19.

Pandemic outbreaks provide unique opportunities to study how different aspects of the immune system contribute to the formation of a novel immune response, for example the protective or risk-associated effects of HLA alleles.[87] Due to the low frequency of shared HLA class II alleles in our cohort, this analysis could not be further explored to the impact of the full range of HLA class II alleles, neither to determine the contribution of age nor of sex. However, the distinction in Ab signatures observed in our study emphasizes the need to better understand the contributions of HLA class II alleles to the maturation of humoral immunity and would require a sufficiently large cohort of HLA-typed healthy controls and COVID-19 patients. The current pandemic outbreak provides a unique opportunity to perform such studies, when large

patient cohorts which include information on antibody responses, HLA class II phenotypes and disease outcome are combined.

Overall, our in-depth serological profiling of healthy children, elderly and COVID-19 patients brings us closer to understanding why the elderly are more susceptible to COVID-19 and provides insights into Ab Fc signatures associated with convalescence of mild/moderate symptomatic individuals. This knowledge is important for the development of improved serological diagnostics,[84] evaluation of convalescent plasma therapeutic trials, and will inform immunogenicity assessment of Ab-based SARS-CoV-2 vaccine strategies, which could potentially extend beyond neutralizing Abs.

2.6 Methods

2.6.1 Study participants and sample collection

Our study assessed antibodies to SARS-CoV-2 in a total of 244 healthy individuals and 43 SARS-CoV-2-infected patients. Children undergoing elective tonsillectomy (age 1.5–19) were recruited at the Launceston General Hospital (Tasmania) and, apart from fulfilling the criteria for tonsillectomy, they were considered otherwise healthy, showing no signs of immune compromise. Healthy adult donors (age 22–63) were recruited via the University of Melbourne. Healthy elderly donors (age 65–92) were recruited at the Deepdene Medical Clinic (Victoria). All healthy donors were recruited prior to SARS-CoV-2 pandemic. SARS-CoV-2-infected patients (age 1–76) were recruited at the Alfred Hospital (AH), at the Murdoch Children's Research Institute (FFX), by James Cook University (D) and University of Melbourne (CP). Eligibility criteria for COVID-19 acute and convalescent recruitment were having at least one swab PCR-positive for SARS-CoV-2. Each patient was categorized into one of the following 6 severity categories: very mild (stay at home, minimal symptoms), mild (stay at home with

symptoms), moderate (hospitalized, not requiring oxygen), severe/moderate (hospitalized with low-flow oxygen), severe (hospitalized with high-flow oxygen) or critical (intensive care unit, ICU). Heparinized blood was centrifuged for 10 min at 300g to collect plasma, which was frozen at −20°C until required. HLA class I and class II molecular genotyping was performed from genomic DNA by the Australian Red Cross Lifeblood (Melbourne).

Human experimental work was conducted according to the Declaration of Helsinki principles and according to the Australian National Health and Medical Research Council Code of Practice. All donors or their legal guardians provided written informed consent. The study was approved by the Human Research Ethics Committee (HREC) of the University of Melbourne (Ethics ID #1443389.4, #2056761, #1647326, #2056689, #1955465) for healthy adult and elderly donors, Tasmanian Health and Medical HREC (H0017479) for healthy child donors, Alfred Hospital (#280/14) for AH donors, RCH HREC (#63666) for FFX donors, James Cook University (#H7886) for D donors and University of Melbourne (#2056689) for CP donors.

2.6.2 Deglycosylation of Escherichia coli-expressed NP

To minimize possible bacterial glycosylation background from the *E. coli* expression system, recombinant hCoV 229E and NL63 NP (Prospec-Tany) were first treated with O-glycosidase and PNGase F. Briefly, 40 µg of NP were treated with a cocktail of 8 µl 10X GlycoBuffer 2, 8 µl 10% NP40, 12 µl O-Glycosidase, 12 µl of Remove-iT PNGase F (New England BioLabs) and water for a final volume of 80 µl and incubated at 37 °C for 2 h on a shaker. The respective mixtures were added to Eppendorf tubes containing 100 µl of PSB-washed Chitin magnetic beads (New England BioLabs) to allow the binding and removal of Remove-iT PNGase F. Tubes were agitated for 10 min then placed onto a magnetic separation rack for 5 min. The supernatant was retrieved and passed through a 100 kDa Amicon Ultra

centrifugal filter (Merck) to remove remaining O-glycosidase. Finally, NPs were washed with PBS using a 3 kDa Amicon Ultra centrifugal filter (Merck) to prepare them for coupling.

2.6.3 Coupling of carboxylated beads

A custom CoV multiplex assay was designed with SARS-CoV-2, SARS-CoV-1, MERS-CoV and hCoV (229E, HKU1, NL63) S and NP antigens, as well as SARS-CoV-2 RBD (gift from Florian Krammer),[62] SARS-CoV-2 Trimeric S (gift from Adam Wheatley) and SClamps of both SARS-CoV-2 and MERS-CoV (gift from University of Queensland) (**Figure 2-1a**). Amino acid sequences for CoV spike and NP are as described in **Figure 2-1a**. Tetanus toxoid (Sigma) and influenza hemagglutinin (H1Cal2009; Sino Biological) were also added to the assay as positive controls, while BSA-blocked beads were included as negative controls. Magnetic carboxylated beads (Bio Rad) were covalently coupled to the antigens using a two-step carbodiimide reaction, in a ratio of 10 million beads-to-100 µg of antigen, with the exception of the deglycosylated NPs mentioned above in which 40 µg were used instead, and SARS-CoV-2 RBD which were used at 49.7 µg instead. Briefly, beads were washed and activated in 100 mM monobasic sodium phosphate, pH 6.2, followed by the addition of Sulfo-*N*-hydroxysulfosuccinimide and 1-Ethyl-3-(3-dimethylaminopropyl) carbodiimide (Thermo Fisher Scientific). After incubation at room temperature (RT) for 30 min, the activated microspheres were washed three times and resuspended in 50 mM MES pH 5.0 (Thermo Fisher Scientific). The respective antigens were added to the activated beads and the mixture was incubated at RT for 3 h on a rotator in the dark. Subsequently, the beads were washed with PBS and blocked with blocking buffer (PBS, 0.1% BSA, 0.02% TWEEN-20, 0.05% Azide, pH 7) for 30 min. Finally, beads were washed in PBS 0.05% Sodium Azide and resuspended as one million beads per 100 µl.

2.6.4 Luminex bead-based multiplex assay

The isotypes and subclasses of pathogen-specific antibodies present in the collected plasma were assessed using a multiplex assay as described[88] (**Figure 2-1b**). Using a black, clear-bottom 384-well plate (Greiner Bio-One), 20 µl of working bead mixture containing 1000 beads per bead region and 20 µl of diluted plasma were added per well. From validation experiments in which cross-reactive Abs present in healthy individuals were titrated, an optimal concentration of 1:100 working dilution of plasma was selected for downstream assays (**Supplementary Figure A-3a, b**). The plate was covered and incubated overnight at 4 °C on a shaker and was then washed with PBS containing 0.05% Tween20 (PBST). Pathogen-specific antibodies were detected using phycoerythrin (PE)-conjugated mouse anti-human pan-IgG, IgG1-4, IgA1-2 (Southern Biotech), at 1.3 µg/ml, 25 µl per well. After incubation at RT for 2 h on a shaker, the plate was washed before the beads were resuspended in 50 µl of sheath fluid. The plate was then incubated at RT for 10 min on a shaker before being read by the FlexMap 3D. The binding of the PE-detectors was measured to calculate the median fluorescence intensity (MFI). Double background subtraction was conducted, removing first background of blank (buffer only) wells followed by removal of BSA-blocked control bead background signal for each well.

For the detection of IgM, biotinylated mouse anti-human IgM (mAb MT22; MabTech) was added at 1.3 µg/ml, 25 µl per well. After incubation at RT for 2 h on a shaker, the plate was washed, and streptavidin, R-Phycoerythrin conjugate (SAPE, Invitrogen) was added at 1 µg/ml, 25 µl per well. The plate was then incubated at RT for 2 h on a shaker before being washed and read as mentioned above. For the detection of FcγR, soluble recombinant FcγR dimers (higher affinity polymorphisms FcγRIIa-H131, lower affinity polymorphisms FcγRIIa-R131, FcγRIIb, higher affinity polymorphisms FcγRIIIa-V158, lower affinity polymorphisms FcγRIIIa-F158) were provided by Bruce Wines and Mark Hogarth. For the detection of C1q, C1q protein (MP

Biomedicals) was first biotinylated (Thermo Fisher Scientific), washed and resuspended in PBS and tertramerized with SAPE. Dimers or tetrameric C1q-PE were added at 1 µg/ml, 25 µl per well, incubated at RT for 2 h on a shaker and then washed. For Dimers, SAPE was added at 1 µg/ml, 25 µl per well, incubated at RT for 2 h on a shaker before being washed and read as mentioned above. Assays were repeated in duplicate. A titration of AH0073 was included in the layout of all multiplex array plates as this patient was known to have IgG, IgM and IgA responses (**Supplementary Figure A-4**). These titrations were used to normalize replicate multiplex array plates.

2.6.5 Enzyme-linked immunosorbent assay (ELISA)

Detection of RBD-specific antibodies was performed as described in Stadlbauer et al.[62,89] with the following modifications; Nunc MaxiSorp flat-bottom 96-well plates (Thermo Fisher Scientific) were used for antigen coating, blocking performed with PBS containing 10% BSA and half-logarithmic serial dilutions (beginning at 1:10 for IgA and 1:31.6 for IgG/IgM) performed with PBST containing 5% BSA. For detection of IgG and IgA, peroxidase-conjugated goat anti-human IgG (Fcγ fragment specific; #109-035-098; Jackson ImmunoResearch) or alkaline phosphate-conjugated rat anti-human IgA (mAb MT20; #3860-9A-1000; MabTech), was used and developed with TMB (Sigma) substrate for IgG or pNPP (Sigma) for IgA. For IgM, biotinylated mAb MT22 (#3880-6-250; MabTech) and peroxidase-conjugated streptavidin (Pierce; Thermo Fisher Scientific) were used. Peroxidase reactions were stopped using 1 M H3PO4 and plates read at 450 or 405 nm on a Multiskan plate reader (Labsystems). All measurements were normalized using a positive control plasma from a COVID-19 patient (AH0073) run on each plate (**Figure 2-5**). Endpoint titres were determined by interpolation from a sigmoidal curve fit (all R^2 values >0.95; GraphPad Prism 8) as the reciprocal dilution of plasma

that produced ≥15% absorbance of the positive control. A total of 28 donors from each cohort was randomly selected for IgA analysis, 14 for IgG and 10–14 for IgM. All assays also included the five same COVID-19 patient samples.

2.6.6 Antibody avidity assay

Avidity of antibodies in plasma samples was measured using urea as the chaotropic agent and only performed on samples with detectable RBD-specific antibodies (IgA and IgM). Following incubation of plasma at a 1:10 dilution (IgA) or 1:100 dilution (IgM) on RBD-coated plates, 6 M of urea was added and incubated for 15 min. Bound antibodies were then detected using respective secondary detection reagents described above. The avidity index is expressed as the percentage of remaining antibody bound to antigen following urea treatment compared to the absence of urea.

2.6.7 Neutralization antibody assay

SARS-CoV-2 isolate CoV/Australia/VIC01/2020[90] was passaged in Vero cells and stored at −80 °C. Serial two-fold dilutions of heat-inactivated plasma or serum were incubated with 100 TCID50 of SARS-CoV-2 for 1 h and residual virus infectivity was assessed in Vero cells; viral cytopathic effect was read on day 5. The neutralizing antibody titre is calculated using the Reed/Muench method as previously described.[91,92]

2.6.8 Cell-based antibody Fc effector assays

To examine the COVID-positive plasma of children and elderly for antibody-mediated activation of FcgRIIa expressing THP-1 monocyte cell lines, a previously described bead-based ADCP assay[93,94] was adapted for use in the context of SARS-CoV2.[95] SARS-CoV-2 S trimer was biotinylated using EZ-Link Sulfo-NHS-LC biotinylation kit (Thermo Scientific) with

20 mmol excess according to manufacturer's instructions and buffer exchanged using 30 kDa Amicon centrifugal filters (EMD millipore) to remove free biotin. Biotinylated S was then used to coat the binding sites of 1 μm fluorescent NeutrAvidin Fluospheres beads (Invitrogen) overnight at 4 °C. S-conjugated beads were washed four times with 2% BSA/PBS to remove excess antigen and incubated with plasma (1:100 dilution) for 2 h at 37 °C in a 96-well U-bottom plate. THP-1 monocytes (10,000/well) were then added to opsonized beads and incubated for 16 h under cell culture conditions. Cells were fixed with 2% formaldehyde and acquired by flow cytometry on a BD LSR Fortessa with a high-throughput sampler attachment (HTS). The data were analysed using FlowJo 10.7.1 and a phagocytosis score was calculated as previously described[96] using the formula: (%bead-positive cells × mean fluorescent intensity)/103. To account for non-specific uptake of S-conjugated beads, the phagocytosis scores for each plasma sample were subtracted with that of the 'no plasma' control.

The bead-based assay was also adapted to use Ramos cells expressing Spike as target cells.[95] THP-1 monocytes were first stained with CellTraceTM Violet (CTV; #C34557; Life Technologies) as per manufacturer's instructions. In a 96-well V-bottom cell culture plate, Ramos S-orange cells (10,000/well) were incubated with plasma from convalescent or uninfected donors (1:5000 dilution) for 30 min. Opsonized Ramos S-orange cells were then washed prior to co-culture with CTV-stained THP-1 monocytes (10,000/well) for 1 h at 37 °C with 5% CO2. After the incubation, cells were washed with PBS, fixed with 2% formaldehyde and acquired using the BD LSR Fortessa with a HTS. The data were analysed using FlowJo 10.7.1. The percentage of Spike-orange-positive THP-1 monocytes was measured for each plasma sample and background-subtracted with the 'no plasma' control.

2.6.9 Statistical analysis

Children versus the elderly Volcano plot was conducted using Prism 8. Statistical significance determined using the Holm-Sidak method, with $\alpha = 0.05$ adjusted for 196 tests (Ab features). Each feature was analysed individually, without assuming a consistent SD. The overall multiplex dataset was analysed for normal distribution using the Shapiro-Wilk test by Prism 8. The data were further analysed by SPSS statistics 26 (IBM Corp.) using the Kruskal-Wallis one-way analysis with a Bonferroni correction to determine the p-values, differences between groups were considered significant at an adjusted p-value of 0.000035. ELISA data were analysed using one-way ANOVA (Kruskal-Wallis one-way analysis with Dunn's multiple comparison) using Prism 8. Comparisons between COVID-positive children and elderly were analysed by two-tailed Mann-Whitney U test. CV accuracies of randomly selected models were compared to the selected model (**Supplementary Figure A-5a, b**) based on previously published methods, which use a one-sided Fisher's permutation test to calculate a CV p-value in Matlab.[97] The CV p-value represents the proportion of randomized signatures that outperformed the original feature selected model in cross-validation accuracy.

2.6.10 Data normalization

For all multivariate analysis, Tetanus, H1Cal2009 antigens (positive controls) were removed, with the exception of HLA analysis. Any healthy samples with a missing age, or missing Ab features were removed ($n = 9$). When analysing COVID-19 samples with healthy samples, only the features where data were available for all COVID-19 samples were included. COVID-19 samples in the initial cohort lacked entire datasets for IgG4, IgA2, FcγRIIaR131, FcγRIIIaF158 and FcγRIIb, thus these detectors were excluded. The second COVID-19 cohort was normalized separately, contained all detectors and no missing data. When COVID-19 samples were analysed based on the time from disease onset, all visit days were used for each patient. In all other

analyses when a patient has two visit days, only the second visit was used. Right shifting was performed on each feature (detector–antigen pair) individually if it contained any negative values, by adding the minimum value for that feature back to all samples within that feature. Following this, all data were log-transformed using the following equation, where x is the right-shifted data and y is the right-shifted log-transformed data: $y = \log10(x + 1)$. This process transformed the majority of the features to having a normal distribution. In all the subsequent multivariate analyses, the data were furthered normalized by mean centering and variance scaling each feature using the z-score function in Matlab. For the HLA analysis, the same data-normalization methods were used, except that positive controls and all samples with any HLA typing were included. Samples with one copy of each most-frequent allele were removed to avoid double classification.

2.6.11 Feature selection using Elastic Net/PLSR and Elastic Net/PLSDA

To determine the minimal set of features (signatures) needed to predict numerical outcomes (age, days from symptom onset) and categorical outcomes (age cohort, COVID-19 infection status, HLA allele) a three-step process was developed based on Gunn et al.[98] First, the data were randomly sampled without replacement to generate 2000 subsets. The resampled subsets spanned 80% of the original sample size, or sampled all classes at the size of the smallest class for categorical outcomes, which corrected for any potential effects of class size imbalances during regularization. Elastic-Net regularization was then applied to each of the 2000 resampled subsets to reduce and select features most associated with the outcome variables. The Elastic-Net hyperparameter, α, was set to have equal weights between the L1 norm and L2 norm associated with the penalty function for least absolute shrinkage and selection (LASSO) and ridge regression, respectively.[99] By using both penalties, Elastic-Net provides sparsity and promotes

group selection. The frequency at which each feature was selected across the 2000 iterations was used to determine the signatures by using a sequential step-forward algorithm that iteratively added a single feature into the PLSR (numerical outcome) or PLSDA (categorical outcome) model starting with the feature that had the highest frequency of selection, to the lowest frequency of selection. Model prediction performance was assessed at each step and evaluated by 10-fold cross-validation classification error for categorical outcomes and 10-fold goodness of prediction (Q2) for numerical outcomes. The model with the lowest classification error and highest Q2 within a 0.01 difference between the minimum classification error and the maximum Q2 was selected as the minimum signature. If multiple models fell within this range, the one with the least number of features was selected and if there was a large disparity between calibration and cross-validation error (overfitting), the model with the least disparity and best performance was selected.

2.6.12 PCA

Principal component analysis (PCA), performed in Eigenvectors PLS toolbox in Matlab, is an unsupervised technique that was used to visualize the variance in the samples based on all of the measured features. Every feature is assigned a loading, the linear combinations of these loadings create a principal component (PC). Loadings and PCs are calculated to describe the maximum amount of variance in the data. Each sample is then scored and plotted using their individual response measurements expressed through the PCs. The percent of variance described by each PC is a measure of the amount of variance in antibody response explained by that respective PC. Separation of groups on the scores plot indicates unsupervised separation of groups based on all features.

2.6.13 PLSDA

Partial least squares discriminant analysis (PLSDA), performed in Eigenvectors PLS toolbox in Matlab, was used in conjunction with Elastic-Net, described above, to identify and visualize signatures that distinguish categorical outcomes (age cohort, COVID-19 infection status). This supervised method assigns a loading to each feature within a given signature and identifies the linear combination of loadings (a latent variable, LV) that best separates the categorical groups. A feature with a high loading magnitude indicates greater importance for separating the groups from one another. Each sample is then scored and plotted using their individual response measurements expressed through the LVs. The scores and loadings can then be cross-referenced to determine which features are loaded in association with which categorical groups (positively loaded features are higher in positively scoring groups, etc.). All models go through 10-fold cross-validation, where iteratively 10% of the data is left out as the test set, and the rest is used to train the model. Model performance is measured through calibration error (average error in the training set) as well as cross-validation error (average error in the test set), with values near 0 being best. All models were orthogonalized to enable clear visualization of results. Statistically significant separation of groups on the PLSDA score plots was determined using a two-tailed t-test on LV1 scores in Prism 8. Confidence ellipsoids (90% confidence level) were plotted for classification groups by calculating the mean and covariance matrix from the scores data of the first and second LVs (or PCs), which follows a chi-square distribution.[100]

2.6.14 PLSR

Partial least squares regression (PLSR), performed in Eigenvectors PLS toolbox in Matlab, was used in conjunction with Elastic-Net, described above, to identify and visualize signatures that distinguish numerical outcomes (age, days from symptom onset). This supervised method assigns a loading to each feature within a given signature and identifies the linear combination of

loadings (a LV) that best describes the variance in the numerical outcome. As in PLSDA, a feature with a high loading indicates greater importance for describing the variance in outcome. Each sample is then scored and plotted using their individual response measurements expressed through the LVs. The scores and loadings can then be cross-referenced to determine which features are loaded in association with which numerical outcomes (positively loaded features are higher in positively scoring samples, etc.). All models go through 10-fold cross-validation, where iteratively 10% of the data is left out as the test set, and the rest is used to train the model. Model performance is measured through R2 (average goodness of fit in the training set) as well as Q2 (average goodness of prediction in the test set), with values near 1 being best. All models were orthogonalized to enable clear visualization of results.

2.6.15 Hierarchical clustering

We visualized separation of numerical (age, days from symptom onset) and categorical (age cohort, COVID-19 infection status) outcomes based on their respective signatures using unsupervised average linkage hierarchical clustering of normalized data. Euclidean distance was used as the distance metric.

2.6.16 Software

PCA, PLSDA and PLSR models were completed using the Eigenvector PLS toolbox in Matlab. Hierarchical Clustering and Correlation Networks were completed using MATLAB 2017b (MathWorks, Natick, MA). PCA, PLSDA and PLSR scores and loadings plots were plotted in Prism version. Statistical analysis was performed in SPSS.

Chapter 3 Systems Serology Identifies Novel Autoantibody Signatures for Sjögren's Syndrome Diagnosis

3.1 Authors and Contributions

Martin Killian,[1,2,3,4*]†, Suzanne K. Shoffner-Beck[5*], Timon Damelang[3], Kevin John Selva[3], Kade E. Wong[5], Samantha K Davis[3], Ebene R Haycroft[3], Bruce D Wines[6,7], P Mark Hogarth[6,7,8], Stephen J Kent[3,9], Lucile Grange[1,2], Baptiste Gramont[1,2], Flora Schein[2], Héloïse Munoz-Pons[2], Isabelle Guichard[2], Jean-Baptiste Gaultier[2], Anne-Emmanuelle Berger[10], Alice Haccourt[10], Blandine Noailly[1], Fabienne Jospin[1], Alexis Bocquet[11], Laurence Bouillet[11,12], Marc Ruivard[13], Yvan Jamilloux[14], Pascal Sève[14], Isabelle Durieu[15], Quitterie Reynaud[15], Jean-Christophe Lega[16], Amélie Servettaz[17], Hubert Marotte[18], Pascal Cathébras[2], Stéphane Paul[1,4,10], Kelly B Arnold[5*], Amy W Chung[3*]†

*These authors equally contributed

[1]Team GIMAP, CIRI, Université de Lyon, UJM, UCBL1, INSERM U1111, CNRS UMR530, F42023 Saint-Etienne, France

[2]Department of Internal Medicine, Saint-Etienne University Hospital, Saint-Etienne, France

[3]Department of Microbiology and Immunology, The Peter Doherty Institute for Infection and Immunity, The University of Melbourne, Melbourne, Victoria, Australia

[4]Clinical Investigation Center, Inserm CIC1408, Saint-Étienne, France.

[5]Department of Biomedical Engineering, University of Michigan, Ann Arbor, MI, USA

[6]Immune Therapies Group, Burnet Institute, Melbourne, VIC, Australia.

[7]Department of Immunology and Pathology, Monash University, Melbourne, VIC, Australia.

[8]Department of Clinical Pathology, University of Melbourne, VIC, Australia.

[9]Melbourne Sexual Health Centre and Department of Infectious Diseases, Alfred Hospital and Central Clinical School, Monash University, Melbourne, VIC, Australia.

[10]Laboratory of Immunology, Saint-Etienne University Hospital, Saint-Etienne, France

[11]Department of Internal Medicine, Grenoble University Hospital, Grenoble, France.

[12]Univ. Grenoble Alpes, T-RAIG unit, CNRS, UMR 5525, VetAgro Sup, Grenoble INP, CHU Grenoble Alpes, TIMC, 38000 Grenoble, France

[13]Department of Internal Medicine, Hôpital Estaing, Clermont-Ferrand University Hospital, Clermont-Ferrand, France

[14]Department of Internal Medicine, Hôpital de la Croix-Rousse, Hospices Civils de Lyon, Lyon, France

[15]Department of Internal and Vascular Medicine, Hôpital Lyon Sud, Hospices Civils de Lyon, Pierre Bénite, France. RESearch on HealthcAre PErformance (RESHAPE), INSERM U1290, Université Claude Bernard Lyon 1, 8 avenue Rockefeller, 69373 Lyon Cedex 08, France

[16]Department of Internal and Vascular Medicine, Hôpital Lyon Sud, Hospices Civils de Lyon, Pierre Bénite, France. University of Lyon, UMR - CNRS 5558, Laboratoire de Biométrie et Biologie Évolutive, F-69100 Lyon, France; Lyon Immunopathology Federation, Lyon, France.

[17]Department of Internal Medicine, Clinical Immunology and Infectious Diseases, Reims University Hospital, Reims, France

[18]Department of Rheumatology, Saint-Etienne University Hospital, Saint-Etienne, France

3.2 Abstract

Sjögren's Syndrome (SjS) has long been associated with elevated autoantibodies to the classical autoantigens: Ro60, Ro52, and La, however defining serostatus continues to be a challenge. Clinically these autoantibody levels are tested via ELISA, but due to threshold requirements, testing may not be very sensitive. Non-SjS sicca patients with dry mouth and dry eye symptoms who do not qualify for disease, present an additional diagnostic challenge. Here we aimed to identify improved autoantibody signatures that distinguish between healthy individuals and patients with non-SjS sicca or SjS. Systems serology approaches were applied to 58 SjS (including 40 ELISA seropositive and 18 ELISA seronegative patients to classical autoantigens), 16 non-SjS sicca syndrome and 40 healthy individuals. Multiplex assays were used to measure antibody isotype, subclass, Fc Receptor (FcR) engagement and complement activation to 14 autoantigens. Machine learning models identified unique autoantibody signatures that distinguish between healthy, non-SjS sicca or SjS individuals. A seven-feature autoantibody signature, that included IgG and FcR binding to Ro, accurately distinguished healthy and SjS. Cell-based assays confirmed an association between increased Ro-specific IgG and FcR binding with Ro-specific antibody-mediated phagocytosis. Non-SjS sicca patients could be distinguished from healthy individuals based upon an antibody signature targeting non-classical autoantigens. Seronegative SjS patients had elevated levels of autoantigens that could be identified by highly sensitive multiplex assays but were not detected via ELISA. Our study provides important insights into the autoantibody responses in SjS and reveals potential diagnostic and therapeutic approaches to differentiate patients who are classically seronegative or non-SjS sicca.

3.3 Introduction

Sjögren's Syndrome (SjS) is an autoimmune disorder in which the exocrine glands are infiltrated by immune cells. Its key feature is sicca syndrome, which manifests as dry eyes (keratoconjunctivitis sicca) and dry mouth (xerostomia). Some patients experience articular symptoms or other more serious systemic involvement of other major organs, including the renal, pulmonary, and nervous systems.[19,101,102] The disease can be primary (Sjögren's disease) or co-exist with another autoimmune disease, such as systemic lupus erythematosus (SLE), rheumatoid arthritis, or scleroderma. The disease pathogenesis is thought to be a multistep process, beginning with an environmental trigger, such as viral infection, in a genetically predisposed person, leading to the production of autoantibodies by autoreactive B cell clones.[20] B cells play a pivotal role in the pathogenesis of SjS, however the precise pathogenic role of the autoantibodies has to be confirmed, as the chronic inflammation of the lacrimal and salivary glands and the other potentially affected target organs is a complex multifactorial process, also involving multiple other cell types and immune pathways.[21,103] Anti-Ro/SSA and anti-La/SSB immunoglobulins G (IgG) have been historically identified as important autoantibodies in SjS, with anti-Ro/SSA antibodies present in 60-80% of patients and anti-La/SSB present in 40-60%.[104,105] Anti-Ro/SSA antibodies can be specific to Ro60/TROVE2,[106] an RNA binding protein involved in removing misfolded RNA transcripts, and Ro52/TRIM21, an intracellular fragment crystallizable (Fc) Receptor also bearing an E3 ubiquitin ligase activity.[107–110] Anti-Ro60 and Anti-Ro52 can appear before symptom onset and have a high positive predictive value for development of disease.[111] Anti-Ro/SSA IgG is also widely used to aid with diagnosis via serologic tests and has been included in all sets of classification criteria to date.[105,112,113] While

many studies have associated individual autoantibodies with SjS, causing them to be used as part of diagnosis, the role of antibodies in the pathogenesis of disease is still largely unknown.

Antibodies are composed of two Fab (Fragment antigen binding) regions, which can bind to antigenic epitopes, and an Fc region, which can bind to immunoglobulin Fc receptors (FcRs) on the surface of innate immune cells or complement to induce functions including phagocytosis, cytotoxicity, release of cytokines leading to inflammatory cascades and/or complement activation. There are multiple antibody isotypes (i.e., IgG, IgA, IgM, IgD, IgE) and subclasses (IgG1-4, IgA1-2), with specific activating and inhibitory FcRs that balance pro-inflammatory and anti-inflammatory effector responses to provide protection against pathogens, though when dysregulated can lead to disease.[114] Fcγ Receptors (FcγR) are IgG receptors that can be induced to activate a range of Fc functions. For example, FcγRIIa is expressed on phagocytes including monocytes and is particularly important for the induction of antibody dependent cellular phagocytosis (ADCP).[115] FcγRIIb is an inhibitory receptor that provides important immune regulation.[4] Aberrant expression or allelic variants of FcγRs have been associated with impaired phagocytosis of autoantibody-autoantigen immune complexes in several autoimmune diseases.[116] In healthy people, expression of the inhibitory FcγRIIb is typically up-regulated to negatively regulate humoral responses, while it appears to be down-regulated in active SLE and SjS,[117,118] Furthermore, single nucleotide polymorphisms (SNPs) and copy-number variations (CNVs) have been identified in the FcγR-coding genes in some autoimmune disorders.[26] For example, individuals with the *FCGRIIA-H131* allele express a FcγRIIa which binds IgG2 more efficiently than patients with the *FCGRIIA-R131* allele, and the former has been found to be a risk factor for several diseases, including SLE.[119] Similarly, the *FCGRIIIA-158F* allele is a risk factor for SLE in comparison to *FCGRIIIA-158V* and is thought to lead to impaired clearance of immune

complexes.[120] Although FcγR-coding variants have been identified in association with SLE and several other autoimmune diseases, the role of Fc receptor activation in SjS is not yet fully understood.[26] One study found Fc receptor mediated clearance to be abnormal in SjS' patients,[121] though others have not found SjS-linked FcγR-coding gene variants.[122] Further evaluation of SjS-associated autoantibodies and related Fc effector activity may lead to the identification of novel specific therapeutic strategies or support the repurposing of currently developed autoantibody-targeting drugs.

Here, we applied systems serology, a fusion of high throughput experimental antibody assays with computational approaches that was originally applied to identify antibody features associated with protection or control of infectious diseases.[5,123–125] This approach, however, can also be applied to any scenario, where antibodies contribute to disease, including certain autoimmune diseases.[125,126] Thus, here we applied high-throughput multiplex assays to measure antibody binding to 14 autoantibodies, antibody-specific FcR engagement, and complement activation in a cohort of SjS, non-SjS sicca syndrome and healthy individuals (**Figure 3-1**) and applied a range of machine learning models that identified unique autoantigen-specific antibody and FcγR signatures associated with SjS.

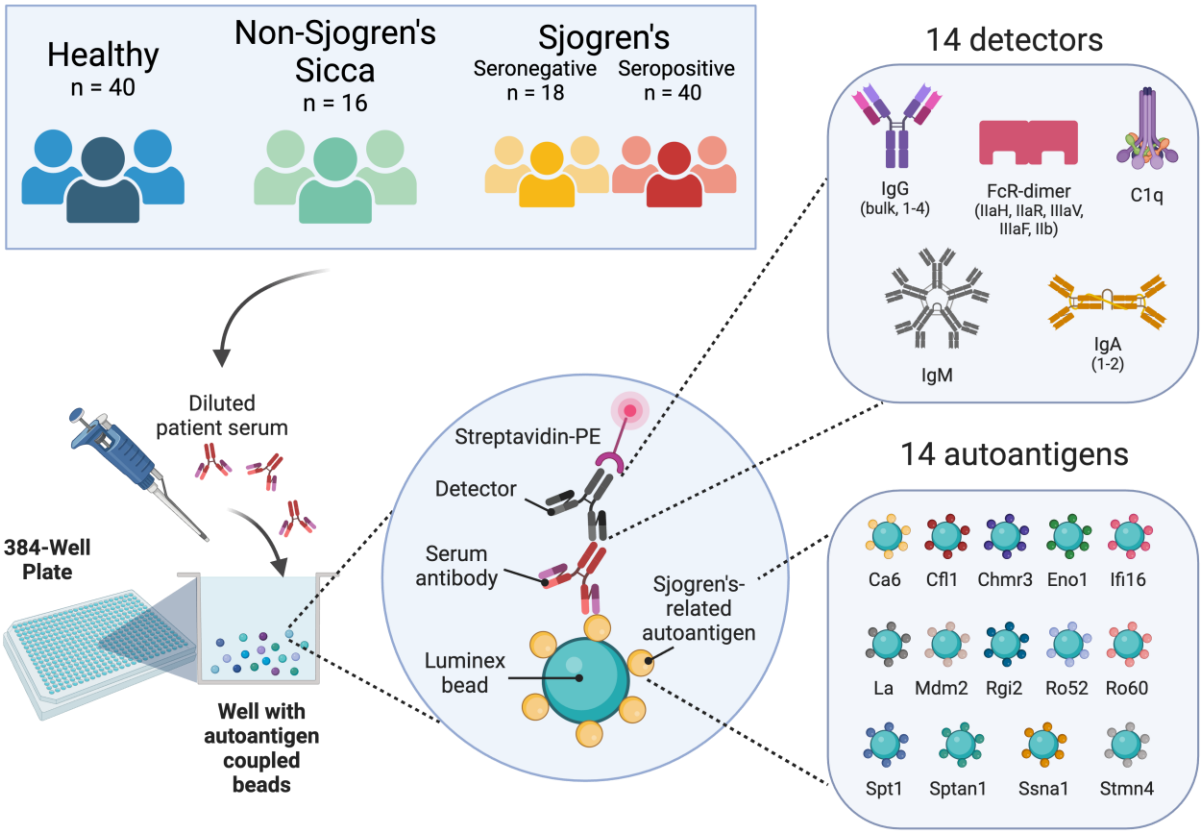


Figure 3-1: Schematic of bead-based multiplex assay.

Patient serum is added to well containing beads coupled to 14 different autoantigens. Plasma antibodies bind the beads and 14 different detectors with markers are added to measure specific autoantibody responses in the serum.

3.4 Results

3.4.1 IgG and FcγR autoantibody signatures distinguish between healthy individuals and those with Sjögren's syndrome

In order to better understand the autoantibody response in SjS versus healthy controls, we designed a multiplex assay with 14 autoantigens and assessed using antibody detectors, as described in **Supplementary Table B-1** and shown in the experimental schematic overview (**Figure 3-1**). The assay allowed us to assess antibody isotypes (IgG, IgM, IgA) and their subclasses (IgG1, IgG2, IgG3, IgG4), C1q binding (classical complement pathway), and FcγR soluble dimer engagement responses to 14 autoantigens relevant to SjS (Ca6, Cfl1, Chmr3, Eno1,

Ifi16, La, Mdm2, Rgi2, Ro52, Ro60, Spt1, Sptan1, Ssna1, Stmn4) (**Supplementary Table B-1**). Overall, 196 autoantibodies-related features (14 antigens x 14 detectors) were measured for 40 healthy controls, 16 patients with non-SjS sicca syndrome, and 58 patients with SjS (**Table 3-1**).

By comparing antibody responses between healthy controls and patients with SjS, univariate analysis confirmed previously observed increases in anti-Ro60 (**Figure 3-2a-b**), anti-Ro52, and anti-La IgG (**Supplementary Figure B-1**) autoantibodies and revealed novel corresponding elevated FcγR responses in SjS relative to healthy controls (**Figure 3-2a-b**). Of particular interest, high activation of FcγRIIa was also observed, suggesting potential high ADCP of these antigens. In contrast, healthy controls had higher levels of complement activation via C1q but only to the Chmr3 antigen. Moreover, autoreactive responses to several other explorative non-classical autoantigens (*e.g.,* Ca6 and Eno1) and respective FcγR engagement were identified in SjS patients (**Figure 3-2a).**

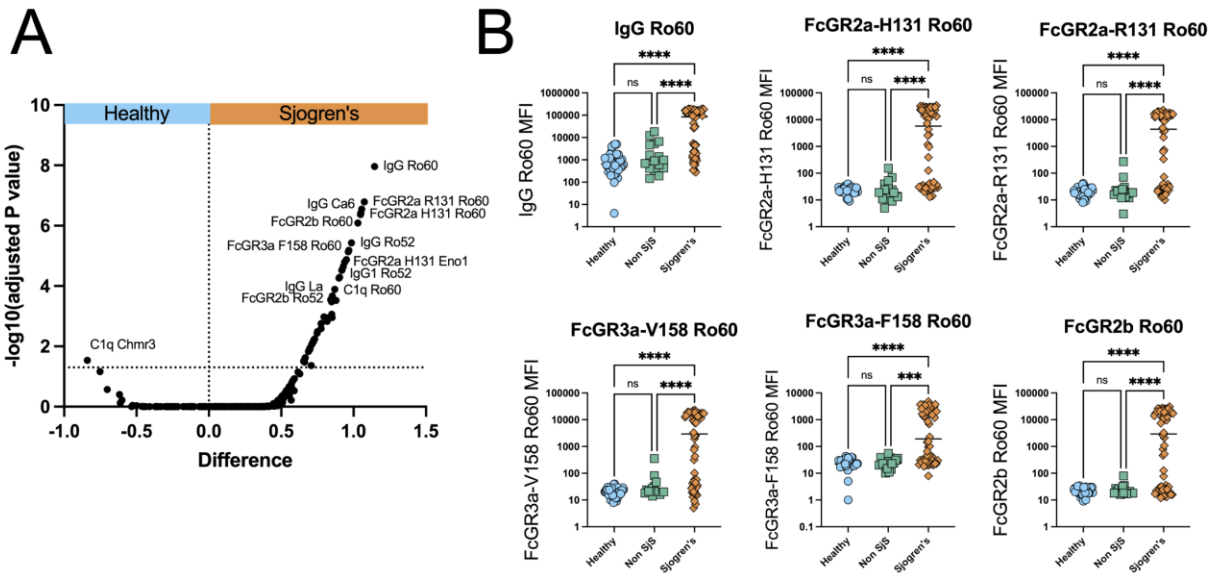


Figure 3-2: Serologic signature identified for Sjögren's (SjS) patients.

a) Volcano plot of healthy controls (blue) versus Sjögren's patients (orange). Data were z-scored prior to analysis. b) Univariate analysis across groups (healthy control, non-SjS sicca syndrome, and all Sjögren's syndrome) for FcR MFI values from the multiplex assay. Significant differences denoted with asterisks.

In order to identify a minimal autoantibody signature that best distinguished Sjögren's patients from healthy controls, we performed feature selection using Elastic-Net regularization followed by a supervised classification method (PLSDA). The identified signature included seven autoantibodies-related features and was able to accurately discriminate between SjS patients and healthy controls with 91.4% calibration and 92.2% cross-validation accuracy. Interestingly, the signature included C1q, FcγRIIa-H131/R131 and FcγRIIIa-V158 engagement specific to Ro60 and IgG specific to Ro60 and Ro52 (**Figure 3-3a-b**). Sensitivity and specificities (**Figure 3-3c**) were calculated from model performance for our seven-antibody signature, with 80.0% sensitivity and 97.5% specificity, and a Ro/La-only PLSDA model with 73.9% sensitivity and 100% specificity. Comparatively, seropositivity for any of the classical autoantibody (either anti-Ro60, anti-Ro52, or anti-La IgG), based on ELISA-like assay results, had a sensitivity of 69.0% (n=40) and seropositivity for Ro60 resulted in a sensitivity of 56.9% (n=33) within our cohort. When using multiplex assay data, 77.6% (n=45) patients with SjS were considered seropositive, with only one (2.5%) healthy individual positive for anti-La and another positive for anti-Ro52 (compared to none with ELISA-like assay). Calibration accuracy of our seven-feature signature was 91.4% and cross validation accuracy was 92.3% compared to 86.0% and 86.8% respectively for a PLSDA model with all classical antigens or Ro-only responses (**Supplementary Figure B-2**). Unsupervised hierarchical clustering showed excellent separation between healthy and SjS patients based on the seven-feature antibody signature identified (**Figure 3-3d)**.

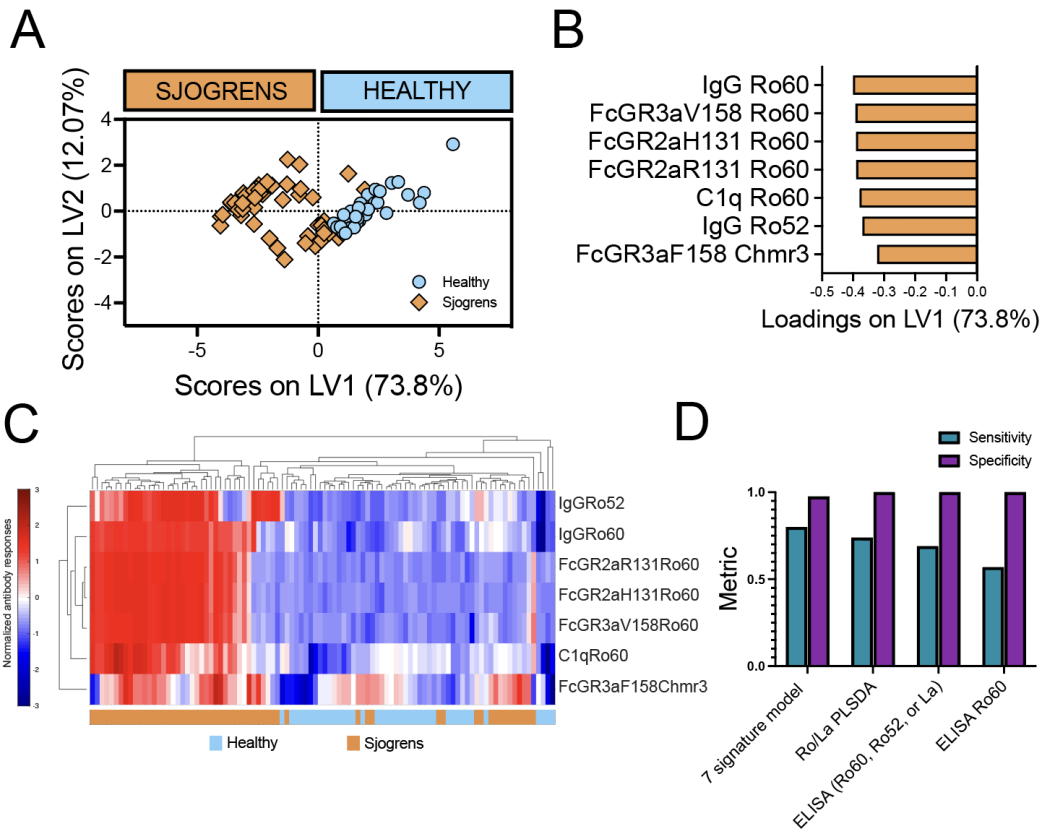


Figure 3-3: Sjögrens versus healthy.

a) PLSDA scores and b) loadings of Sjögren's patients (orange) versus healthy controls (blue) with variance explained by each LV in parentheses. c) Hierarchical clustering was performed using the seven feature elastic net-selected antibody signature. Data were z-scored prior to analysis. d) Sensitivity and specificity for our seven feature antibody signature versus clinical use of ELISA-like assay positivity for Sjögren's diagnosis.

3.4.2 Unique autoantibody responses between non-Sjögren's sicca syndrome and Sjögren's syndrome differentiate these individuals from healthy controls

We next investigated differences in autoantibody signatures between individuals with SjS and a group of non-SjS sicca patients. Univariate analysis of the antibody responses for this group revealed many non-significant differences in antibody responses between the non-SjS Sicca group and healthy controls (**Figure 3-2b**). In comparing minimal multivariate signatures using the feature selection/PLSDA analysis pipeline described above, results indicated that non-SjS Sicca patients had autoantibody signatures more similar to healthy controls than individuals with SjS, as

indicated by separation across latent variable (LV)1 (**Figure 3-4a-b**). As in the previous analysis, SjS was associated with anti-Ro60 and anti-Ro52 IgG and FcγRIIa, IIb, and IIIa engagement specific to these autoantigens. Interestingly, the results indicated that the Sicca patients separated from the healthy population across the second LV2, which involved increases in non-classical autoantibodies-related features including anti-Chmr3, anti-Cfl1, anti-Rgi2, and anti-Ifi16 (**Figure 3-4a, c**). In line with this, 25% (n = 4/16) of the non-SjS Sicca patients (who are all seronegative according to ELISA-like assay data) were IgG-positive to at least one of the non-classical autoantigens (Chmr3, Cfl1, Rgi2, Ifi16 and/or Ca6) according to multiplex data, including two who were not positive for any other autoantibody, and with that addition both would be "reclassified" as SjS according to the international criteria. As a matter of fact, despite not being identified as major drivers of the non-SjS sicca patients' autoantibody signature *via* the feature selection/PLSDA analysis pipeline, 25% (n = 4/16) were positive for anti-Ro60 IgG, and 12.5% (n = 2/16) for anti-La IgG, compared to 0% and 2.5% (n = 1/40) of the healthy controls, respectively, likely due to these features mainly driving LV1.

When including multiplex data regarding classical (*i.e.,* anti-Ro60 and anti-La in such case, as none were anti-Ro52 IgG positive) and non-classical (*i.e.,* anti-Cfl1, anti-Rgi2, anti-Spt1, anti-Ca6, anti-Chmr3) IgG autoantibody positivity into account, a total of eight non-SjS Sicca patients would become seropositive, including 75% (n = 6/8) who would be "reclassified" as SjS according to the international criteria. Interestingly, low levels of corresponding autoantigen-specific FcγR binding were detected in 66.7% of these 6 patients, but none of the other Sicca patients with multiplex-only autoantigen IgG positivity. Hierarchical clustering enabled visualization of clear separation of Sjögren's from heathy and non-Sjögren's using the LV1 feature-selected antibody signature (**Figure 3-4d**).

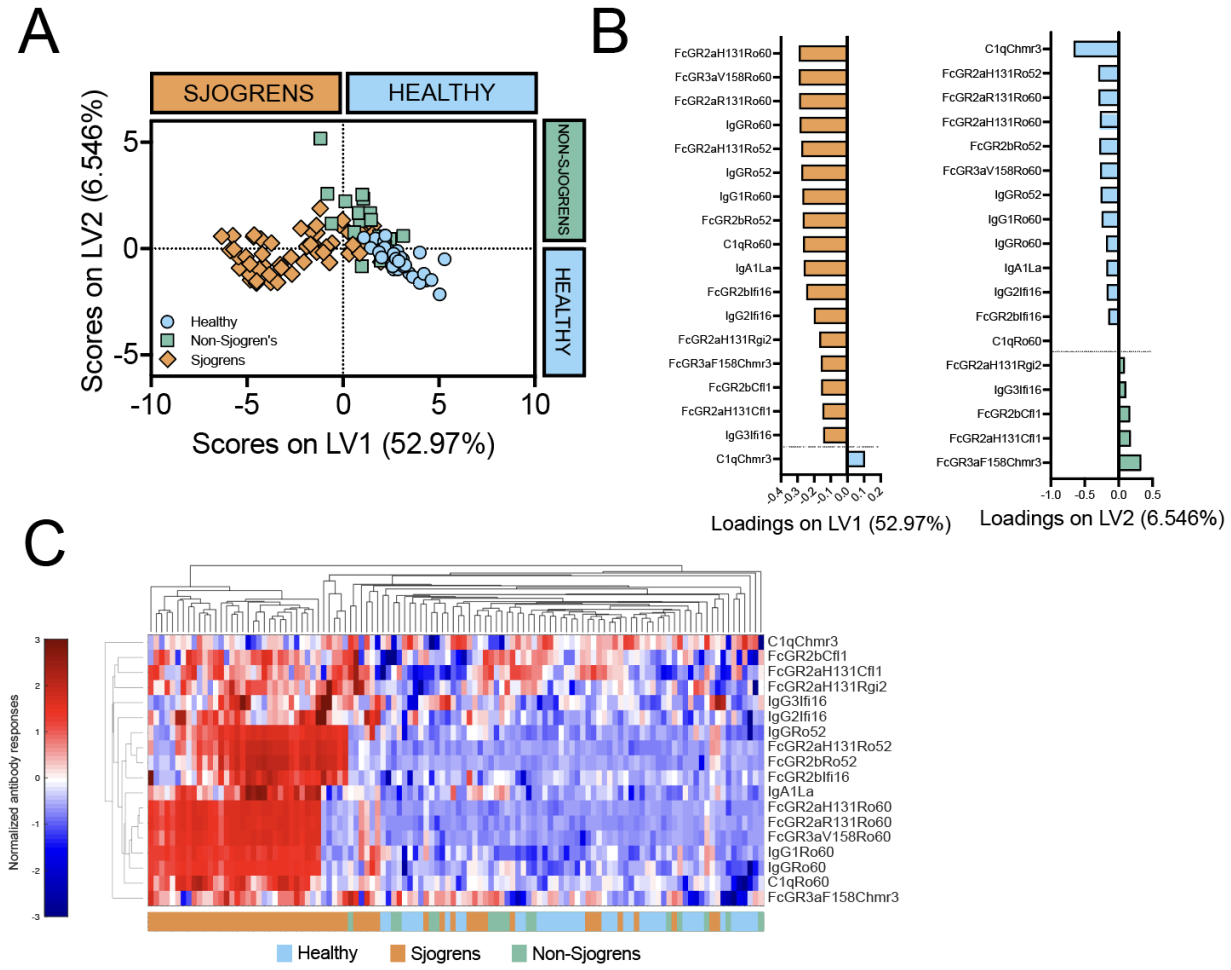


Figure 3-4: PLSDA of healthy controls vs. non-Sjogren sicca patients vs. Sjögren's patients

a) Scores plot shows separation of Sjögren's (orange) from healthy (blue) and non-Sjögren's sicca (green) across LV1 while healthy and non-Sjögren's are distinguishable across LV2. Elastic-net selected feature loadings for LV1 (b) and LV2 (c). Calibration accuracy of the model was 88.1% and cross validation accuracy was 85.0%. d) Hierarchical clustering performed on elastic-net-selected features.

3.4.3 N-linked glycosylation profiling reveals variations in IgG glycans associated with Sjögren's syndrome

As autoantigen-specific FcγRIIa, FcγRIIb and FcγRIIIa binding was identified as an important contributor to the autoantibody signatures associated with SjS, we examined IgG N-linked glycosylation, an important factor that can modulate the strength of IgG-Fc/FcγR engagement, in the cohort. Total IgG of SjS patients were more frequently lacking galactose

residues (referred to as G0) compared to non-SjS Sicca patients (27.7% ± 1.2 versus 20.4% ± 1.8, $p = 0.0037$) and healthy controls (27.7% ± 1.2 versus 18.6% ± 1.0, $p < 0.0001$). Accordingly, the relative abundance of highly galactosylated IgG (referred to as G2) followed the exact opposite trend in the three groups. Non-SjS sicca patients and healthy controls were not different regarding G0 ($p = 0.74$) or G2 relative abundance ($p = 0.84$).

IgG lack of fucosylation, which is classically associated with improved FcγRIII binding, was also more frequent in SjS patients compared to healthy controls, with levels of fucosylation respectively 81.1% ± 0.6 versus 86% ± 0.4 ($p < 0.0001$). Sicca controls also had lower amounts of fucosylated IgG compared to healthy controls (82.1% ± 1.0 versus 86% ± 0.4, $p = 0.0052$), but were not different from SjS patients regarding that feature ($p = 0.70$).

When analysing N-linked glycosylation profiling in seropositive and seronegative SjS (**Figure 3-5a**) according to the results of the ELISA-like assay, the same trend was identified, with seropositive SjS having the higher amount of G0 IgG (28.3% ± 1.3), then seronegative SjS (25.3% ± 2.8), non-SjS sicca patients (20.4% ± 1.8) and healthy controls (18.6% ± 1.0). The increase in G0 relative abundance in seropositive SjS was statistically significant when compared to non-SjS sicca controls ($p = 0.0036$) and healthy controls ($p < 0.0001$), whereas for seronegative SjS it was only significantly increased compared to healthy controls ($p = 0.0446$) (**Supplementary Figure B-3**). Regarding IgG fucosylation, analysing separately the seropositive and seronegative SjS subgroups did not modify the results, with healthy controls having significantly higher amounts of fucosylated IgG compared to all the other groups (**Figure 3-5b**).

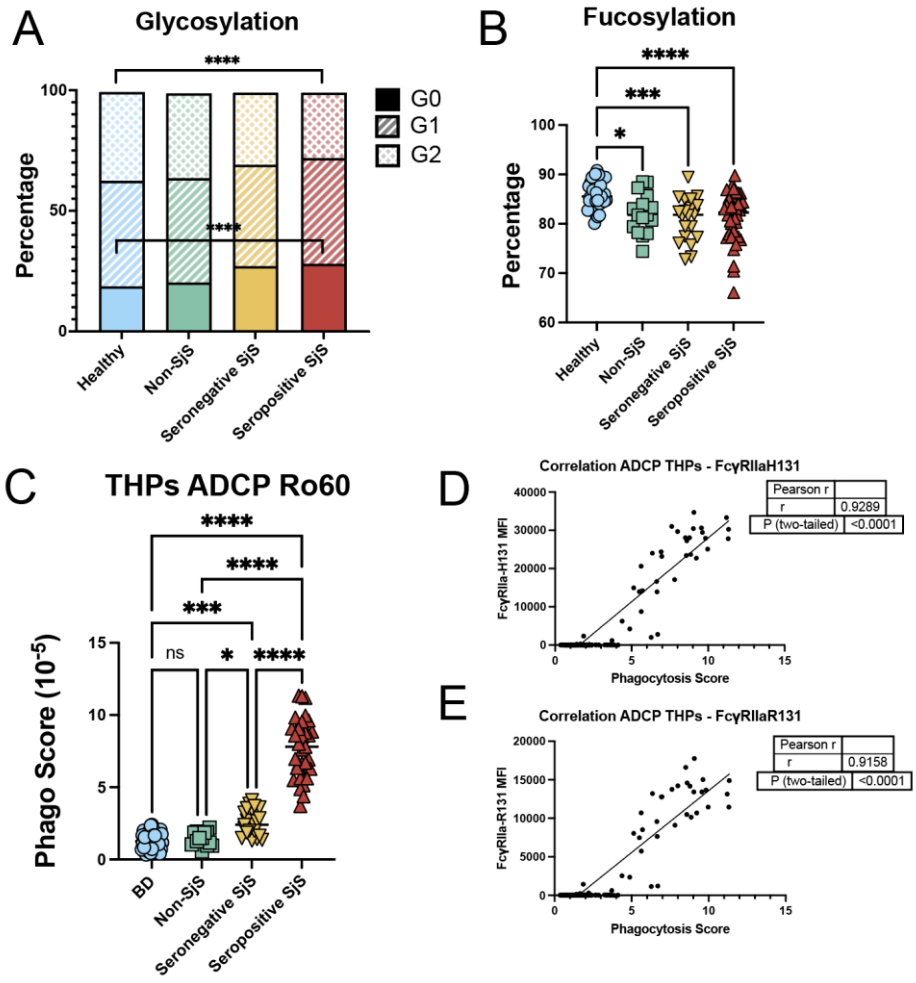


Figure 3-5: Cell-based phagocytosis assays and glycans.

a) Total IgG glycosylation profiles and fucosylation (b). c) Comparison of anti-Ro60 specific antibody-dependent cellular phagocytosis between healthy, non-Sjögren's, seronegative and seropositive Sjögren's patients using the THP-1 cell-based assay. Correlation with FcγRIIa-H131 (d) and FcγRIIa-R131 (e) dimers binding in multiplex.

3.4.4 Cell-based phagocytosis assay suggests autoantibody-associated FcγR binding is linked to elevated autoantigen-specific phagocytosis in Sjögren's syndrome

As FcγRIIa (both the H131 and R131 polymorphisms) binding of anti-Ro60 autoantibodies was a critical feature associated within all SjS-associated autoantibody signatures, we evaluated their functionality *via* an anti-Ro60 bead-based ADCP assay (**Figure 3-5c**)._Anti-Ro60 IgG seropositive (according to the ELISA-like assay) SjS patients (n = 33) had the higher phagocytosis scores among all groups, with a mean score of 7.7 ± 0.4 versus 2.5 ± 0.2 ($p < 0.0001$) for anti-

Ro60 IgG negative SjS patients (n = 25), 1.4 ± 0.1 ($p < 0.0001$) for non-SjS sicca controls (n = 16) and 1.3 ± 0.1 ($p < 0.0001$) for healthy controls. Anti-Ro60 IgG negative SjS patients also had higher phagocytosis scores than non-SjS sicca controls ($p = 0.0347$) and healthy donors ($p = 0.0011$), whose respective phagocytosis scores were, however, not statistically different ($p = 0.98$). In comparison, SjS patients who were anti-Ro52 IgG only (n = 6) or anti-La IgG only (n = 1) positive, without anti-Ro60 IgG positivity, had low phagocytosis scores, comparable with seronegative patients (i.e., a mean phagocytosis score of 2.3 ± 0.3 and a phagocytosis score of 3.6, respectively). Finally, phagocytosis scores from the whole cohort were significantly correlated with FcγRIIa-H131 (Pearson correlation coefficient $r = 0.93$; $p < 0.0001$) and FcγRIIa-R131 ($r = 0.92$; $p < 0.0001$) specific engagement of anti-Ro60 autoantibodies (**Figure 3-5d, e**).

3.4.5 Seronegative SjS patients can be differentiated from healthy controls based on an autoantibody signature driven by non-classical antigens

A major remaining challenge in SjS diagnosis is recognizing individuals who are not seropositive for classical antigens, requiring performing an invasive minor salivary gland biopsy to meet the international classification criteria for SjS. Thus, we wanted to explore what autoantibodies might be driving this difference between healthy controls and seronegative SjS patients. Univariate results revealed significantly higher Ro60, Ro52, and La responses in seropositive SjS patients compared to seronegative SjS patients, but the differences between healthy controls and seronegative SjS was non-significant (**Supplementary Figure B-4**). Using feature selection and PLSDA, we were able to identify an autoantibody signature that successfully distinguished between healthy individuals and seronegative patients (**Figure 3-6a**). The 17 elastic net selected features in this model included some anti-Ro60, anti-Ro52, and anti-La autoantibody-related features, such as anti-Ro60 IgG, anti-Ro52 FcγRIIb, and anti-Ro60 FcγRIIIa-V158 (**Figure**

3-6b). In line with this, based on multiplex assay instead of ELISA-like assay data, some patients would have been considered seropositive among the seronegative group: three for anti-Ro60 IgG, three for anti-Ro52 IgG and two for anti-La IgG.

Interestingly, there are also many non-classical autoantibody-related features that are part of the 17 feature signature, including anti-Ifi16 IgG3, anti-Ca6 FcγRIIa-H131, and anti-Cfl1 FcγRIIb and FcγRIIa-H131. This suggests that elevated autoantibodies to non-classical antigens may be important features in seronegative SjS patients. By plotting ROC curves (**Figure 3-6c**), we were able to show the improved sensitivity and specificity of the 17 feature seronegative autoantibody signature in comparison to the Ro/La PLSDA model, and the seven feature healthy vs. SjS autoantibody signature. Our model had a cross validation accuracy of 82.5% in comparison to cross validation accuracies of 75.0% using the seven-feature healthy vs. SjS signature and 61.3% using a PLSDA model with classical antigens only (**Supplementary Figure B-5**). The sensitivities and specificities for each model are shown in **Figure 3-6d**, with 80.4% sensitivity and 72.2% specificity for the 17 feature seronegative PLSDA model, 82.7% sensitivity and 66.7% specificity using the seven feature healthy vs. SjS model, and 65% sensitivity and 46.7% specificity for a Ro/La only PLSDA model.

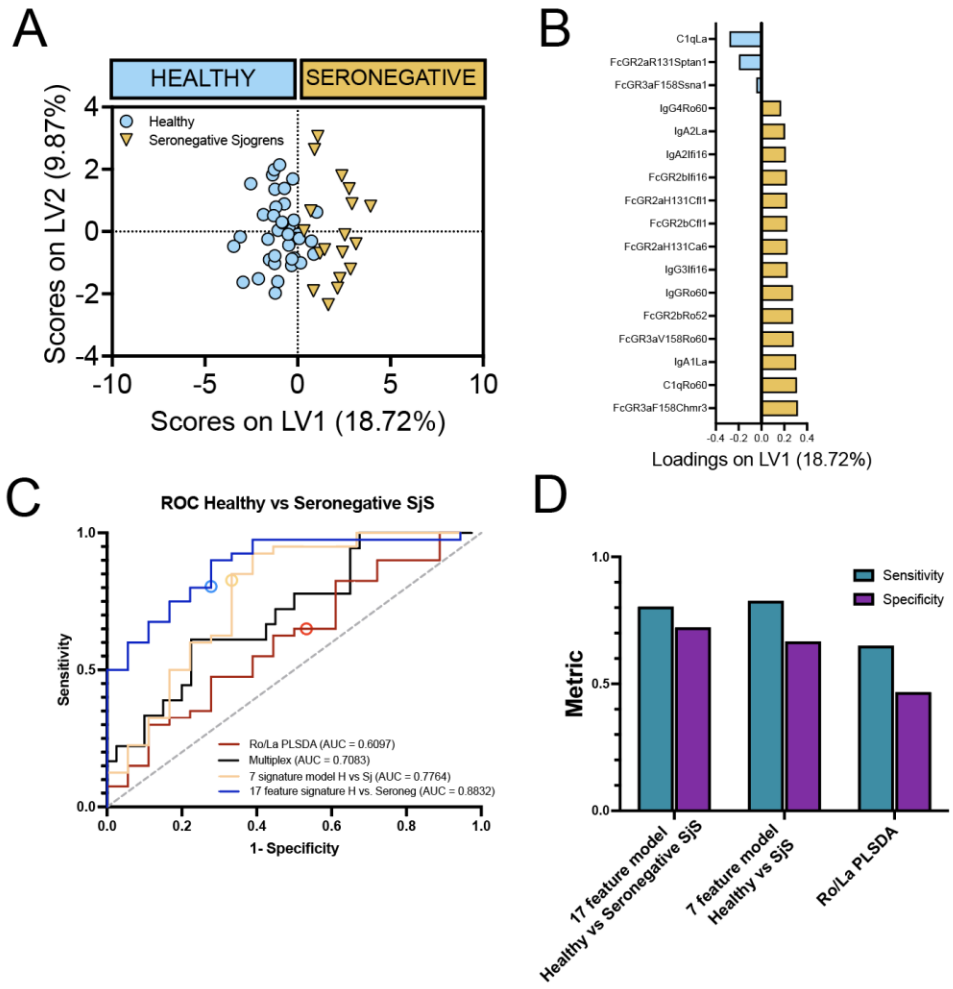


Figure 3-6: Healthy vs. Seronegative Sjögren's patients.

a) PLSDA scores and b) loadings of Seronegative Sjögren's patients (light orange) versus healthy controls (blue) with variance explained by each LV in parentheses. C) Receiver operating characteristic (ROC) curve showing the improved sensitivity and specificity of the 17 feature seronegative signature in comparison to the seven feature SjS signature, multiplex positivity, and Ro/La-only PLSDA. D) Sensitivity and specificity for the 17 feature Sjögren's antibody signature versus the seven feature Sjögren's antibody signature and the clinical use of ELISA-like assay positivity for Sjögren's diagnosis.

3.5 Discussion

In this study, we have used a novel SjS-dedicated systems serology approach, combining different high-throughput technologies, including a custom SjS-multiplex assay, IgG N-linked glycosylation profiling and a cell-based autoantigen-specific phagocytosis assay, to study differences in autoantibody responses between SjS patients, non-SjS sicca patients and healthy

controls. Systems serology approaches have almost exclusively been applied in the field of infectious diseases to date [7,123,125] but have the ability to provide new insight in understanding complex autoantibody responses and improve autoimmune patients' care.[126–128]

We have been able to confirm the pivotal association of the classical anti-Ro60/SSA, anti-Ro52/SSA and anti-La/SSB IgG autoantibodies, which were overrepresented in patients compared to healthy individuals, and also identified high levels of corresponding FcγR and C1q engagement. Fc-related effector functions have been scarcely studied in autoimmune diseases,[114] and never in SjS at a system level. In this study, they have been identified as prominent components of all the autoantibody signatures associated with SjS, whether considered seropositive or – more surprisingly – seronegative beforehand. The inclusion of FcγR and C1q engagement, along with IgG measurement, as in the identified SjS-associated seven feature autoantibody signature, has the ability to significantly improve SjS diagnostics' performances as represented in **Figure 3-3c**. Moreover, as anti-Ro60-associated autoantibody features were the most represented in this seven feature signature (accounting for 5 of them), but also in the more complex signatures represented in **Figure 3-3c**, **Figure 3-4b** and **Figure 3-6b**, such an assay could be adapted for clinical settings (contrary to its current version) with a curated set of autoantigens, including Ro60, and detectors, making one potentially alleviating the need for some patient biopsies. Moreover, in line with the literature,[129] choosing a particle-based multiplex instead of a classical solid phase technology has been associated with improved sensitivity for classical autoantibodies' detection (+8.6% anti-Ro/SSA and/or anti-La/SSB seropositivity in the SjS group), again allowing for quicker and less invasive diagnostic procedures, without significant loss of specificity. Accordingly, in the non-SjS sicca group, the multiplex-associated improved sensitivity for classical autoantibodies' detection

would allow for the reclassification of four patients (25% of the group) and none of the healthy individuals, as having SjS according to at least one set of international classification criteria.[112,113]

Apart from the classical anti-Ro60, anti-Ro52 and anti-La autoantibodies, the SjS-dedicated custom multiplex assay from this study was designed to include several previously described non-classical autoantibodies, to evaluate their potential value in identifying SjS and non-SjS patients. Hence, multiple non-classical autoantibodies (anti-Chmr3, anti-Cfl1, anti-Rgi2, anti-Ifi16 and/or anti-Ca6) were included in all the signatures associated with SjS (see in **Figure 3-3b**, **Figure 3-4b** and **Figure 3-6b**), but also in non-SjS sicca patients, with two (12.5%) additional individuals who would be "reclassified" as SjS when taking non-classical autoantibodies' data into account. Bridging the "seronegative gap" has been a key goal in SjS – and more globally in systemic autoimmune diseases – for many years, with different approaches, including the use of human proteome assays in recent publications.[130] Such approach allows for wider autoantigen screening, such as the proteome array comprising 19500 proteins that cover >75% of the human proteome, that identified 11 novel SjS autoantibodies with low individual frequencies (using the same threshold determining method as we did), as we similarly found for non-classical autoantibodies in this study. In contrast to proteomic approaches, current multiplex bead technologies are limited to a maximum of 500 antigens but are more rapid and easily portable to the clinical setting. This approach also allowed for the simultaneous evaluation of the autoantigen-specific main immunoglobulin isotypes, subclasses as well as FcγR engagement, which were identified as prominent for classical autoantibodies but also detected in more than 2/3 of the non-classical autoantibody-seropositive patients in our cohort. Using similar machine learning approaches, Longobardi et al.[130] have identified a 30-feature (only including autoantibodies-specificities) signature which was able to identify seronegative SjS from healthy individuals, with

an AUC of 0.79 (95% CI 0.64 to 0.93), compared to our 17 feature signature (including both Fab and Fc-related features) whose AUC was 0.88 (95% CI 0.79 to 0.97) for the same purpose. Regarding autoantibody specificities, there was some overlapping antigens between both approaches, as they also detected anti-Cfl1 and anti-Stmn4 in their cohort, but others were not, either because the autoantigens were absent from the array (e.g., Spt1, Sptan1) or probably for technical differences in the detection methods, especially protein conformation issues, as raised by the authors themselves.[130] Due to its very nature, the SjS-dedicated custom multiplex assay we have designed and evaluated in this study used native or recombinant proteins, without conformational issues, however its intrinsic qualities are necessarily highly dependent on the protein quality themselves.

As FcγR engagement was associated with all the identified autoantibodies and as an important signature in our cohort, we investigated the potential role of IgG N-linked glycosylation, a well-known pivotal factor in modulating IgG Fc binding to their receptors.[131] Previous SjS glycosylation studies have observed decreases in sialylation[132] (which was not observed in our cohort, shown in **Supplementary Figure B-4**). However, reduced levels of IgG galactosylation (**Figure 3-5a**) in both seronegative and seropositive SjS patients is in line with previous studies along with a range of autoimmune diseases and thought to be reflective of their common proinflammatory state.[133,134] However, the precise impact of galactosylaton on FcγR/IgG binding is subject to debate and is hard to affirm without antigen-specific IgG glycosylation data (which is sample-consuming and difficult to conduct with clinical samples[135] where small sample volumes are collected). On the other hand, the increased binding of afucosylated IgG to FcγR (especially FcγRIIIa, but also weakly FcγRIIa) is more widely described, and interestingly, the relative fucosylation of IgG was the lowest in seropositive SjS patients in our cohort (**Figure 3-5b**).

Moreover, seronegative SjS and non-SjS patients also had lower levels of IgG fucosylation than healthy controls, as afucosylation is associated with enhanced FcγR engagement, this is in line with our observation of higher FcγR binding to classical autoantibodies as well as non-classical autoantibodies in both groups.

To confirm the important role for autoantibody/FcγR engagement suggested by multiplex and total IgG N-linked glycosylation data in SjS, we have designed a Ro60-specific ADCP cell-based assay. As expected, anti-Ro60 seropositive SjS patients had the highest Ro60-specific phagocytosis scores, suggesting a possible novel pathogenic role for these autoantibodies which could contribute to disease *via* inflammatory cytokine production by phagocytes after Ro60 internalisation. Ro60 is an ubiquitous and mainly intracellular ribonucleoprotein, however it can be exposed to the immune system through cellular death and tissue damage.[136] Interestingly, seronegative SjS patients had at low levels, significantly higher phagocytosis scores than non-SjS sicca and healthy controls. One explanation could be the non-specific stimulation of THP-1 cells by the patients' diluted serum enriched in proinflammatory cytokines which was used in the assay (and not purified IgG). Whereas patients with non-anti-Ro60-autoantibodies (including anti-Ro52 or anti-La autoantibodies which are part of the same ribonucleoproteic complex) had comparable phagocytosis as controls. Nevertheless, if confirmed by further studies with other SjS-related autoantibodies and with primary cells, this finding could strengthen the rationale of targeting autoantibodies-producing cells and/or autoantibodies in clinical trials.[114]

A limitation of this study is the relatively limited number of individuals in each group. Although the association of FcγR engagement and related effector functions were consistently identified for all the different autoantibodies and *via* different technical approaches including functional assays, additional studies incorporating multiple cohorts are needed to confirm and

precise our results. In order to address this, we also compared the performance of our antibody signatures against 100 randomly generated signatures of the same size and found that our models performed significantly better ($p<0.05$) than all of the random models for each group comparison (**Supplementary Figure B-6**).

Overall, our study provides further insight into the autoantibody responses in Sjögren's syndrome, especially identifying a novel association and presumed pivotal role for classical, but also non-classical, autoantibody-specific Fc/FcγR-related effector functions, unveiling novel areas of research for known and lesser-known autoantibodies, with possible practical beneficial consequences for patients' diagnosis and treatment.

3.6 Methods

3.6.1 Study participants and sample collection

Samples were collected as part of the I GET DRY (NCT03003572) multicentric cohort, whose patients were recruited in the Auvergne-Rhône-Alpes region in France between March 2018 and December 2019, after Ethics Committee (Comité de Protection des Personnes Est-III) approval under the reference IDRCB 2016-A01851-50. The cohort (**Table 3-1**) contains healthy blood donors (who have all provided written consent before blood donation; n=40), non-SjS sicca syndrome patients (i.e., patients presenting with sicca syndrome but not fulfilling any classification criteria for SjS; n=16), and SjS patients (i.e., patients fulfilling the 2002 American-European Consensus Group [AECG][113] and/or the 2016 American College of Rheumatology [ACR]/European League Against Rheumatism [EULAR] classification criteria ; n=58).[112] Among non-SjS sicca syndrome patients and SjS syndrome patients, EULAR Sjögren's Syndrome Disease Activity Index (ESSDAI), EULAR Sjögren's Syndrome Patient Reported Index (ESSPRI) and focus score (i.e., number of mononuclear cell infiltrates containing at least

50 inflammatory cells in a 4 mm^2 minor salivary glandular section) were available [137]. Recommended biological tests for SjS workup were available for all non-SjS sicca syndrome and SjS patients, including anti-Ro/SSA and anti-La/SSB IgG. Patients were classified as seropositive (n=40) or seronegative (n=18) using the ELISA-like Phadia™ 250 system (Thermo Fisher Scientific), based on positivity for at least one of any of the Ro or La antigens.

Table 3-1: Cohort demographics

Group	N	Sex F/M # (%)	Age Mean (Range)	Time from Symptom Onset (months) Mean (Range)	ESSDAI Mean (Range)	ESSPRI Mean (Range)	Sialadenitis (Focus Score ≥ 1) n (%)
Healthy	40	34/6 (85%)	37.8 (19 – 68)	N/A	N/A	N/A	N/A
Non-SjS Sicca syndrome	16	14/2 (87.5%)	53.4 (33 – 75)	86 (2 – 342)	N/A	N/A	2 (12.5%)
Seronegative Sjögren's	18	16/2 (94.3%)	58.7 (28 – 84)	98.8 (14 – 308)	5.6 (0 – 23)	4.9 (0.3 – 10)	18 (100%)
Seropositive Sjögren's	40	36/4 (90%)	57.8 (30 – 91)	98.8 (2 – 477)	5.4 (0 – 31)	5 (1.3 – 8.3)	38 (95%)

3.6.2 Customized Sjögren's syndrome bead-based multiplex assay

A customized multiplex assay **(Supplementary Table B-1)**[127,138,139] was designed including an array of relevant autoantigens: the classical autoantigens (Ro60/SSA, Ro52/SSA, La/SSB; AROTEC Diagnostics), as well as non-classical "investigative" autoantigens found to have some association with SjS syndrome in the literature (carbonic anhydrase 6 [Ca6], cofilin 1 [Cfl1], cholinergic muscarinic receptor 3 [Chmr3], enolase 1 [Eno1], interferon gamma-inducible protein 16 [Ifi16], La, mouse double minute 2 homolog [Mdm2], rho GDP-dissociation inhibitor

2 [Rgi2], salivary gland protein 1 [Spt1], alpha fodrin [Sptan1], Sjögren's syndrome nuclear autoantigen 1 [Ssna1], stathmin 4 [Stmn4]; MyBioSource Inc., USA).[105]

The presence of autoantibodies in the donors and patients' serum was examined (**Figure 3-1**) using pan-IgG, IgG1-4, IgA1-2, IgM, C1q (an indicator of complement engagement), along with soluble FcRs dimers (activating FcγRIIa-H131 and -R131, inhibitory FcγRIIb, and activating FcγRIIIa-V158 and -F158), that have been previously described to correlated with a range of Fc functions.[140,141] Tetanus toxoid (Sigma) and influenza hemagglutinin (H1Cal2009; Sino Biological) were also added to the assay as positive controls. Magnetic carboxylated beads (Bio Rad) were covalently coupled to the antigens using a two-step carbodiimide reaction, as previously published[127,142] and methods are described in detail within supplementary materials. A titrated pool of anti-Ro60 seropositive SjS patient plasma control was included in all multiplex array plates. These titrations were used to normalize replicate multiplex array plates.

3.6.3 Data normalization

For all multivariate analyses, Tetanus and Influenza (positive control antigen) data was removed. As the majority of the multiplex data was non-parametric, all data was log-transformed, first thresholding any values below zero for each detector–antigen pair individually, by adding the minimum negative value for that feature to all samples within that feature. Positivity threshold for each feature was determined as the mean value in healthy blood donors + 3 standard deviations. For all multivariate analyses the data was normalized by mean centering and variance scaling for each feature using Matlab.

3.6.4 Statistical analyses:

Healthy versus Sjögren's syndrome Volcano plot was created using Prism 9, using the two-stage step-up method of Benjamini, Krieger, and Yekutieli to adjust for multiple comparisons with a False Discovery Rate of 1%. Welch t-test was used to avoid assumptions about consistent standard deviation. For univariate comparisons between three or more groups, ordinary one-way ANOVA was used for normally distributed data, and Kruskall-Wallis with Dunn's multiple comparisons was used otherwise.

3.6.5 IgG antibody purification

IgG antibodies were purified from the collected serum via Melon Gel chromatography according to manufacturer's protocol as previously described[143] (Melon Gel IgG Purification Kit, Thermo Fisher Scientific) and is described in detail in the supplementary materials.

3.6.6 IgG N-linked glycosylation profiling:

N-linked glycosylation profiles of purified IgG antibodies were measured on the LabChip® GXII Touch instrument (PerkinElmer) according to the ProfilerPro glycan profiling LabChip® GXII Touch protocol and is described in detail in the supplementary materials.[143]

3.6.7 Bead-based THP-1 antibody-dependent phagocytosis assay

To examine ADCP mediated by SjS' autoantibodies, a previously described bead-based assay[143,144] was adapted to Ro60/SSA antigens. Methods are described in detail in the supplementary materials.

3.6.8 Feature selection and data-driven methods

To determine the minimal set of features (signatures) needed to predict categorical outcomes (healthy, non-SjS sicca, seronegative SjS, seropositive SjS) a three-step process was developed based on Gunn et al.[145] Partial least squares discriminant analysis (PLSDA) performed in the Eigenvector PLS toolbox in Matlab was used in conjunction with Elastic-Net (described above) to identify and visualize signatures that distinguish categorical outcomes (age cohort, COVID-19 infection status) and are described in detail in the supplementary materials.

3.6.9 Receiver operating characteristic (ROC) curves

To explore the diagnostic ability of binary classifiers, ROC curves for PLSDA antibody classification signatures were generated using the Eigenvectors toolbox in Matlab. Graphpad Prism 10 was used for multiplex positivity. Sensitivity and specificity were calculated based on model performance for PLSDA models or our cohort data for assays.

3.7 Acknowledgements

We thank all the I GET DRY (NCT03003572) study participants, investigators and administrative staff, as well as all the blood donors for their involvement in this study. The I GET DRY study was supported by a Programme Hospitalier de Recherche Clinique Interregional AURA (PHRCI-16-006). This work was supported by a NHMRC Investigator Grant #2008092 (AWC). MK was supported by Villa M (GPM Hospitaliers), L'Institut Servier and ADPMIS research grants.

Chapter 4 Decoupling Antibody Levels from Fc Effector Functions: An Ordinary Differential Equation Framework Challenges the 'More is Better' Assumption for Polyfunctionality

4.1 Authors and Contributions

Suzanne K. Shoffner-Beck[1*], Kade E. Wong[1], Amy Chung[2], Kelly Arnold[1]

[1]Department of Biomedical Engineering, University of Michigan, Ann Arbor, MI, USA

[2]Peter Doherty Institute for Infection and Immunity, The University of Melbourne, Melbourne, Victoria, Australia

4.2 Abstract

The role of neutralizing antibodies and non-neutralizing antibodies in responses to Human Immunodeficiency Virus (HIV) have been studied for decades, but the complex polyfunctionality of Fc receptor effector responses is not yet fully understood. The only HIV vaccine trial shown to have modest efficacy (RV144) correlated increased IgG1 and IgG3 levels ("more antibody") with increased antibody-dependent cellular cytotoxicity (ADCC) FcγRIIIa responses and found that this resulted in protection from infection. Because these are cause-and-effect assumptions only, a theory-driven mathematical model can provide a unique opportunity to explore the underlying mechanism. While ordinary differential equation models have been studied previously to evaluate personalized differences in FcR activation, these models only

considered a single function or FcR type at a time and thus fail to accurately represent the complex dynamics of a polyfunctional system. Here we create an ordinary differential equation model that is able to simultaneously able to consider antibody-dependent cellular cytotoxicity ADCC and antibody-dependent cellular phagocytosis (ADCP) across different tissues using parameters from the literature to explore heterogeneity in immune responses between individuals, and within the same individual across mucosal or systemic circulatory environments. We found that the "more is better" antibody paradigm was not always true, and that increases in IgG3 while increasing ADCC, could decrease ADCP and likewise increases in IgG1 increased ADCP but decreased ADCC. We applied the model to vaccinee data from the RV144 trial and confirmed that boosting maximal single or combined FcR effector functions did not occur at the maximum concentration for either antibody, and thus boosting could result in increases in one function but decreases in another. Additionally, FcR polymorphisms that affect binding affinity were more influential in the blood than in mucosal tissues. These results could play a critical role in bettering our understanding of polyfunctionality in HIV and drive therapeutic and prophylactic interventions.

4.3 Introduction

Antibodies play a vital role within the immune system by providing protection against infection through a wide variety of functions. One main way that antibodies defend against invaders is by "neutralizing" or tightly binding to pathogens via the Fab portion of the antibody, which can be prophylactic. However, because it relies so heavily on tight binding of the Fab to antigen, pathogen mutations can have a negative effect on neutralization potential. Thus, antigenically variable pathogens, such as Human Immunodeficiency Virus (HIV), present a challenge because the rapid mutation of the viral antigens can easily escape the high-affinity

antibody recognition required for neutralization. Fortunately, antibodies can also utilize the Fc portion of the antibody to bind Fc Receptors (FcRs) on innate immune cells to induce multiple cellular functions. Polyfunctional responses include antibody-dependent cellular phagocytosis (ADCP) and antibody- dependent cellular cytotoxicity (ADCC) via cellular Fc receptors. These functions are enacted when immune complexes (antibody IgG dimers bound to antigen) bind different types of Fc receptors, including the Fc gamma receptor (FcγR), with FcγRIIa being primarily found on monocytes for phagocytosis and FcγRIII found mainly on natural killer (NK) cells to secrete cytotoxic factors. FcγR binds the four subclasses of IgG (IgG1-4), each of which can bind FcRs at different rates. The antibody subclass distribution also varies in each individual, leading to heterogeneity in FcR activation across populations. Furthermore, FcR receptor genetic polymorphisms have been identified, which can affect the binding affinity of IgG to the FcR (e.g. FcγRIIa-H has a higher affinity for IgG than FcRIIa-R) and can be inherited in homozygous or heterozygous patterns. There are also post-translational modifications that affect the subclass distribution profiles as well as binding affinities. For example, glycosylation and fucosylation of the Fc portion of an antibody (the addition of a carbohydrate group) can modify FcR binding and subsequently modulate immune responses. These intertwining parts build a complex system of antibody dynamics that lend itself well to mathematical modeling in order to further elucidate the most important aspects of the system, thereby identifying potential targets for intervention.

4.3.1 Antibody and Fc Receptor responses in HIV infection and vaccination

Due to the exceptionally high rate of spontaneous mutation within the HIV genome, FcRs are thought to play a particularly important role in HIV infection and protection, although the exact mechanism is not yet fully understood. There have been numerous studies that have explored the role of neutralizing antibodies in HIV and potential mechanisms for HIV prevention.[146–150]

Recently, broadly neutralizing antibodies (bNAbs) have been of particular interest as potential prophylactic or therapeutic targets as well as guides for HIV vaccine design.[150] Passive transfer and vaccination have been shown to provide some protection against vaginal and rectal HIV virus challenge in animal studies.[151] To date, there has been only one clinical trial of a vaccine with modest effectiveness at preventing HIV infection, the RV144 vaccine trial in Thailand (60% at one year, 31.5% at 3.5 years after vaccination).[28] RV144 showed no increase in broadly neutralizing Abs, but rather induction of non-neutralizing Abs with the ability of activating ADCC. The trial remains controversial, as the results have not been able to be replicated and follow-up studies have had limited success. Systems serology studies have previously shown that "more is better," indicating that higher levels of IgG1 and IgG3 correlated with improved Fc effector responses and thus reduced risk of infection, while decreased IgG3 led to decrease Fc effector responses.[29,152] Particularly, it has been found that in the absence of high IgG1 levels, IgG3 antibodies have limited functional potential.[152] It was also observed that, over time, IgG3 levels decreased, and this effect correlated with the decrease in vaccine efficacy over time.[153,154] Other studies have explored potential antibody "boosting" to maintain protection over time, but have found that these elevated total IgG, but skewed subclasses towards IgG2 and IgG4 which led to overall decreased Fc effector functions.[153,155–157] Thus, the link between Fc effector functions and protection against HIV remains not yet fully understood and there is much left to be explored involving the dynamics between the "more is better" mantra, IgG1/IgG3 collaboration, and polyfunctionality.

4.3.2 HIV transmission and immune responses across different tissues

In addition to the previously stated studies on prevention, there have been numerous studies on the transmission of HIV and local immune responses, further supported by the differences in

transmission across different tissues. The risk of HIV transmission depends on the method of exposure, with sexual transmission being the highest risk. Receptive anal intercourse has the highest rates of transmission (1 in 72 sex acts), with receptive penile-vaginal intercourse resulting in intermediate transmission rates (1 in 1250 sex acts), and penile-oral sex causing very few infections (0-4 in 10,000).[158] Bloodborne and vertical transmission is also possible, with mother-to-child transmission the highest risk (as high as 25%),[159] followed by needle sharing (1 in 150 exposures) and needle-stick (1 in 435).[160] Transmission rates also depend on a variety of factors, including viral load or treatment status, circumcision status, coinfection with other sexually transmitted diseases, and genetic background. The wide range of transmission rates further indicate that heterogeneity of responses in different tissues, particularly in mucosal tissues versus the blood, lead to variable levels of protection. These results have been supported by several studies, including a study in macaques that indicated rectal mucosal tissue was the most permissible to infection, while genital tissue had much lower mucosal permeability.[161]

4.3.3 A new framework for a multiple FcR model to explore competition and polyfunctionality

While data-driven systems serology studies can be powerful for exploring correlations in a complex system, these methods are unable to provide a mechanistic understanding of the system and do not give information about cause-effect relationships. Due to the large number of variables contributing to the system, Fc receptor activation lends itself well to a theory-driven model, that can be used to unravel individual components of the system contributing to the heterogeneity of responses. Lemke et al. (2021)[9] was able to create an ordinary differential equation (ODE) model to represent this framework and look at personalized responses in individuals participating in the RV144 clinical trial. However, their study had several limitations: first, the model was performed using in vitro assay parameters, which are vastly different in range from physiologic in vivo

parameters. Furthermore, the model only considered the binding of IgG dimer-antigen complexes to one type of FcγR at a time (FcγRIIa or FcγRIIIa, but not both simultaneously). In reality, FcγRs are competing for the same antibody and antigen substrates and in order to truly consider polyfunctionality, it is necessary to consider the dynamic between the receptors present on immune cells coexisting in the same environment.

In this paper, we use computational systems serology approaches to enable quantitative evaluation of the relationship between antibody features and immunological function. Here we will create a novel ordinary differential equation (ODE) model that is able to account for interaction between multiple FcRs which can help us better understand genetic variability between individuals or multiple simultaneous polyfunctional responses due to cells expressing different classes of Fc gamma receptors. Furthermore, the two FcR model will be simulated using in vivo physiologic parameter values rather than in vitro assay parameters. The model schematic is shown in **Figure 4-1**, with an example reaction equation displayed below. Our computational approach also provides a unique opportunity to simulate responses within various tissue environments that would otherwise be difficult to study in vivo. Using powerful computational methods to explore a complex parameter space, we will be able to better unravel heterogeneity in immune responses due to polyfunctionality.

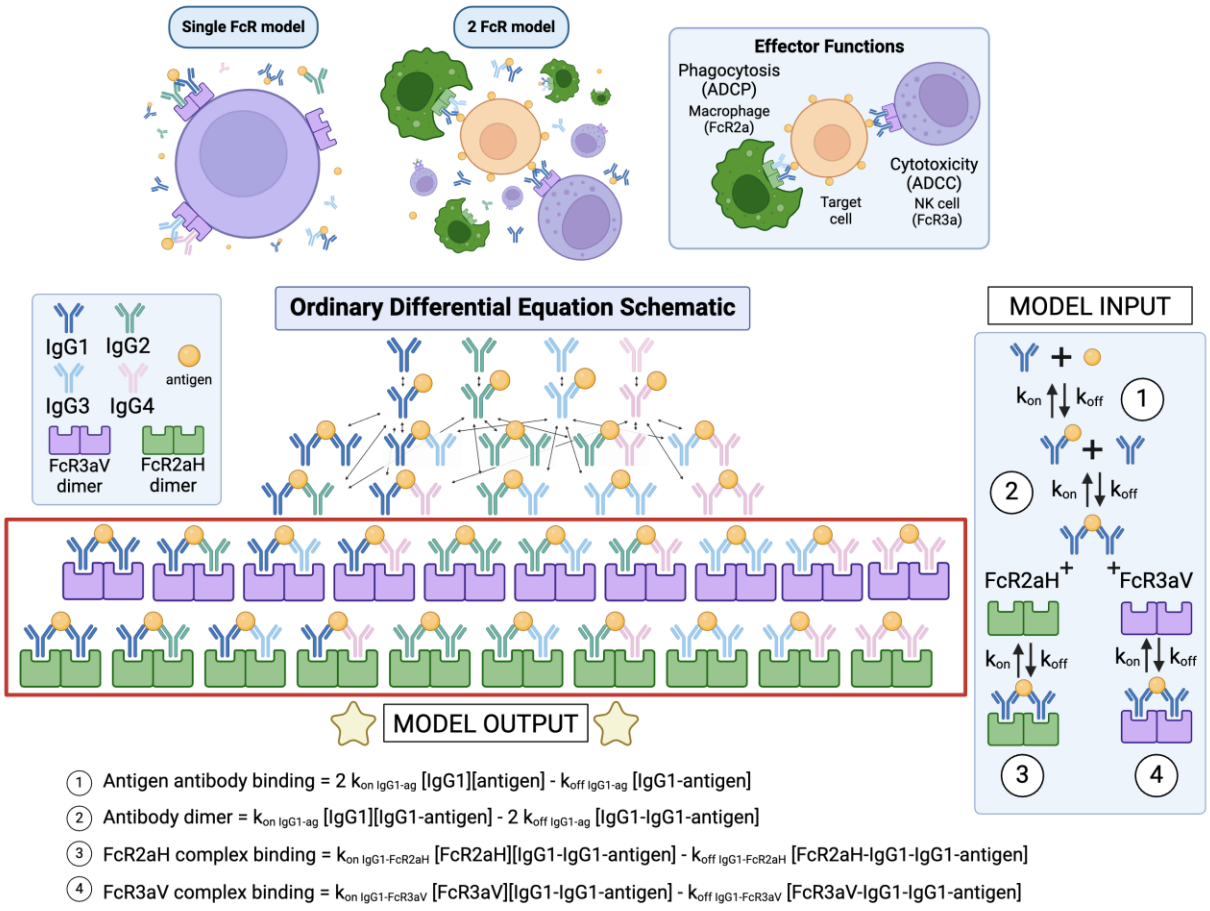


Figure 4-1: Model Schematic

Illustration of FcR2a on macrophages and FcR3a on natural killer cells as examples for antibody-dependent cellular phagocytosis (ADCP) and antibody-dependent cytotoxicity (ADCC) respectively. Forward and reverse reactions shown for binding of antibody to antigen, formation of a dimer, then subsequent binding of either FcR2a or FcR3a.

4.4 Results

4.4.1 A sensitivity analysis highlights importance of IgG1- and IgG3-related parameters

In order to understand which IgG and FcR features have the most significant impact on FcγRIIa and FcRγIIIa complex formation in blood, we performed a one-dimensional sensitivity analysis, in which FcγRIIa and FcRγIIIa complex formation were calculated after each parameter was varied individually by 0.05-20x (**Figure 4-2**). Unsurprisingly, the most sensitive parameters for both FcγR outputs involved IgG1 and IgG3, including IgG1 and IgG3 concentration as well as

parameters related to antigen binding (on and off), binding to each respective FcγR (FcγRIIa and FcγR concentration. In terms of IgG subclass concentrations, the model predicted increases in FcγRIIa complex formation with increases IgG1, whereas increases in FcγRIIIa complex formation was driven by increases in IgG3. Both of these results were expected given the higher affinity of FcγRIIa for IgG1 and FcγRIIIa for IgG3. Intriguingly, however, the model also suggested that IgG1 and IgG3 have the potential to negatively impact FcγRIIIa and FcγRIIa, respectively. When IgG1 was increased by 20-fold, the model predicted a 26.6% decrease in FcγRIIIa. Likewise, the model suggested that a 20-fold IgG3 may decrease FcγRIIa by as much as 54.9%. The global sensitivity analysis revealed similar results, highlighting the importance of IgG1 and IgG3 concentration and affinity parameters and suggesting negative relationships between IgG1 and IgG3 with FcγRIIIa and FcγRIIa, respectively (**Supplementary Figure C-1**). Inspection of the model revealed that the unexpected decreases in FcR complex formation with increased in IgG titers was likely due to competition between IgG1 and IgG3 subclasses for antigen, with stronger versus weaker binding for FcγRIIIa vs. FcγRIIa. At very high IgG1 concentrations, antigen remains bound in anti-IgG1 intermediate complexes, thus reducing antigen availability for IgG3 and lowering formation of FcγRIIIa complexes. A similar mechanism was observed for IgG3 and FcγRIIa. Overall, these results provide a mechanism by which increased levels of IgG1 and IgG3 may negatively impact FcγR complex formation and downstream activation of ADCC and ADCP.

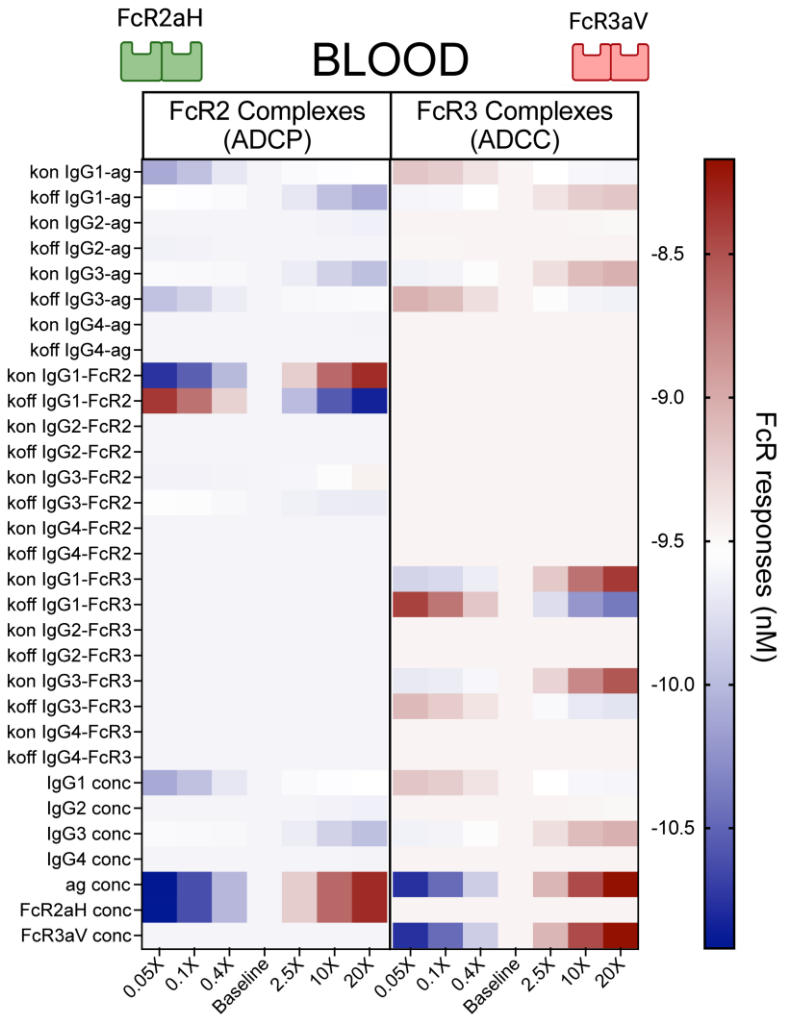


Figure 4-2: 1D sensitivity analysis of two-FcR model using in vivo blood parameters

4.4.2 The model reveals mechanisms that underpin individual heterogeneity in ADCP and ADCC responses depending on IgG1 and IgG3 concentrations

In order to further explore the interaction between IgG1 and IgG3 and their combined effects on FcγRIIa and FcγRIIIa complex formation, we next performed a two-dimensional (2D) sensitivity analysis by tuning each over 0.001x – 1000x and computing complex formation for FcγRIIa and FcγRIIIa (**Figure 4-3a**). The resulting landscape highlighted changes in ADCP (FcγRIIa complexes) and ADCC (FcγRIIIa complexes) that might be expected with increases in IgG1 and IgG3 that result from vaccine boosting (**Figure 4-3**). The model suggested that more antibody is

not necessarily ideal and that maximizing one Fc effector function tends to lead to decreases in another function at certain combinations of IgG1 and IgG3. For example, for FcγRIIa complexes, the landscape illustrates sensitivity to IgG1 up to 100 nM at low levels of IgG3 ($<10^3$ nM), however this sensitivity has a limit and IgG3 has the capacity to reduce complex formation at high titers (**Figure 4-3a**). Conversely, FcγRIIIa is predicted to be highly sensitive to IgG3 from 10 to 500 nM, but at high levels of IgG1, IgG3 would be reduced to XXX. (**Figure 4-3c**). Interestingly, at constant levels of IgG1, the model predicts that increases in IgG3 would increase FcγRIIIa complex formation (ADCC) but decrease FcγRIIa functions (ADCP). For example a 1000-fold increase in IgG3 would increase ADCC by 616%, but in parallel it would expected to decrease ADCP by 74.7%. This is likely due to the increased relative affinity of FcγRIIIa for IgG3 in comparison to FcγRIIa, which leads to competition between antibodies for antigen and less antigen-bound IgG1to activate ADCP via FcγRIIa. A similar effect was observed for constant IgG3, where increases in IgG1 were predicted to result in increases in FcγRIIa functions (ADCP), but decreases in FcγRIIIa functions (ADCC). For example, a 1000-fold increase in IgG1 leads to a 734% increase in ADCP while simultaneously leading to a 69.5% decrease in ADCC (Figure 3). Perhaps most interestingly, parallel increases in both IgG1 and IgG3 were not predicted to maximize FcγRIIa and FcγRIIIa complexes due to the potential for high IgG1 to significantly reduce FcγRIIIa complex formation.

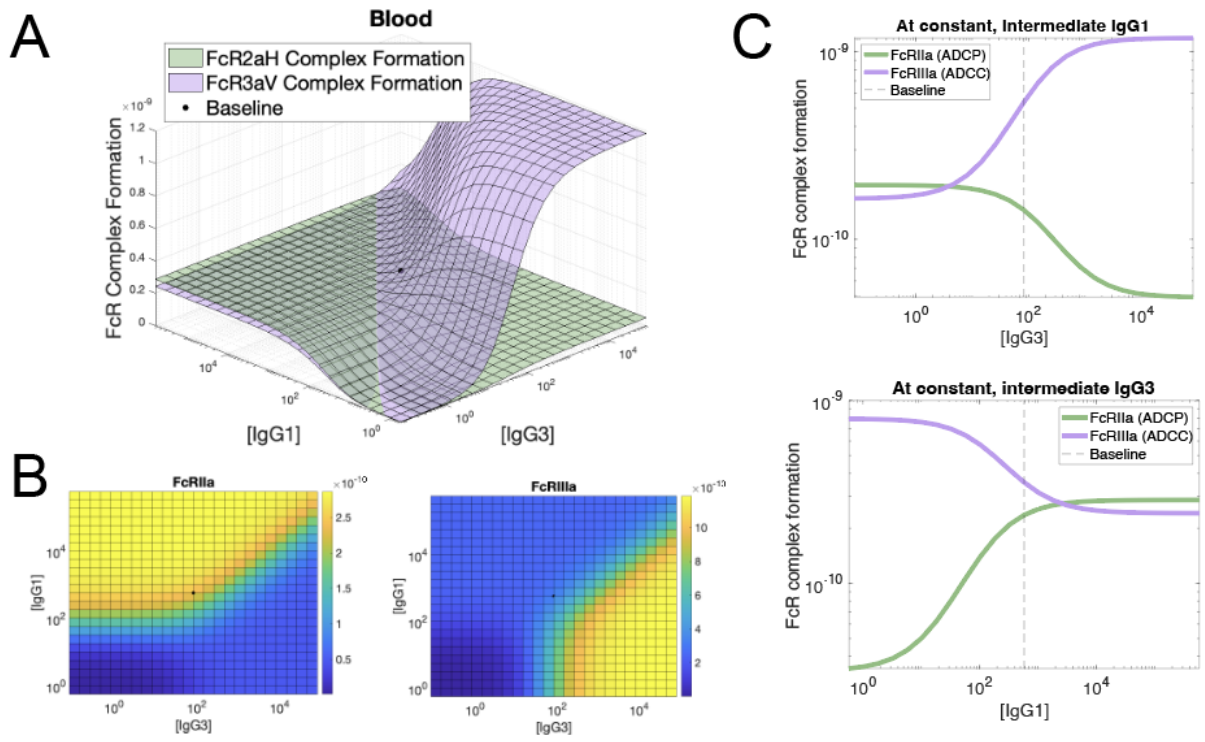


Figure 4-3: 2D Sensitivity Analysis and relationship between IgG1 and IgG3.

A) FcRγIIaH complex formation (green surface) and FcRγIIIaV (purple surface) plotted across a combination of IgG1 and IgG3 concentrations with baseline blood parameter values indicated with a black point. B) Heatmap showing complex formation with yellow indicating higher values and blue indicating lower values. The curved line indicates the region with the highest gradient (regions which are very sensitive to small perturbations). C) Cross-section of surface shown at constant IgG1 = 100nM (above) and constant IgG3 = 100 nM (below), showing the baseline x parameter value with a dashed line and the inverse relationship between FcRγIIaH formation and FcRγIIIaV formation as antibody levels increase.

In order to evaluate heterogeneity in a vaccine population after boosting-related increase in IgG1 and IgG3, we used data from the RV144 HIV clinical trial, where antigen-specific IgG1, IgG2, IgG3, and IgG4, as well as antigen-specific FcγRIIa and FcγRIIIa responses were measured in 105 plasma samples. Experimental IgG subclass measurements made in mean fluorescent intensity (MFI units) were converted to concentration as described in the methods and previously published (Lemke 2021)..[9] We used converted concentration values as personalized input into our two FcR model and predicted in vivo blood FcγRIIa and FcγRIIIa complex formation using the model. The vaccinee samples are plotted at baseline in vivo conditions on the surface in **Figure**

4-4a, with an average FcγRIIa complex formation of 2.76e-10 nM and mean FcγRIIIa complex formation of 2.77e-10 nM.

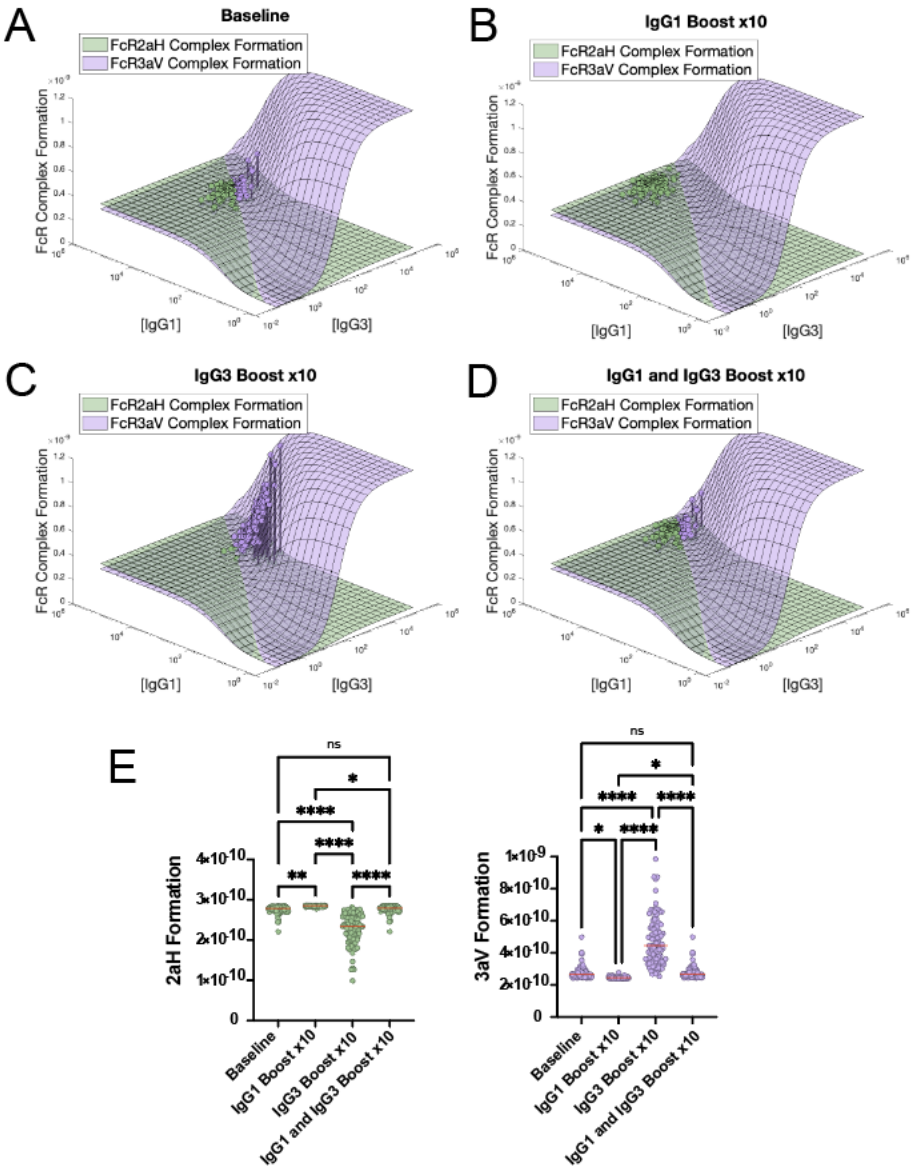


Figure 4-4: Simulation of the impact of antibody boosting in RV144 vaccinee data on FcR complex formation.

A) Baseline plasma values of gp120-specific IgG1 and IgG3 values with simulated FcR complex formation plotted on the surface. Simulated boosting of IgG1-only x10 (B), IgG3-only x10 (C), and simultaneous IgG1 and IgG3 boosting x10 plotted. E) Statistical significance between the population FcRIIa and FcRIIIa formation across baseline and various interventions with significant adjusted p-value denoted by asterisks.

Because some vaccinees fall on a steep gradient for the FcγRIIIa, while others fall more on the plateau of FcγRIIa, we next utilized the model to predict FcγRIIa and FcγRIIIa complex

formation after a simulated "boost" in IgGI and IgG3, separately and in combination. Boosting IgG1-only by 10-fold shifted all the vaccinees into a non-sensitive plateau region of the landscape (**Figure 4-4b**) where mean FcγRIIa complex formation was significantly higher than baseline (2.85e-10 nM, adjusted p-value = 0.0069). The IgG1-only boost decreased FcγRIIIa significantly (2.46e-10 nM, adjusted p-value = 0.03). Boosting IgG3-only by 10-fold significantly decreased FcγRIIa by 17.5% (2.28e-10 nM, adjusted p-value < 0.0001) and increased FcγRIIIa by 70.0% (4.71e-10 nM, adjusted p-value < 0.0001) (**Figure 4-4c**). Interestingly, simultaneously boosting both IgG1 and IgG3 by 10-fold each led to no significant difference in either FcγRIIa or FcγRIIIa complex formation due to the shifting of the vaccinees along the FcγRIIa ≅ FcγRIIIa intersection (**Figure 4-4d**). The statistical significances between boosting interventions are summarized in **Figure 4-4e**.

4.4.3 Host genetics influence optimization of effector functions

We next used the model to investigate differences predicted to arise from genetic differences in Fc receptor polymorphisms, which have the potential to change IgG binding to FcγRs. We evaluated two known polymorphisms for FcγRIIa, the higher affinity FcγRIIa-H131 and the lower affinity FcγRIIa-R131, as well as the higher affinity FcγRIIIa-V158 and the lower affinity FcγRIIIa-F158.[162] For each polymorphism, we evaluated both homozygous and heterozygous combinations. The landscapes for FcR formation with the two heterozygous combinations (H131/F158 and R131/V158) are shown in **Figure 4-5a**. With the R131/V158 genotype, FcγRIIIa is always greater than FcγRIIa regardless of IgG1 and IgG3 levels. There is also a much lower maximum for ADCP (FcγRIIIa) with this combination in comparison to the H131/F158 combination. Example points A (high IgG1 and low IgG3) and B (high IgG3 and low

IgG1) were used to display the balance of FcγRIIa and FcγRIIIa across the four different polymorphism genotype combinations. **Figure 4-5b** illustrates this, where the horizontal line indicates equivalent FcγRIIa and FcγRIIIa formation; above the line is higher ADCP responses (FcγRIIa), while below the line is higher ADCC (FcγRIIIa) responses. While ADCC responses are relatively consistent across phenotypes, the R1131/V158 combination is the only genotype to flip to higher levels of ADCC rather than ADCP at high levels of IgG1.

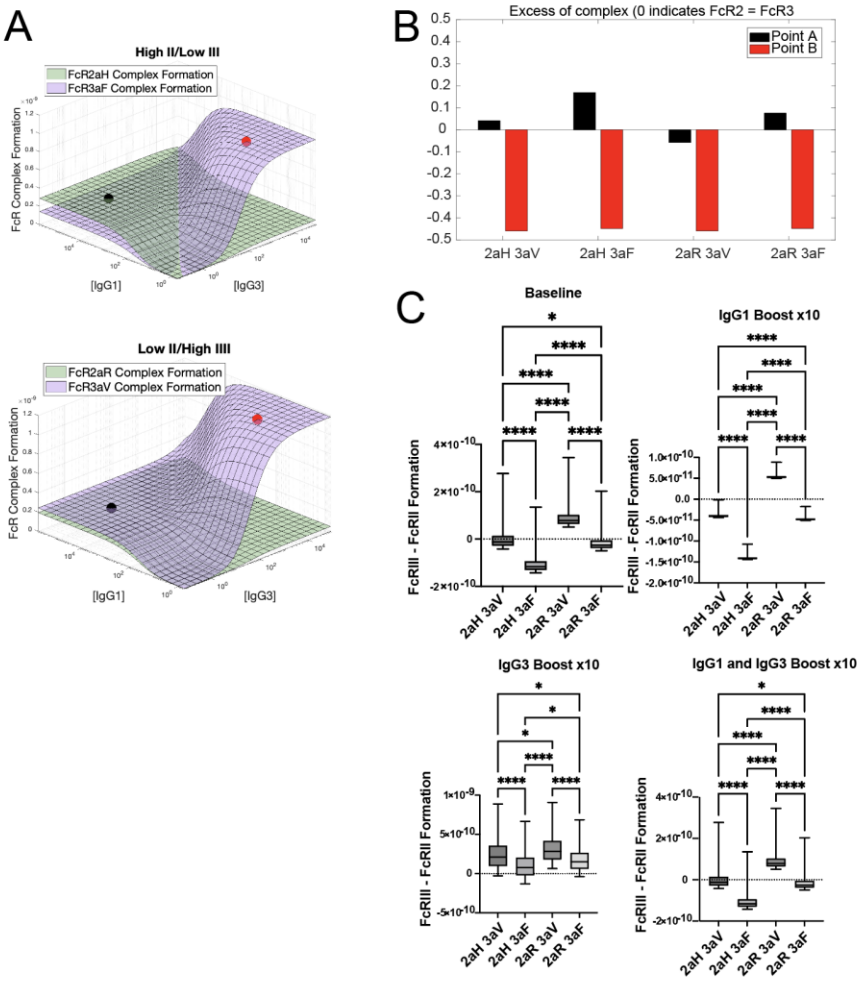


Figure 4-5: Simulating FcR complex formation across different polymorphisms combinations

A) Antibody landscapes for two of the four possible combinations of FcγR genotypes (high-affinity FcγRIIaH131 paired with low affinity FcγRIIIaV158 and low-affinity FcγRIIaR131 paired with high affinity FcγRIIIaV158) show that ADCP has lower potential in the R131/V158 combination. B) Excess complex formation as defined by the formation above 50% correlating with an equal balance of FcγRIIa/IIIa. C) Difference between FcγRIIIa and FcγRIIa complex formation across different boosting conditions for the RV144 vaccinee data.

Next, we took the vaccinee data and applied it to our polymorphism landscapes in combination with our boosting simulations to show how individuals could respond differently to interventions based on their genetic polymorphism combination. We saw significant differences for baseline FcγRIIa formation between any combination that included H131 versus R131 (2.76e-10 nM for H131 versus 1.86e-10 nM for R131, adjusted p-value < 0.0001). There were no significant differences in FcγRIIa formation with H131 (or R131) when comparing a genetic pairing with F158/V158. We observed a similar pattern for FcγRIIIa formation (2.77e-10 nM for V158 versus 1.71e-10 nM for F158, adjusted p-value < 0.0001). **Figure 4-5c** summarizes the significance in the difference between FcγRIIIa and FcγRIIa formation in all four polymorphism combinations, with the greatest difference observed between R131/V158 (higher ADCC) and H131/F158 (higher ADCP). The same pattern was observed across all of the boosting patterns, including IgG1-only boost, IgG3-only boost, and IgG1 and IgG3 boost. These results indicate that personalized differences in affinity of binding based on genetic polymorphism combinations could play an important role in an individual's capacity for maximizing specific FcR effector functions in some settings, but not in others.

4.4.4 Model illustrates the potential for vastly different Fc responses in mucosal tissues

Fc effector functions play an important role in ADCP and ADCC in mucosal tissues[163], however these functions are difficult to evaluate in vivo because of challenges associated with obtaining human mucosal samples. We next used the model to make predictions for how FcR complex formation might changes in mucosal tissues, as a function of differences mucosal viral load, Fc receptor expression, and IgG titers. We used parameters from the literature as shown in **Supplementary Table C-1, Supplementary Table C-2,** and **Figure 4-6a**. Viral load (antigen concentration) is highest in the rectal mucosa and antibody concentrations are more than 100x

lower in the mucosal tissues than in the blood. In the blood, there are similar levels of FcγRIIa and FcγRIIIa (42%/58%) but the balance is much more skewed in the mucosal tissue (**Figure 4-6b**). For instance, in the rectal tissue there are more monocytes and thus higher expression of FcγRIIa or ADCP (78%), while in the penile tissue there are more natural killer cells present and thus higher expression of FcγRIIIa or ADCC (98%).

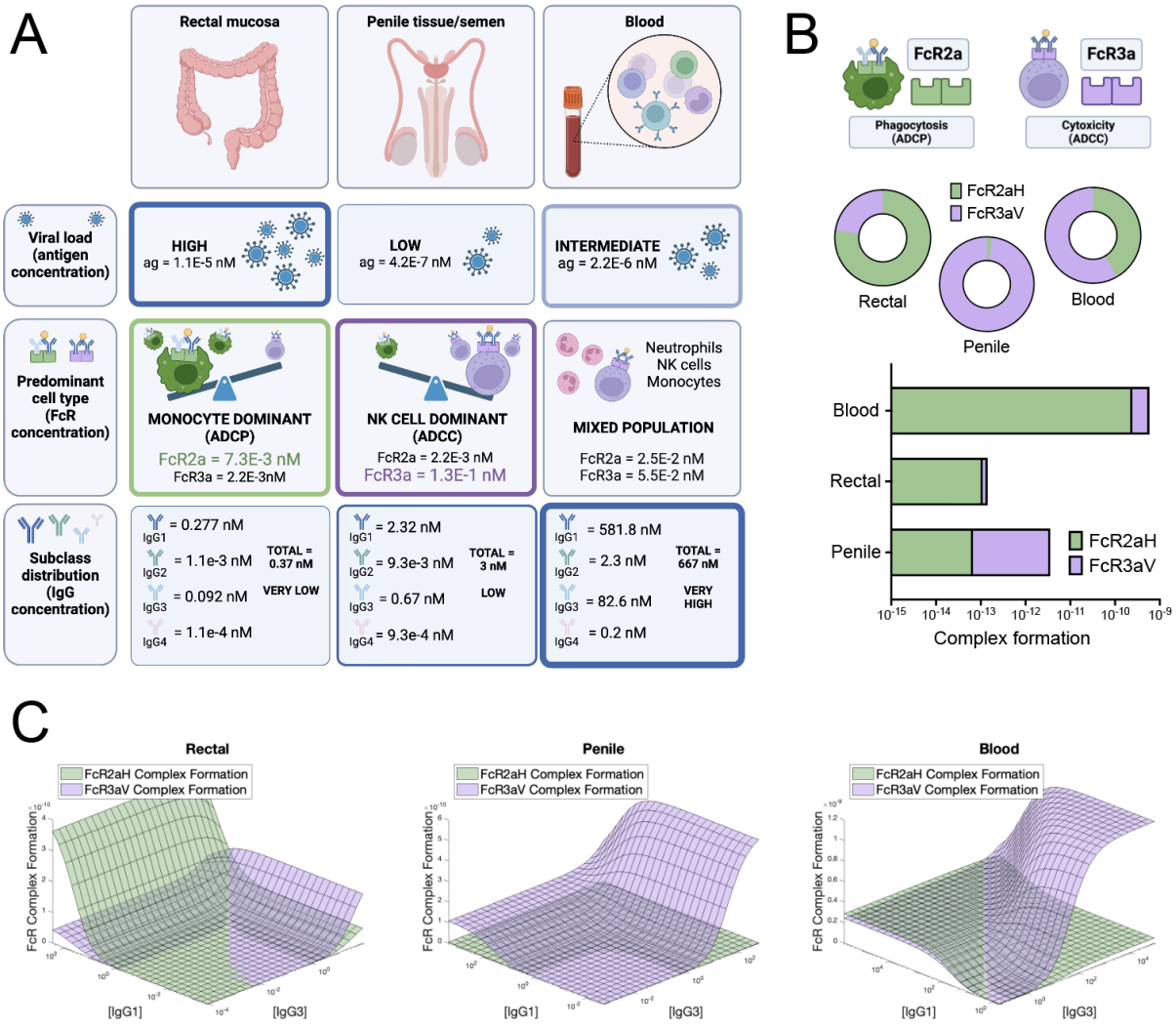


Figure 4-6: Fc receptor functions across different tissues.

A) Visualization of baseline parameters used as input for mucosal (rectal and penile) and blood models. Sources summarized in **Supplementary Table C-1** and **Supplementary Table C-2**. B) Baseline simulation results showing complex formation involving FcγRIIa and FcγRIIIa as log complex formation or percentage of total FcγR complexes. C) 2D landscapes showing IgG1 and IgG3 combinations affect ADCP and ADCC model output as measured by FcγR complex formation.

This pattern is also clearly visualized by looking at the FcR landscapes across variable combinations of IgG1 and IgG3 (**Figure 4-6c**). In the penile tissue, ADCC is dominant and boosts in IgG1 or IgG3 mainly cause increases in ADCC without much change in ADCP. In the rectal tissues, high IgG1 at any level of IgG3 causes a steep increase in ADCP, a pattern which is not present in other tissues. These results could be important for potential local boosting interventions, or for modeling antibody decay in different tissues. Likewise, if ADCC is thought to be protective against HIV transmission,[164–166] interventions like increase ADCP (like increasing IgG1) in the rectal tissue could actually be harmful, while increasing IgG1 or IgG3 in the penile tissue would have an advantageous affect. Furthermore, we explored how polymorphism combinations affect FcR effector functions in the mucosal tissues. Unlike in the blood model, polymorphisms did not make as much of a difference in the balance of ADCP and ADCC in the tissues, likely because of the much smaller scale of antibody levels putting the landscape in a region in which FcR-antibody affinity is not as sensitive of a parameter as antibody concentrations (**Supplementary Figure C-3**).

4.5 Discussion

Overall, our polyfunctionality two FcγR model helped to unravel complex dynamics involving the balance between ADCP and ADCC in HIV immune responses. In particular, the model non-intuitively challenges the "more is better" assumption that increasing antibody levels in the blood always leads to increases Fc effector functions. Due to the competition between IgG subclasses for the antigen, more availability of one or another subclass can lead to skewing of the system towards maximizing one or the other antibody-dependent Fc responses, but not both. Increasing IgG1 leads to increases in ADCP, but decreases in ADCC and increasing IgG3 increases ADCC, but decreases ADCP. The overall maximum for ADCC or ADCP does not occur at a maximum of both antibodies; rather, it occurs at an intermediate value.

When examining patient data from the RV144 clinical trial and adjusting for the experimental dilution to represent dynamics in vivo in the blood, we can see that the patient values fall close to the baseline parameters used for our model. The patients fall on a sensitive region of the landscape with a large gradient, such that increases or decreases in IgG1 or IgG3 lead to significant differences in Fc effector functions. While one may predict that simultaneous boosting of IgG1 and IgG3 might maximize both Fc effector functions, there is no significant different in complex formation from baseline due to patients falling on the intersection of the two FcγR surfaces.

Polymorphisms have also been shown to be of importance for heterogeneity in responses and we are able to directly model this with the two FcγR model. The 2aH/3aF and 2aR/3aV polymorphism combinations had the largest statistically significant difference between complex formation. The 2aR/3aV genotype is the only genotype for which FcγRIIIa formation is always greater than FcγRIIa, meaning that these individuals would be ADCC dominant in most scenarios and may have more difficulty maximizing ADCP in comparison to those with the high affinity FcγRIIa polymorphism. Interestingly, when we evaluated the polymorphisms across the mucosal tissues, we did not see a large difference in complex formation in the mucosal tissues as we had seen previously in the blood. This is likely due to the much lower levels of antibody present in the mucosa, changing the limiting reagents for Fc complexes to form.

As expected, due to the larger number of monocytes in the rectal mucosa, ADCP is the more prominent function in this tissue type, which may explain the higher rates of transmission via anal sex acts. The rectal mucosa is also paired with a very high antigen load, which we know can also increase transmission. The penile tissue and semen had lower levels of antigen, and mostly NK cells which leads to prominence of ADCC. The blood has a mixture of the two functions as

discussed previously, but has much higher levels of antibodies than the mucosal tissues, leading to overall higher Fc effector responses.

In summary, the expansion of a theory-driven model to include a representation of polyfunctionality of Fc responses was able to accurately depict previously observed experimental patterns in immune responses, but it was also able to provide important insights about how the combination of IgG1 and IgG3 levels may contribute to paradoxical decreases in opposing FcR effector functions. Furthermore, by mimicking the local environment, we were able to better predict how interventions may affect immune response. The model could be applied in the future to develop potential new therapies, such as mucosal boosting, modulation of primary resident cell type, or alterations in binding affinities. We believe that this approach provides unique insight into mechanisms of antibody competition and polyfunctionality that are otherwise difficult or impossible to study clinically.

4.6 Methods

4.6.1 Computational methods

4.6.1.1 System of Ordinary Differential Equations (ODEs) (adapted from Lemke et al. 2021)[9]

We expanded the system of ODE equations established in Lemke et al. (2021) to account for the potential binding of antigen-bound IgG dimers to multiple different classes of FcγRs, thereby considering potential competition between substrates and receptors within the system. The env-IgG-FcγRIIa and -FcγRIIIa framework is illustrated in the schematic shown in **Figure 4-1**. The system of equations is written using the laws of mass action kinetics, in combination with conservation equations for total antigen, total FcR, and each IgG subtype. We assumed no degradation or production of species over the short time span of the model. The initial IgG subclass

concentrations were estimated from Raux et al. (2000)[167] based on gp120 antigen-specific IgG1 and IgG3 EU/mL values measured in the serum, seminal secretions, and rectal secretions in HIV-type 1 infected subjects (asymptomatic CDC stage II/III infection). The IgG2 and IgG4 were found to be very low in HIV-infected individuals and were estimated to be 100 EU/mL and 10 EU/mL respectively. The EU/mL values were then converted to estimated concentrations based on total IgG concentration measured in untreated HIV-infected individuals in Pillay et al. (2019)[168] and subsequently using the expected proportions of each subclass in serum, seminal secretions, and rectal secretions to calculate the subclass concentrations across each tissue. The antigen concentrations in each tissue were obtained from Zuckerman et al. (2004),[169] in which HIV RNA levels were measured in untreated HIV-infected individuals in the plasma, rectum, and semen. The RNA levels were converted to nanomolar concentrations assuming 20 envelope proteins on the surface of each virus[170] and then using Avogadro's number. The FcR concentrations were calculated based on a study by Cheeseman et al. (2016)[171] in which they measured the distribution of CD14+ monocytes and natural killer (NK) cells in whole blood, penile tissue, and colorectal tissue. They then used flow cytometry to characterize the expression of various Fc receptors on the different cell types. We used these values accounting for the distribution of cell types in each tissue and then the expression of FcγRIIa and FcγRIIIa on each cell type to calculate a summed total FcγR concentration for each tissue type. **Supplementary Table C-1** and **Supplementary Table C-2** contain a summary of the affinity and concentration parameter values and sources for the model respectively.

The initial concentration of each complex was set to zero and binding affinities for lgG1, lgG2, lgG3, lgG4, and FcγR dimers were set based on literature values.[162] Envelope binding affinities were determined via SPR measurements as described in ***4.6.2.3*** (**Supplementary Table**

C-1). We obtained K_As for each IgG subclass binding to FcγRIIIA-V158 from the literature[162] and converted these K_As to k_{on}s by estimating a universal k_{off} from pooled RV144 serum samples (0.01 s^{-1}), as done in Lemke et al. (2021).[9] MATLAB's ode113 solver function was utilized to predict the concentration of each complex over 10^5 seconds, with an absolute error tolerance of 1e-50 and a relative tolerance of 1e-10. We assumed sequential IgG antibody binding to antigen prior to engagement of any antigen-IgG-IgG complex with any FcγR dimer. We assumed no cooperativity in IgG binding antigen (such that affinity parameters were independent of the presence of another IgG on the same antigen). For antigen-IgG complexes containing two of the same IgG subclass we used literature values for the reported value of that subclass.[162] For complexes containing two different IgG subclasses, we averaged the two individual IgG subclass affinities.

4.6.1.2 MFI conversion to nM (adapted from Lemke et al. 2021)[9]

When plotting RV144 vaccinee data for boosting simulations, experimental MFI measurements (as described in ***4.6.2.2***) were converted to concentration measurements using a conversion factor based on a reference IgG1 concentration of 10,000 ng/mL,{Citation} as done in previous work by Lemke et al. (2021).[9] For multiplex readings, there is a log-linear relationship between MFI and concentration when measurements are within the machine's dynamic range.[172] Conversion formulas were based on this typical relationship. We assumed that MFI measurements were in the dynamic range, and that the average IgG1 concentration was 10,000 ng/mL. The conversion factor found for IgG1 was then applied to the remaining species within that given assay. The concentrations for species IgGn (where n = 1 through 4) were converted from assay concentrations to plasma concentrations by multiplying by a factor of 200 to account for dilution of plasma samples for the assay.

$$\text{Conversion Factor} = \frac{\log_{10} \text{Reference Concentration}}{\text{mean}(\log_{10} \text{MFI}_{\text{IgG1}})}$$

$$[\text{IgGn}] \text{ in nM} = \frac{10^{(\log_{10} \text{MFI}_{\text{IgGn}}) * \text{Conversion Factor}}}{\text{Molecular weight}_{\text{IgGn}}} * 200$$

4.6.1.3 Sensitivity analyses (adapted from Lemke et al. 2021)[9]

We first performed a one-dimensional sensitivity analysis across each of the tissues for the two FcγR model. This was done by calculating the model output (FcγRIIa complex formation and FcγRIIIa complex formation) at the baseline parameter value, and then also varying each parameter, one at a time across a physiological relevant range, from 0.05x the baseline parameter to 20x the baseline. The outputs of the model are shown in **Figure 4-2**, where red indicates higher FcγR complex formation and blue indicates lower FcγR complex formation.

We also performed a global uncertainty and sensitivity analysis[173] using the baseline parameters described in ***4.6.1.1*** (results shown in **Supplementary Figure C-1**). In the global sensitivity analysis algorithm provided by the Kirschner lab at the University of Michigan (Figures 2B, 2C, S3, and S4), we assigned log-uniform probability density functions (pdfs) to each parameter (initial concentrations and affinities) with a minimum 0.05X of baseline and a max 20X of baseline for all parameters.[173] These pdfs were sampled using Latin hypercube sampling (LHS) to create random combinations of parameter values. The model was evaluated under each of the 2,000 sets of random parameter combinations, allowing for a multidimensional exploration of the system. Partial rank correlation coefficient (PRCC) calculated within the algorithm determined the correlation between each input variable's variance throughout multidimensional analysis and the output variable, giving a sensitivity measure for each parameter and a statistical significance of its effect on complex formation.

4.6.1.4 Generation of IgG1 versus IgG3 landscapes (adapted from Lemke et al. 2021)[9]

625 simulations were run with differing combinations of initial IgG1 and IgG3 concentrations with tissue-specific baseline values for all other parameters. All combinations of 25 IgG1 and IgG3 concentration values were uniformly spaced on a logarithmic scale between 0.001X-1000X baseline concentrations. Results were plotted as a grid surface for each FcγR, with FcγRIIa (green) and FcγRIIIa (purple) complex formation across the IgG1 and IgG3 combinations plotted on the same graph. Heatmaps showing the complex formation for each FcγR type were also generated (**Figure 4-3b**). Cross-sections at an intermediate value of IgG1 or IgG3 (100 nM) were visualized as well (**Figure 4-3c**).

For boosting simulations using RV144 vaccinee data (**Figure 4-4**), we predicted individual FcγRIIa and FcγRIIIa complex formation (n = 105) based on IgG subclass 1-4 concentrations. Individuals were plotted as circles at their specific IgG1 and IgG3 initial concentrations with their individually predicted complex formation concentration. Simulations of IgG1, IgG3, or simultaneous IgG1 and IgG3 boosting were performed at 10x personal baselines. Ordinary one-way ANOVA and Tukey's multiple comparison test were performed to determine significance across the different boosting simulations or FcγR polymorphisms. When evaluating the landscapes for the four different polymorphism combinations, the FcγR polymorphism and IgG class specific affinity parameters were taken from the literature, reported in **Supplementary Table C-1**. Example points A and B (using first and third quartile of IgG1 and IgG3 concentrations) were used for demonstration of differences in FcγR complex formation.

4.6.2 Experimental methods

4.6.2.1 RV144 samples (adapted from Lemke et al. 2021)[9]

RV144 phase III clinical trial plasma samples[174] were provided by the U.S Military HIV Research Program (MHRP). Samples from week 26 (2 weeks post vaccination) RV144 vaccine recipients (n = 30; n = 75 from two separate shipments) were evaluated using data from a previously published study.[48] All relevant human research ethics committees approved all experimental studies. All plasma samples were provided de-identified of demographics including gender and age.

4.6.2.2 HIV-specific multiplex IgG subclass and rs FcR dimer-binding assay (adapted from Lemke et al. 2021)[9]

HIV-specific IgG subclass and recombinant soluble FcγR (rsFcγR) dimer binding multiplex data was used from a previously published RV144 study.[48] Extracted multiplex data included previously published IgG1, IgG2, IgG3, IgG4, rsFcγRIIa-H131, rsFcγRIIIa-V158, rsFcγRIIIa-F158 dimer data from the customized multiplex or ELISA binding assays using HIV-1 Clade AE A244 gp120 (NIH AIDS reagents catalog #12569), HIV-1 Clade B BAL gp120 (NIH AIDS reagents catalog #4961) recombinant protein antigens and Influenza Hemagglutinin (HA) protein (H3/Switzerland/2013, Sinobiological) as a positive control antigen, as nearly all individuals have previously been exposed to Influenza A virus.

These dimeric rsFcγR assays have been applied to several HIV and other infectious disease studies, which have demonstrated that they correlate with and hence are predictive of in vitro cell based ADCC and ADCP assays.[48,56,69–71] All multiplex data was reported as an arbitrary Median Fluorescence Intensity (MFI).

4.6.2.3 Surface plasmon resonance (adapted from Lemke et al. 2021)[9]

SPR was conducted as previously described.[175] Briefly biotinylated gp120 BAL (NIH AIDS Reagents) was immobilized onto a SA sensor chip at approximately 300, 500 and 800 response units. A blank flow cell with no immobilized ligand was used as a reference flow cell. Injections of 60 µl of purified HIV-IgG (NIH AIDS Reagents program) at 1:3 dilutions ranging from 0.5 to 0.006 mg/ml were passed across flow cells at a flow rate of 20µg/ml, with subsequent 360 s dissociation time to determine IgG disassociation. Regeneration after each injection used two pulses of 10mM glycine HCl, pH 2.5. SPR measurements were conducted in HBS-EP buffer (0.01M HEPES (pH 7.4), 0.15M NaCL, 3mM EDTA, 0.005% [vol/vol]). Kinetic data was calculated using BIA evaluation program, with data being fitted to the simplest 1:1 langmuir binding model.

4.6.2.4 Software (adapted from Lemke et al. 2021)[9]

ODE modeling, sensitivity analyses, and 3-D plots were completed using MATLAB 2022b (MathWorks, Natick, MA). Visualization of the remaining plots, and statistics were completed using GraphPad Prism version 10. Custom MATLAB code is available to run the simulations necessary to generate the data and figures (steady state complex formation concentrations) used in this analysis.

4.6.2.5 Statistical analysis (adapted from Lemke et al. 2021)[9]

Statistical significance for the IgG boosting vaccinee simulations and polymorphism simulations were determined using an ordinary one-way ANOVA performed in GraphPad Prism with multiple comparisons and the Tukey test with a single pooled variance and no matching or pairing ($\alpha = 0.05$). Statistical significance denoted with adjusted p-value less than 0.05 shown with one asterisk, less than 0.01 with two asterisks, continuing down to less than 0.0001 with four asterisks.

Chapter 5 Conclusions and Discussion

5.1 Scientific contributions

In this work, we demonstrate the flexibility and capability of computational system serologies techniques to learn more about infection and autoimmune disease. In summary, here are several key themes about the insights our models were able to provide.

5.1.1 Elucidating heterogeneity across diseases

Overall, our data-driven and theory-driven approaches helped us gain new ideas about which antibodies are key players involved in heterogeneity of disease, whether based on a demographic group, disease severity, or transmission rates. By evaluating three different diseases (COVID-19, Sjogren's syndrome, and HIV) we demonstrate how different systems serology approaches add value, depending on the data available and the posed questions. In **Chapters 2 and 3**, COVID-19 and Sjogren's syndrome both presented situations with a plethora of high-throughput antibody and FcR data, where little was known about the disease and underlying biology. Data-driven approaches were useful in both cases for classifying immune responses based on heterogeneity within a disease presentation. Our model identified antibody signatures that distinguished groups based on demographics (COVID-19) or disease state (Sjogren's). In **Chapter 2** we focused on cross-reactive SARS-CoV2 antibodies that differentiated healthy children and elderly individuals, though we have also used the approach to understand heterogeneity of responses within a family in which the parents were virologically positive and the children mounted targeted SARS-CoV-2 antibody responses (without ever testing positive for the virus),[11]

in addition to another study distinguishing between mild and severe COVID-19 disease by looking at the Ab responses in the respiratory secretions in comparison to the blood.[176] In **Chapter 3**, we used the same approach to identify differences in Ab and FcR activation between healthy individuals and Sjogren patients, as well as between seronegative Sjogren's patients and non-Sjogren's Sicca patients. Applying data-driven techniques here helped us understand how Abs are intertwined in relationship with FcRs in a disease where the underlying mechanisms are largely unknown.

In contrast, in **Chapter 4**, we used a mechanistic model to explore the heterogeneity of Ab responses in HIV infection and vaccination. In contrast to Sjogren's and COVID-19, more knowledge is available regarding immune responses and Fc activation in HIV; thus a theory-driven model is useful for testing hypotheses that would otherwise be difficult to explore experimentally or clinically. We expanded on a previous ODE model of single FcR activation[9] to include both receptor FcγRIIa and FcγRIIIa and explore polyfunctionality (ADCP and ADCC effector functions) or simultaneous competition between Abs and receptors in a multiple FcR environment. Our results found that ADCC was protective against transmission in the penile tissue, while ADCP was more prevalent in the rectal tissue where transmission rates are highest. Our model confirmed results seen experimentally in vaccine trials and transmission studies, also providing mechanistic insights regarding Fc effector functions in mucosal tissues, where sampling can be challenging and clinical studies are not performed easily. Through the lens of systems serology and Fc receptor activation, we were able to better understand the variability in disease presentation and new mechanisms that link antibody features to FcR activation and effector functions.

5.1.2 Developing diagnostic tools

In one of our COVID studies, we discovered (what would later be confirmed in many studies) that individuals, especially children, can be exposed to SARS-CoV-2 and mount antigen-specific antibody responses without ever testing virologically positive. This was an important concept early in the pandemic as a challenge in diagnostics for identifying individuals who could be spreading the disease. The data-driven model also provided a better understanding of the differences in Ab responses between people with variable severity of symptoms (or lack thereof) on presentation. In Sjogren's, our data-driven approaches provide valuable biomarkers which could be used for improved diagnostics. Current diagnosis relies on high Ab responses to classical antigens in addition to a particular clinical presentation. Our more nuanced approach could help identify sets of Abs, including Abs to non-classical antigens, that could aid in diagnosis. Furthermore, there remains the challenge of diagnosing individuals with Sjogren's syndrome who are seronegative on basic testing for classical antigens, and our model identified a set of additional biomarkers that could be used to distinguish between healthy, non-Sjogren's, and seronegative Sjogren's patients. Collectively, these studies identified new relationships between Ab formation and FcR activation that could help improve diagnostics in the future.

5.1.3 Guiding vaccination and therapeutic interventions

In each of our studies, our results can help drive guidelines for vaccination, boosting, and other therapeutic targets for intervention. In our study on COVID, we found that elderly individuals, who tend to have more severe disease, had cross-reactive antibody responses that were not specific to SARS-CoV-2. These results help inform Ab-based SARS-CoV-2 vaccine strategies, which subsequently went on to be developed with specific targeting of SARS-CoV-2 antigen to develop neutralizing Abs. It also provided information about potential for expanding vaccine strategies beyond neutralization based on the importance of FcR activation in COVID-

19. The information is also useful for guidelines for boosting as well as future convalescent plasma therapeutic trials.

In our Sjogren's study, our model revealed the importance of FcγRIIa responses to the Ro and La classical antigens, which could be important for new therapeutic strategies. Since the role of FcγRs in Sjogren's is still unknown, our results provide new indications that FcγRs could be a target for decreasing autoimmune activity through drugs or other interventions.

Lastly, in our HIV study, we found that simulated boosting or "more antibody" did not always maximize Fc effector functions and that there is a compromise that takes place between Ab subclasses leading to elevated ADCP or ADCC depending on the individual circumstances and potential boosting interventions. This also introduces the concept of how local boosting (mucosal Ab transfer) could potentially provide important changes to the environment leading to alterations in transmission or viral load.

5.2 Limitations

While systems serology can be extremely useful for understanding complex antibody systems across multiple disease applications, there are several limitations of our work that must be considered.

5.2.1 Early pandemic constraints

Our study on antibody-responses in COVID-19 was conducted very early on during the pandemic, during a time at which little was known about the pathogenesis and treatment of the SARS-CoV-2 virus. Pre-pandemic samples were used as healthy controls, which would likely be less relevant now, given the widespread exposure to SARS-CoV-2 and global vaccination efforts. The cohort of COVID-19 infected individuals was quite small but was an important first step in

understanding heterogeneity of disease severity based on age. The small sample size of the study also made it difficult to elucidate protective or risk-associated effects of HLA alleles. Since then, several studies have been published using larger datasets and have found several associations: the HLA-C*04 and HLA-B*35 carrier states were linked with more severe infection, HLA-B*15 was associated with asymptomatic infection, and HLA-DQB1*06 alleles were associated with decreased breakthrough infections.[177–180]

5.2.2 Lack of validation cohort

Another limitation of our studies is the lack of a validation cohort. For our COVID-19 data-driven study and our Sjogren's syndrome data-drive study, we identified a set of biomarkers associated with a group of interest. Our models are created using a subset of the data as the training set and reserving a small fraction of samples as a test set. However, in order to appropriately confirm our findings, it would be important to apply our antibody signature to a new sample set different from the training cohort to ensure that the results are reproducible across different populations. This would also help generalize the results beyond the study population for a broader applicability in clinical practice. Due to limited sample access, we were unable to perform validation studies, and thus we do not have as strong of an evidence base to draw conclusions.

5.2.3 Limitations of the multiplex assay and ODE model

As with all experimental models, there are some assumptions made to represent the system we are modeling as closely as possible. In the case of the multiplex assay, we often need to dilute the plasma samples for the MFI to be in a dynamic range. For example, IgG values in Sjogren's tend to be extraordinarily high and, in order not to maximize out the readings such that there is no variability between people, dilutions must be done. Likewise, some antibodies at very low

concentrations may not be in the dynamic range of the system. The background signal is subtracted for each feature but deciphering between background and low-level binding can still be a challenge. There are measures taken and quality control to prevent these from affecting the results, but it remains a consideration.

Additionally, for our theory-driven model we need to convert MFI to concentrations, which is difficult to do given the above constraints. The relationship between fluorescence intensity and concentration is non-linear and there is not a standard calibration method. Thus, as per Lemke et al. (2021)[9], we developed a conversion method using a reference concentration of expected IgG1 levels in the blood. This makes our results less useful for absolute concentration predictions, but still maintains relative concentration predictions for comparison between individuals on a rank-order basis. The actual reference concentration is likely dependent on many factors, including the disease and antigen considered.

It is a challenge to identify physiologically accurate parameters in the literature across many different diseases. HIV presents a unique challenge because the parameters can fall across a wide range depending on the timeline of infection: parameters can be vastly different for acute infection versus chronic infection. In our study, we assumed that penile tissue FcR expression is related to semen antigen and antibody concentrations, although these are different environments as well. Our global sensitivity analysis accounts somewhat for the potential wide range of physiologically relevant parameters possible and helps us evaluate the model across many possible parameter sets, but it is important to consider that there are a wide range of definitions for HIV infection that can result in vastly different parameter sets. Additionally, at extreme parameter values, computation time can increase drastically leading to the need for pursuing different ODE solvers, thereby making it somewhat difficult to assess all possible parameter sets.

Lastly, our model uses Fc complex formation as a surrogate for downstream Fc effector functions themselves. This assumption is reasonable for our purposes given the high association of levels of FcγRIIa with ADCP and FcγRIIIa with ADCC, but the assumption is not perfect. We would also like to link these functions by confirming with cellular assays, such as the cellular phagocytosis assay used in **Chapter 3**, but our model currently does not account for the downstream cellular effector functions given the constraints of potential measurements within the multiplex assay.

5.3 Future directions

5.3.1 New theory-driven model applications: COVID-19 infection and vaccination

As discussed in **Chapter 2**, SARS-CoV-2 is an example of a virus capable of evading neutralization through the development of new Variants of Concern. Thus, Fc effector functions may be important for sustained immunity. Our group plans to use theory-driven mechanistic models to unravel how SARS-CoV-2 variant-related changes in IgG subclass distributions and binding can influence IgG-FcR complex formation. Additionally, given the new research that has linked certain genetic profiles with increased or decreased risk of infection, application of a theory-driven model could help determine the role of host genetics, including IgG1 allotypes and FcR polymorphisms, in the formation of immune complexes. Furthermore, there have been several vaccines (including Pfizer-BNT162b2, Sinovac-CoronaVac, and Moderna bivalent booster) developed to protect against COVID-19 infection and there has been some hesitancy and controversy surrounding boosting schedules.[181] Because our model is uniquely suited to mimic boosting, this provides an excellent opportunity to learn more about the complex dynamics of changes in IgG subclass concentrations resulting from boosting. Using computational systems serology approaches to explore IgG-FcR complex formation in response to infection or vaccination

will help drive vaccine and therapeutic development, boosting criteria, future targets for vaccine modifications, and different potential vaccine or therapeutic mechanisms to maximize Fc effector functions.

5.3.2 Linking antibody neutralization and other Fc effector functions

In this study, we expanded an ODE model to consider a complex system consisting of multiple Fc receptors and antibodies competing for antigen and substrate in order to activate antibody-dependent cellular functions. However, there are other opportunities to build on our framework to better represent the spectrum of functions in antibody responses. First, our model only considers antibodies used for Fc activation, while antibody neutralization is a huge component of protection from pathogens. Expanding the model to include antigen-specific antibody neutralization would help better understand the balance between neutralizing and non-neutralizing antibodies, especially since neutralizing antibodies play such a key role in protection from diseases like SARS-CoV-2. Furthermore, neutralizing monoclonal antibodies quickly became an important area of interest for treating COVID-19 disease during the pandemic and were approved for emergency use authorizations in November 2020.[182] Development of new monoclonal antibodies continues and early monoclonal antibody use has been associated with lower risk of hospitalization or death.[182] Similarly, neutralizing monoclonal antibody development has been an ongoing area of research for preventing HIV infection.[183] Monoclonal antibody treatment use could be mimicked in our model by expanding the system to include antibody binding to IgG that further blocks binding of Fc receptors. This element would help us evaluate neutralization and Fc effector functions in parallel to better understand the relative importance of parameters in the system and balance between these important immune functions. Complement-dependent cytotoxicity (CDC) is another Fc effector function that would be interesting to explore

as part of our mechanistic model. Complement activation is an important part of the immune system that is relevant for many infectious and autoimmune diseases.

5.3.3 Diagnosing autoimmune disease

As discussed previously in **Chapter 3**, diagnosing autoimmune diseases can be challenging due to non-specific symptoms that can overlap with many conditions, heterogeneity of symptoms, complex clinical diagnostic criteria, and inaccessibility of specialized laboratory tests. In particular, with Sjogren's syndrome, it is not yet fully understood how and if non-classical autoantibodies play a role in pathogenesis.[184] While our initial results have revealed an association between antibodies to many non-classical antigens, further studies are needed in order to link this to a mechanism involved in disease pathogenesis. Theory-driven models could also be useful in the future to test hypotheses about mechanisms involved in FcR activation in Sjogren's. These data- and theory-driven techniques could also be applied to other autoimmune diseases, including diseases which have more background knowledge on links between FcR activation and disease status.

We also hope to explore heterogeneity in disease severity in Sjogren's syndrome by attempting to identify antibody signatures that can distinguish between more active disease versus inactive disease. Preliminary unpublished results show elevated FcγIIa responses are associated with more severe Sjogren's syndrome (**Appendix D:** Preliminary cellular assays also confirmed higher levels of phagocytosis in more severe disease (**Supplementary Figure D-5**). There appeared to also be a trend showing that increased glycosylation (more galactose residues, G2) was associated with less severe disease, while decreased glycosylation (G0) was associated with more severe disease (**Supplementary Figure D-6**). Larger sample sizes and further studies are needed in order to further explore the link between disease severity and Fc receptor activation.

5.4 Overall conclusions

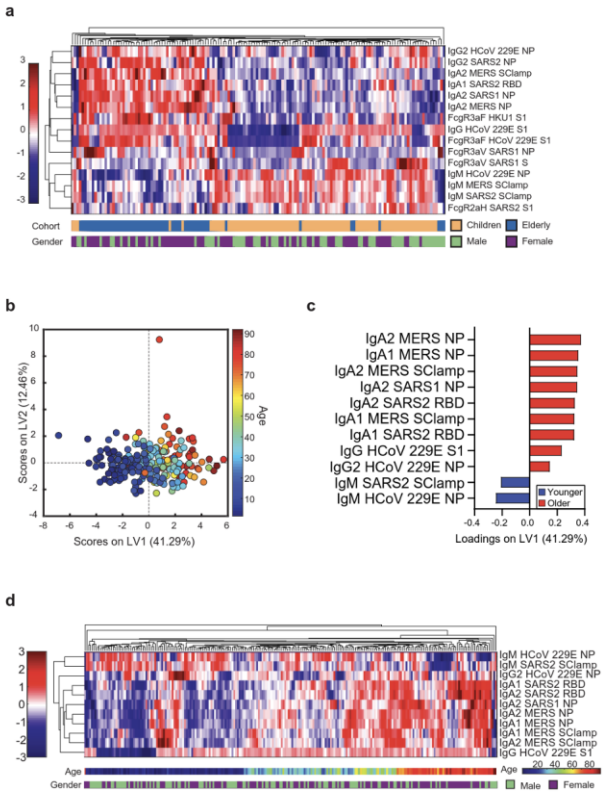
Overall, in this work we have provided novel insights using systems serology approaches applied to two infectious diseases (COVID-19 and HIV) and an autoimmune disease (Sjogren's syndrome). Based on the existing knowledge of the disease, we used data-driven approaches as an exploratory initial step when disease pathogenesis is not fully understood and used theory-driven approaches for more thoroughly studied systems with predicted mechanisms. We were able to address heterogeneity of disease in multiple difference ways across diseases, including by disease severity between age groups, autoantibody seropositive versus seronegative patients, or differences in transmission across tissues. Our methods and models are widely applicable to many infectious and autoimmune diseases and have the potential to provide important insights into patterns and mechanisms valuable for disease.

Appendices

Appendix A: Supplement to Systems Serology Detects Functionally Distinct Coronavirus Antibody Features in Children and Elderly

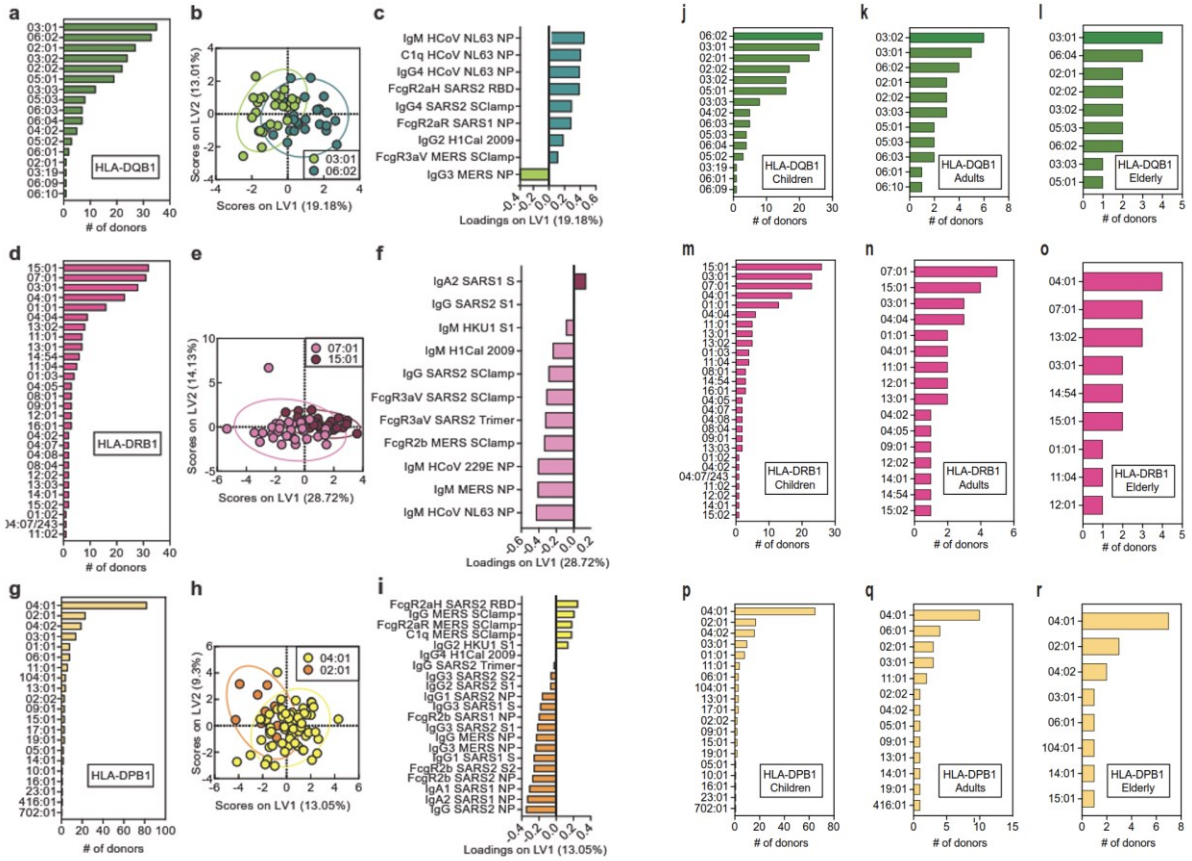
Supplementary Figure A-1: SARS-CoV-2 serological signatures differ between healthy children, adults, and elderly

(a) Hierarchical clustering of Elastic-Net selected features for children and elderly. Levels are coloured from low (dark blue) to high (dark red). PLSR model scores plot (b) loadings plot (c) for all healthy patient data on Elastic-Net 11-feature signature. The model goodness of fit (R2) was 0.6421 and goodness of predication (Q2) was 0.6144. Percent variance explained by each latent variable in parentheses. (d) Hierarchical clustering of signature in (b-c).



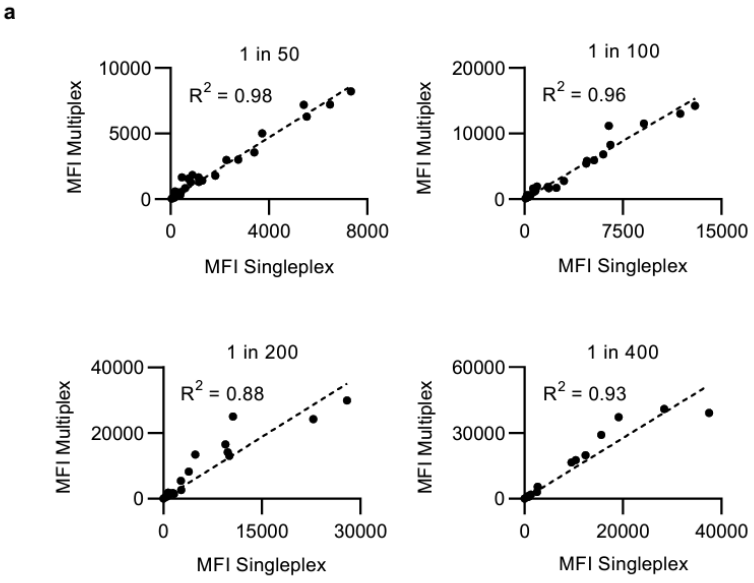
Supplementary Figure A-2: HLA class II alleles influence Ab signatures

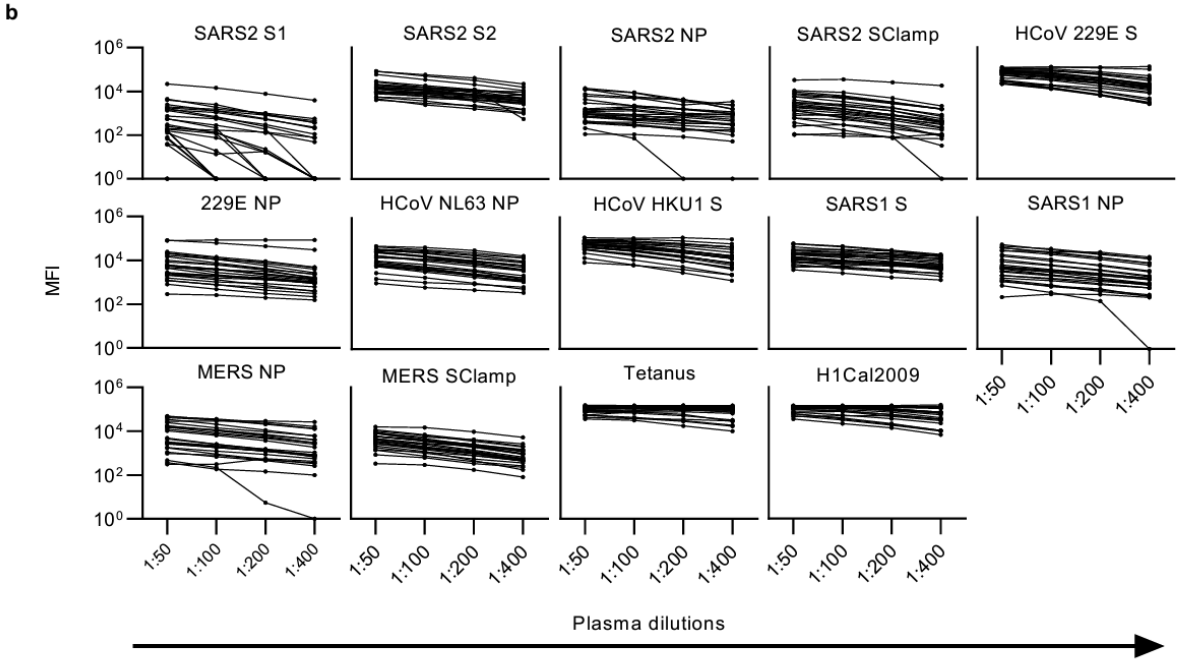
HLA-DQB1, -DRB1 and -DPB1 alleles in our healthy donor cohort (a,d,g), PLSDA scores (b,e,h) and loadings (c,f,i) plots using the Elastic-Net selected signatures for the two most frequent alleles (HLA-DQB1*03:01 and 06:02, 82.59% cross-validation accuracy, 86.44% calibration accuracy; HLA-DRB1*15:01 and 07:01, 76.32% cross-validation accuracy, 77.83% calibration accuracy; HLA-DPB1*04:01 and 02:01, 74.23% cross-validation accuracy, 82.44% calibration accuracy). Variance explained on each LV is in parentheses. Analysis was performed on a subset of the healthy individuals (n=111) for whom HLA class II type was available. Donors heterozygotes for the two most frequent HLA alleles were excluded from PLSDA and loading analysis. Distribution of HLA-DQB1 (j-l; green), -DRB1 (m-o; pink) and -DPB1 (p-f; yellow) alleles detected in healthy donor children (j, m, p), adults (k, n, q), and elderly (f, o, p). HLA class II alleles analyzed in figure 4 are indicated by a bold outline



Supplementary Figure A-3: Multiplex Assay setup and optimization

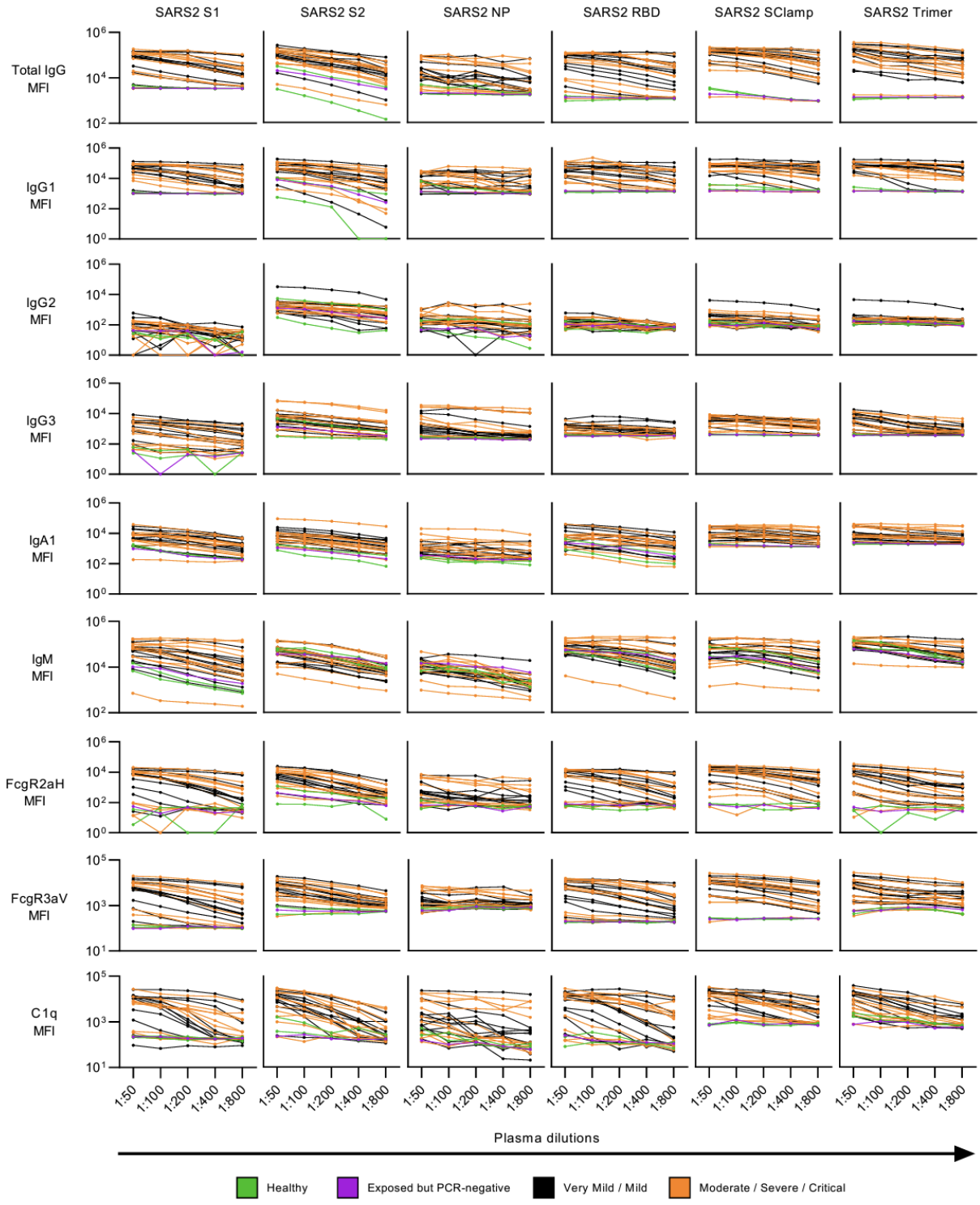
(a) Multiplex was validated by measuring a subset of healthy samples both in singleplex and multiplex. Strong correlations suggest that multiplexing did not affect measurement of Ab responses, especially at 1:50 and 1:100 dilutions. (b) Serial dilution of a subset of healthy samples against 14 antigens included in the custom multiplex assay to select dilutions where saturation was not observed. A final dilution of 1:100 showed not only strong correlation between singleplexed and multiplexed antigens, but was also not saturated for most antigens and was selected for subsequent assays.





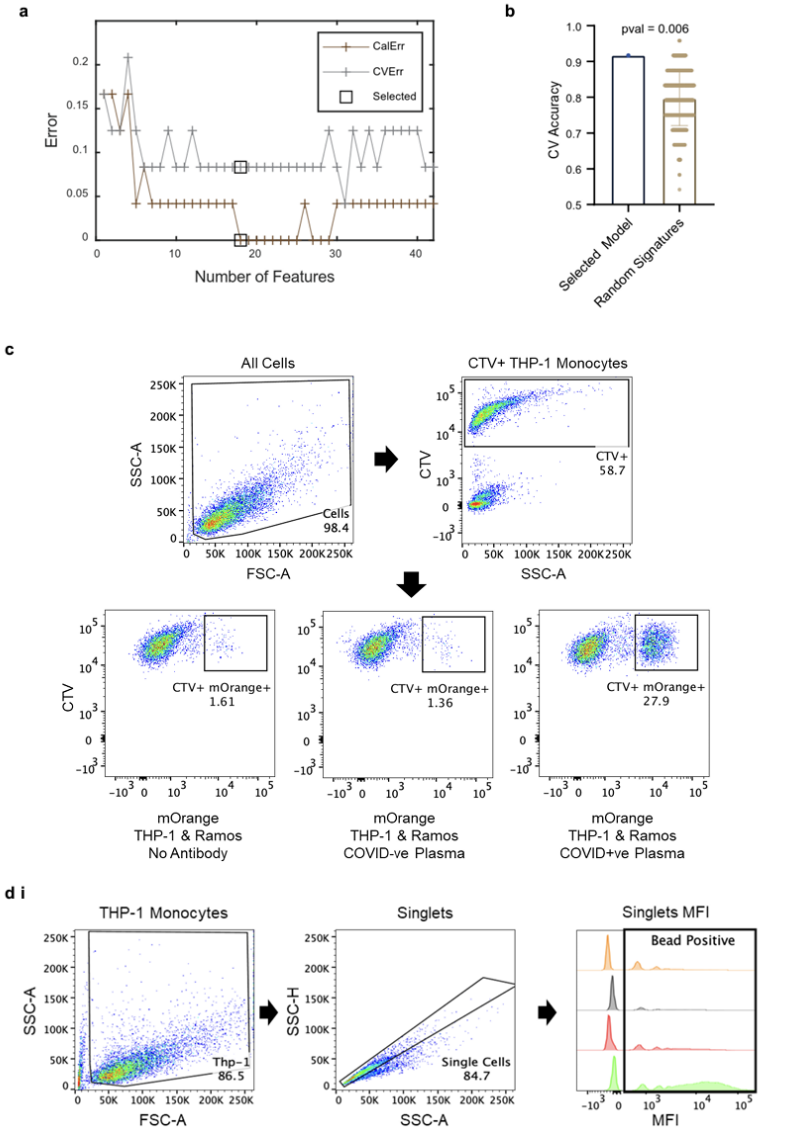
Supplementary Figure A-4: SARS2 Ab titrations

Serial dilutions of COVID-19 plasmas against the six SARS-CoV-2 antigens in the assay. Very mild and mild cases were coloured black, while moderate to severe cases were coloured orange. For comparison, two healthy elderly plasma were included (green). D1, who was SARS CoV-2-exposed but remained SARS CoV-2 PCR-negative, was also included (purple).



Supplementary Figure A-5: Accuracy of feature selection between COVID+ Children and Elderly model

An 18-feature model was selected from the 169 Ab features with 100% calibration and 91.37% Cross validation (CV) (a). CV accuracy of the selected model was compared with randomly selected antibody features (b).



	Sample ID	Bead Positive Cells		Phagocytosis score (x10^3)
		MFI	%	
	Uncoated beads	1894	47.9	9.07
	S-trimer beads-No Ab	1822	37.1	6.76
	S-trimer beads-COR98	1907	39.4	7.51
	S-trimer beads-CP04 T1	9374	77.4	72.55

Appendix B: Supplement to Systems Serology Identifies Novel Autoantibody Signatures for Sjögren's Syndrome Diagnosis

Supplementary Table B-1: Sjogren's related autoantigens, their known functions and the reported clinical manifestations in the respective seropositive patients

Autoantigen	Name	Use	Known function of the protein	Clinical association with the autoantibody	References
Ca6	Carbonic Anhydrase 6	Investigative / non-classical	Ionic exchange in acinar cells, potentially involved in salivary and lacrimal fluid production	Early form of SjS, seronegativity for Ro/La, glandular manifestations	Shen et al. (2012) [185]
Cfl1	Cofilin 1	Investigative / non-classical	Regulates organization of the actin cytoskeleton	MALT lymphoma	Cui et al. (2017) [186]
Chmr3	Muscarinic receptor M3	Investigative / non-classical	Acetylcholine-dependent glandular secretion	Glandular manifestations	Mona et al. (2021) [187]
Eno1	Enolase 1	Investigative / non-classical	Glycolysis, fibrinolysis, immunoglobulin production	MALT lymphoma	Cui et al. (2017) [186]
Ifi16	IFN gamma inducible protein 16	Investigative / non-classical	DNA sensor related to IFN pathway and inflammasome, anti-inflammatory	Glandular manifestations	Baer et al. (2016) [188]
La/SSB	Sjogren's Syndrome B	Clinical / classical	RNA protection from degradation	Systemic manifestations, lymphoma	Deroo et al. (2022) [189]
Mdm2	Mouse double minute 2 homolog	Investigative / non-classical	Nuclear-localized E3 ubiquitin ligase, binds to p53	Cytopenia, systemic manifestations	Liu et al. (2017) [190]
Rgi2	Rho GDP-dissociation inhibitor 2	Investigative / non-classical	Regulates organization of the actin cytoskeleton	MALT lymphoma	Cui et al. (2017) [186]
Ro52/SSA/ Trim21	Sjogren's Syndrome A/Tripartite motif containing-21	Clinical / classical	Cytosolic Fc receptor, ubiquitin E3 ligase, type 1 IFN pathway	Systemic manifestations, lymphoma	Deroo et al. (2022) [189]
Ro60/SSA/ Trove2	Sjogren's Syndrome A/Trove domain family member 2	Clinical / classical	RNA-binding protein, type 1 IFN pathway	Systemic manifestations, lymphoma	Hung et al. (2015) [106] Deroo et al. (2022) [189]4/3/2024 1:58:00 PM
Spt1	Salivary gland protein-1	Investigative / non-classical	Isolated from salivary glands	Early form of SjS, glandular manifestations,	Shen et al. (2012) [185]

				seronegativity for Ro/La	
Sptan1	Alpha fodrin	Investigative / non-classical	Movement of the cytoskeleton, interaction with calmodulin	Low specificity, neuropathy, seronegativity for Ro/La	Ulbricht et al. (2003) [191] Zheng et al. (2023) [192]4/3/2024 1:58:00 PM
Ssna1/NA14	Sjogren syndrome nuclear autoantigen 1	Investigative / non-classical	Microtubule-stabilizing and damage sensing protein	Seronegativity for Ro/La	Lawrence et al. (2021) [193]
Stmn4	Stathmin 4	Investigative / non-classical	Microtubule-associated protein, role in neurons	Neuropathy	Duda et al. (2017) [194]

Materials and Methods:

Plasma Sample collection:

Blood was collected from recruited patients in the Auvergne-Rhône-Alpes region in France between March 2018 and December 2019, as part of the I GET DRY (NCT03003572) multicentric cohort, after Ethics Committee (Comité de Protection des Personnes Est-III) approval under the reference IDRCB 2016-A01851-50. Blood was collected in BD Vacutainer™ SST™ II Advance Tubes (Becton Dickinson) and centrifuged for 15 min at 2500g to collect serum, which was frozen at −20°C until required.

Customized Sjogren's syndrome bead-based multiplex assay:[127,138,139]

A customized multiplex assay **(Table 2)** was designed including an array of relevant autoantigens: the classical autoantigens (Ro60/SSA, Ro52/SSA, La/SSB; AROTEC Diagnostics), as well as non-classical "investigative" autoantigens found to have some association with SjS syndrome in the literature (carbonic anhydrase 6 [Ca6], cofilin 1 [Cfl1], cholinergic muscarinic receptor 3 [Chmr3], enolase 1 [Eno1], interferon gamma-inducible protein 16 [Ifi16], La, mouse

double minute 2 homolog [Mdm2], rho GDP-dissociation inhibitor 2 [Rgi2], salivary gland protein 1 [Spt1], alpha fodrin [Sptan1], Sjogren's syndrome nuclear autoantigen 1 [Ssna1], stathmin 4 [Stmn4]; MyBioSource Inc., USA).

Tetanus toxoid (Sigma) and influenza hemagglutinin (H1Cal2009; Sino Biological) were also added to the assay as positive controls. Magnetic carboxylated beads (Bio Rad) were covalently coupled to the antigens using a two-step carbodiimide reaction, as per manufacturer's instructions. Briefly, beads were washed and activated in 100 mM monobasic sodium phosphate, pH 6.2, followed by the addition of Sulfo-N-hydroxysulfosuccinimide and 1-Ethyl-3-(3-dimethylaminopropyl) carbodiimide (Thermo Fisher Scientific). After incubation at room temperature for 30 min, the activated microspheres were washed three times and resuspended in 50 mM MES pH 5.0 (Thermo Fisher Scientific). The respective antigens were added to the activated beads and the mixture was incubated at room temperature for 3 h on a rotator in the dark. Subsequently, the beads were washed with phosphate buffered saline (PBS) and blocked with blocking buffer (PBS, 0.1% BSA, 0.02% Tween-20, 0.05% sodium azide, pH 7) for 30 min. Finally, beads were washed in PBS 0.05% sodium azide and resuspended as one million beads per 100 µl.

The isotypes and subclasses of SjS-specific autoantibodies present in the collected serum were assessed using a multiplex assay as described (Figure 1).[127] Using a black, clear-bottom 384-well plate (Greiner Bio-One), 20 µl of working bead mixture containing 1000 beads per bead region and 20 µl of diluted serum were added per well. From validation experiments in which cross-reactive antibodies present in healthy individuals were titrated, an optimal concentration of 1:800 working dilution of serum was selected for downstream assays. The plate was covered and incubated overnight at 4 °C on a shaker and was then washed with PBS containing 0.05% Tween-

20. SjS-specific autoantibodies were detected using phycoerythrin (PE)-conjugated mouse anti-human pan-IgG, IgG1-4, IgA1-2, IgM (Southern Biotech), at 1.3 µg/ml, 25 µl per well. After incubation at room temperature for 2 h on a shaker, the plate was washed before the beads were resuspended in 50 µl of sheath fluid. The plate was then incubated at room temperature for 10 min on a shaker before being read by the FlexMap 3D (Luminex). The binding of the PE-detectors was measured to calculate the median fluorescence intensity (MFI). Background subtraction was conducted by removing background of blank (buffer and beads only) wells.

For the detection of FcγR, biotinylated soluble recombinant FcγR dimers (higher affinity polymorphisms FcγRIIa-H131, lower affinity polymorphisms FcγRIIa-R131, FcγRIIb, higher affinity polymorphisms FcγRIIIa-V158, lower affinity polymorphisms FcγRIIIa-F158; provided by Bruce Wines and Mark Hogarth, Burnet Institute) were added at 1.3 µg/ml, 25 µl per well. After incubation at room temperature for 2 h on a shaker, the plate was washed, and streptavidin-R-Phycoerythrin conjugate (SAPE, Invitrogen) was added at 1 µg/ml, 25 µl per well. The plate was then incubated at room temperature for 2 h on a shaker before being washed and read as mentioned above. For the detection of C1q, C1q protein (MP Biomedicals) was first biotinylated (Thermo Fisher Scientific), washed and resuspended in PBS and tertramerized with SAPE. Tetrameric C1q-PE were added at 1 µg/ml, 25 µl per well, incubated at room temperature for 2 h on a shaker and then washed, and read as mentioned above. Assays were repeated in duplicate.

IgG antibody purification:

IgG antibodies were purified from the collected serum via Melon Gel chromatography according to manufacturer's protocol as previously described[143] (Melon Gel IgG Purification Kit, Thermo Fisher Scientific). IgG antibody samples were centrifugated through 100kDa Amicon

Ultra filters (Merck) at 14000g for 10 min to remove excess albumin proteins and buffer exchanged into PBS. The IgG concentration and purity were quantitated using a human IgG ELISA development kit (Mabtech AB). The IgG antibody samples were diluted in PBS to adjust concentration to 0.25 mg/mL. The samples were stored at -20°C until further use.

IgG N-linked glycosylation profiling:

N-linked glycosylation profiles of purified IgG antibodies were measured on the LabChip® GXII Touch instrument (PerkinElmer) according to the ProfilerPro glycan profiling LabChip® GXII Touch protocol as previously described.[143] Microchip capillary electrophoresis-laser-induced fluorescence (CE-LIF) analysis of digested and labelled *N*-linked glycans was performed. The relative prevalence of several glycosylation profiles of IgG antibodies were analyzed using the LabChip GX Reviewer (PerkinElmer) software. Peaks were assigned based on migration of known standards and glycan digests. Peak area and therefore the relative prevalence of each glycan pattern was calculated, and results were presented as mean ± standard error of the mean.

Bead-based THP-1 antibody-dependent phagocytosis assay:

To examine antibody-dependent cellular phagocytosis (ADCP) mediated by SjS' autoantibodies, a previously described bead-based assay was adapted.[144,195] Ro60/SSA was biotinylated using EZ-Link Sulfo-NHS-LC biotinylation kit (Thermo Scientific) with 20mmol excess according to the manufacturer's instructions and buffer exchanged using 30kDa Ultra filters (Merck) to remove free biotin. The binding sites of 1 μm fluorescent NeutrAvidin Fluospheres beads (Invitrogen) were coated with biotinylated Ro60/SSA at a 1:1 ratio overnight at 4°C. Ro60/SSA-conjugated beads were washed four times with 1% BSA/PBS to remove excess antigen

and incubated with serum (1:1600 working dilution) for 2 hours at 37°C in a 96-well U-bottom plate. THP-1 monocytes (100 000/well) were then added to opsonized beads and incubated for 22 hours under cell culture conditions. Cells were fixed with 2% formaldehyde and acquired on a BD LSR Fortessa with a HTS (Becton Dickinson). The data was analyzed using FlowJo 10.7.1 and a phagocytosis score was calculated as previously described[196] using the formula: (%bead-positive cells × mean fluorescent intensity)/10^5. Results were presented as mean ± standard error of the mean. To account for non-specific uptake of Ro60/SSA-conjugated beads, the phagocytosis scores for each serum sample were subtracted with that of the "no serum" control.

Feature selection using Elastic Net/PLSR and Elastic Net/PLSDA:

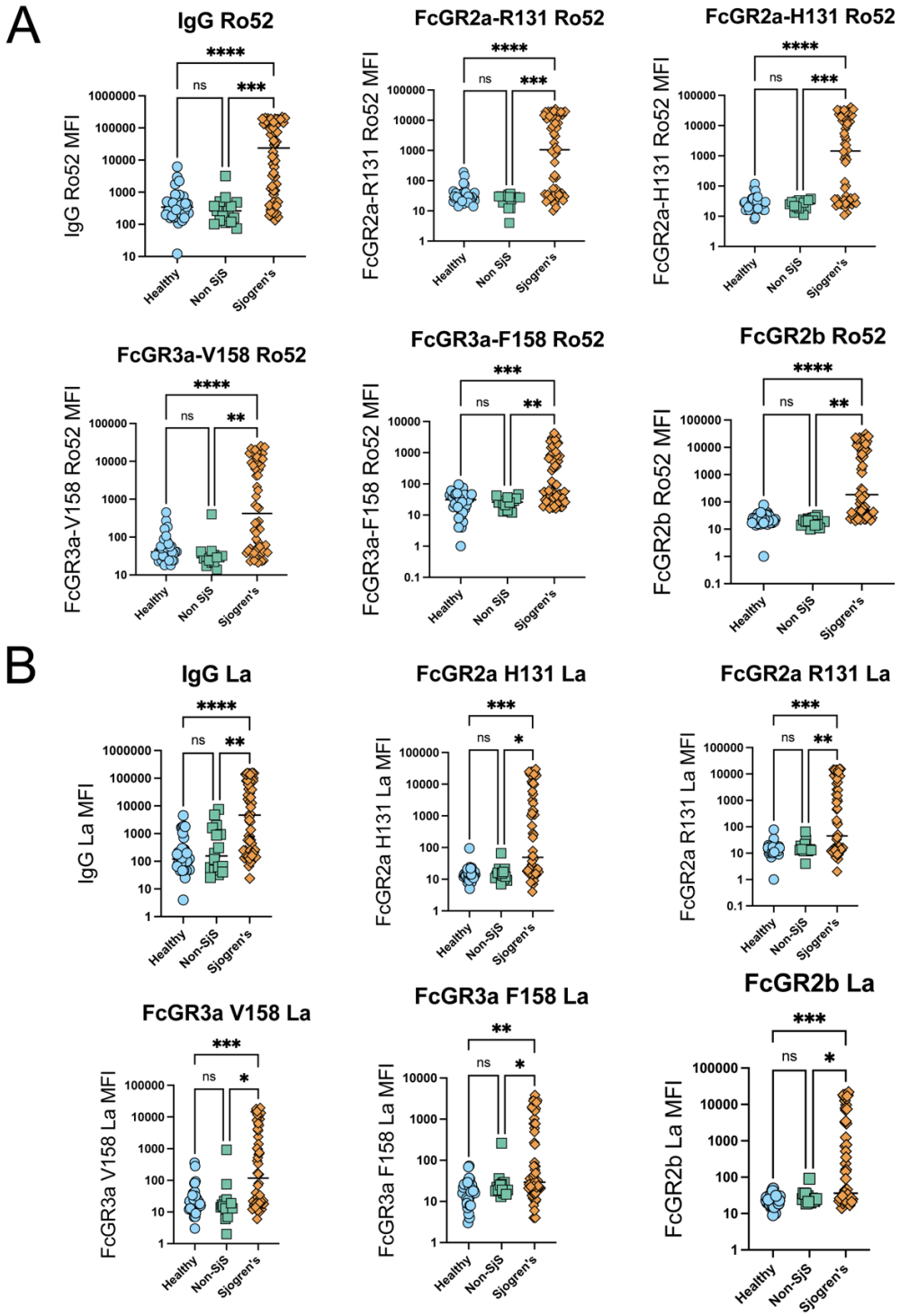
To determine the minimal set of features (signatures) needed to predict categorical outcomes (healthy, non-SjS Sicca, seronegative SjS, seropositive SjS) a three-step process was developed based on Gunn et al..[145] First, the data were randomly sampled without replacement to generate 2000 subsets. The resampled subsets spanned 80% of the original sample size or sampled all classes at the size of the smallest class for categorical outcomes, which corrected for any potential effects of class size imbalances during regularization. Elastic-Net regularization was then applied to each of the 2000 resampled subsets to reduce and select features most associated with the outcome variables. The Elastic-Net hyperparameter, α, was set to have equal weights between the L1 norm and L2 norm associated with the penalty function for least absolute shrinkage and selection (LASSO) and ridge regression, respectively.[197] By using both penalties, Elastic-Net provides sparsity and promotes group selection. The frequency at which each feature was selected across the 2000 iterations was used to determine the signatures by using a sequential step-forward algorithm that iteratively added a single feature into the PLSDA model starting with the feature

that had the highest frequency of selection, to the lowest frequency of selection. Model prediction performance was assessed at each step and evaluated by 10-fold cross-validation classification error. The model with the lowest classification error within a 0.01 difference between the minimum classification error was selected as the minimum signature. If multiple models fell within this range, the one with the least number of features was selected.

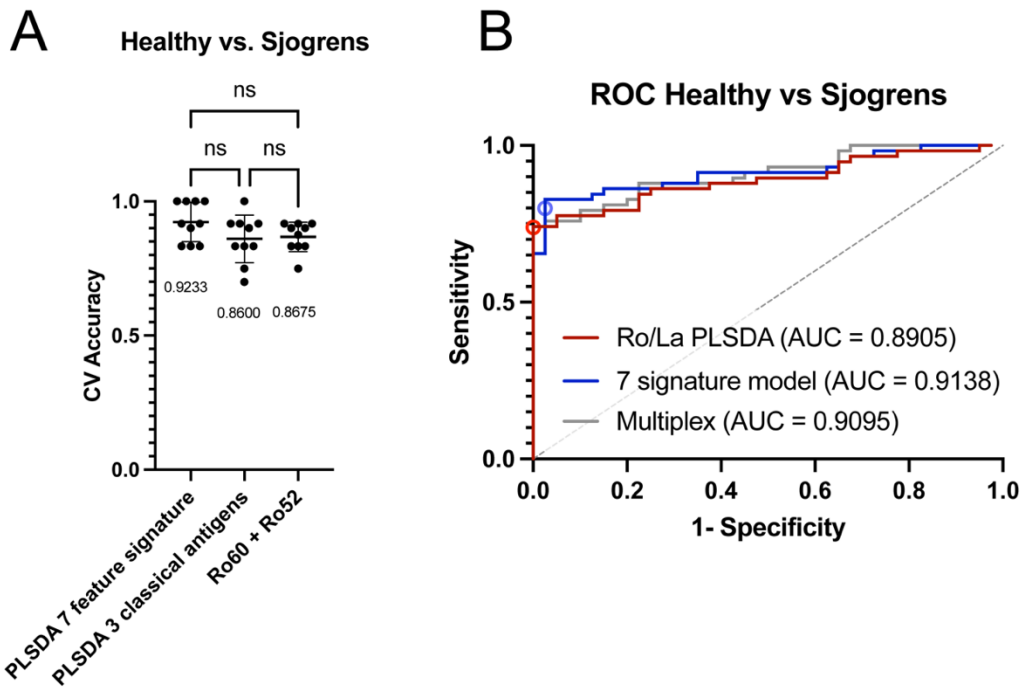
Supervised data-driven methods: Partial Least Squares Discriminant Analysis and Partial Least Squares Regression:

Partial least squares discriminant analysis (PLSDA) performed in the Eigenvector PLS toolbox in Matlab was used in conjunction with Elastic-Net (described above) to identify and visualize signatures that distinguish categorical outcomes (age cohort, COVID-19 infection status). This supervised method assigns a loading to each feature within a given signature and identifies the linear combination of loadings (a latent variable, LV) that best separates the categorical groups. A feature with a high loading magnitude indicates greater importance for separating the groups from one another. Each sample is then scored and plotted using individual response measurements expressed through the LVs. The scores and loadings can then be cross-referenced to determine which features are loaded in association with which categorical groups (positively loaded features are higher in positively scoring groups, etc.). All models go through 10-fold cross- validation, where iteratively 10% of the data is left out as the test set, and the rest is used to train the model. Model performance is measured through calibration error (average error in the training set) as well as cross-validation error (average error in the test set), with values near 0 being best. All models were orthogonalized to enable clear visualization of results.

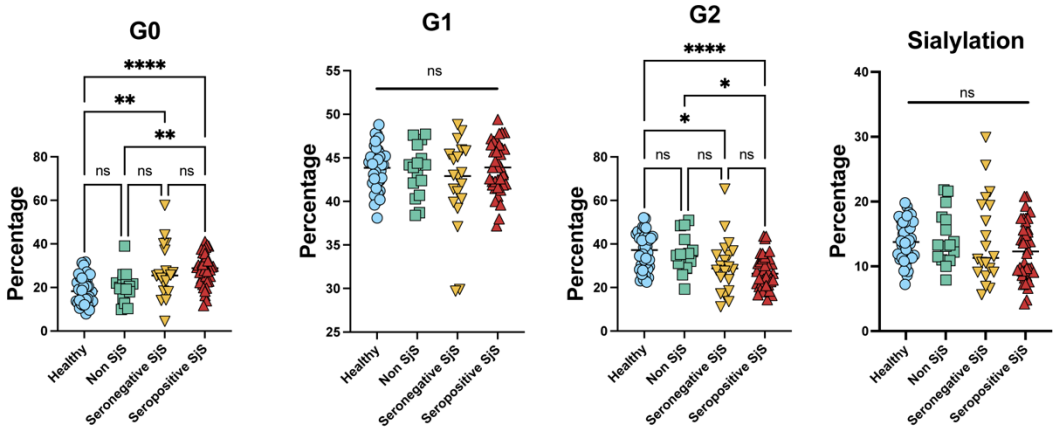
Supplementary Figure B-1: Univariate analysis across groups for Ro52 (a) and La (b) specific responses (healthy control, non-SjS sicca syndrome, and all Sjogren's syndrome). Significant differences denoted with asterisks



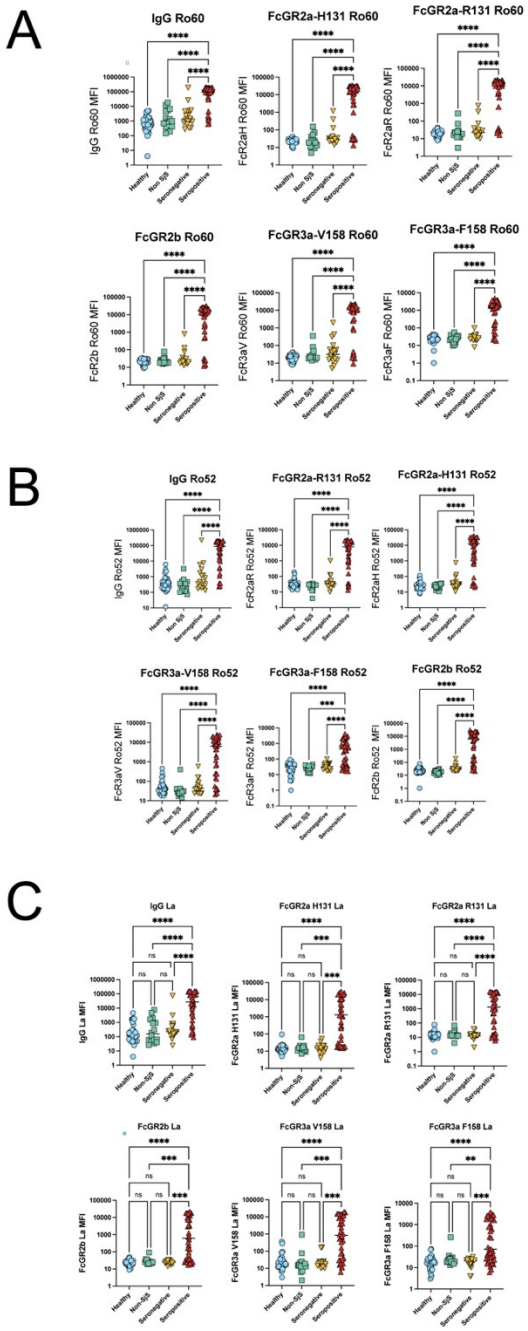
Supplementary Figure B-2: a) Comparison of cross validation errors for the models plotted in Figure 3d. ROC curve showing sensitivity and specificity for the classical antigen PLSDA model, our seven-feature signature Healthy vs. Sjogrens PLSDA model, and multiplex positivity.



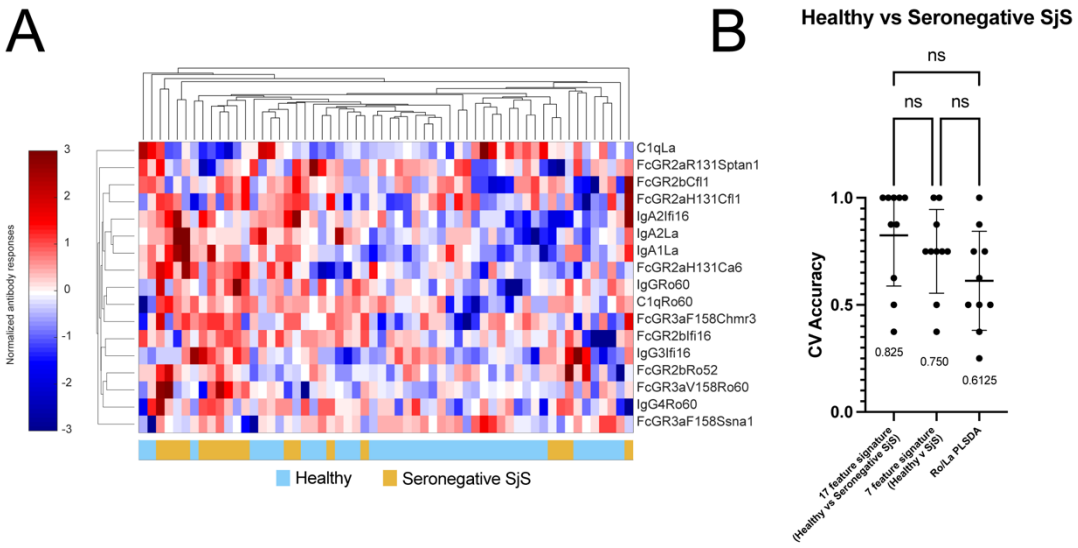
Supplementary Figure B-3: a) Glycosylation profiles from Figure 5a plotted by individuals across the different disease groups. b) Sialylation profiling showed no significant differences between groups



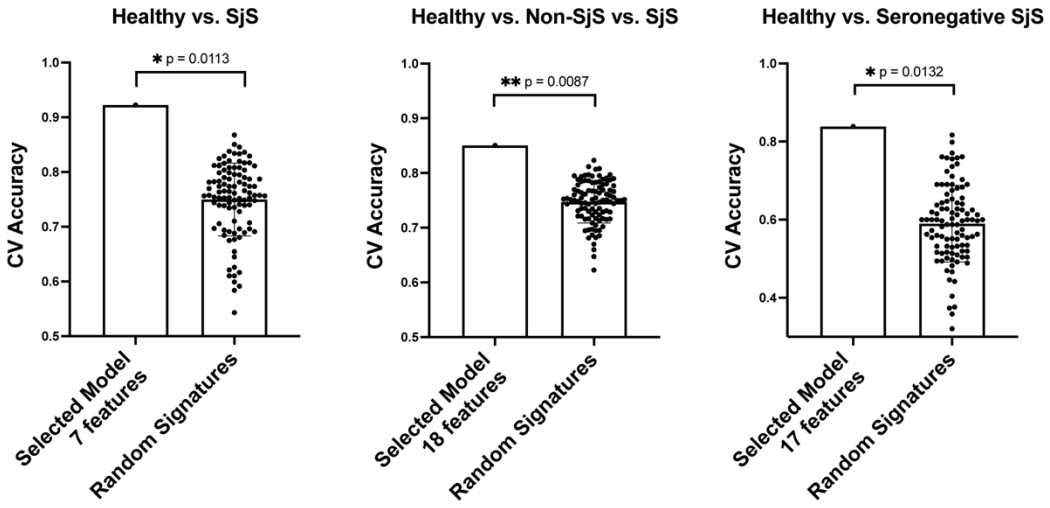
Supplementary Figure B-4: Univariate analysis across groups for Ro60 (a), Ro52 (b) and La (c) specific responses (healthy control, non-SjS sicca syndrome, and Sjogren's syndrome subdivided into seropositive and seronegative SjS). Significant differences denoted with asterisks.



Supplementary Figure B-5: a) Hierarchical clustering for seronegative vs. healthy model from Figure 6. b) Comparison of cross validation errors for the PLSDA models plotted in Figure 6d.



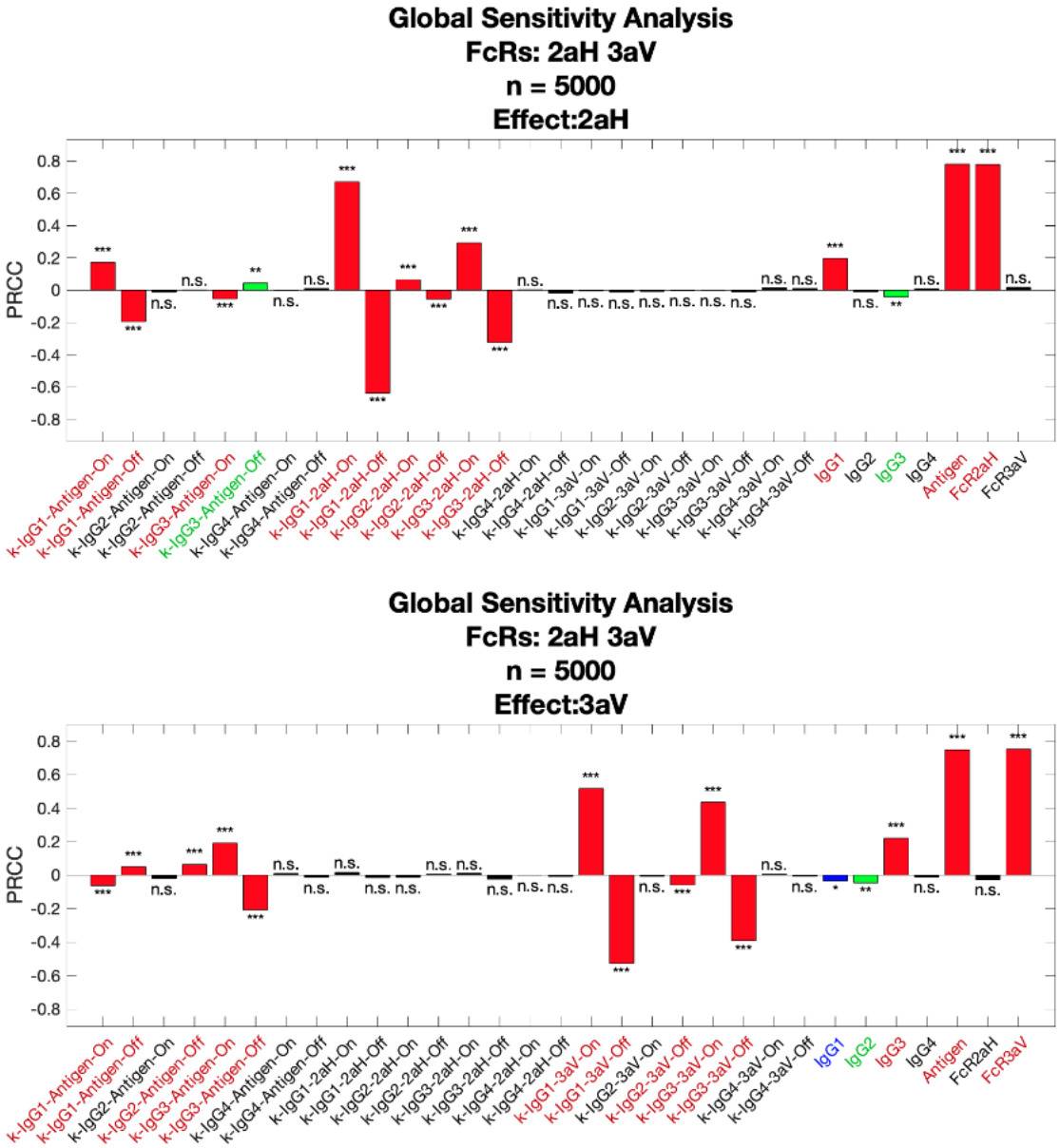
Supplementary Figure B-6: Comparison of cross validation accuracy for our chosen PLSDA models to 100 randomly generated signatures with the same number of features. Significance denoted by asterisks.



.

Appendix C: Supplement to Decoupling Antibody Levels from Fc Effector Functions: An Ordinary Differential Equation Framework Challenges the 'More is Better' Assumption for Polyfunctionality

Supplementary Figure C-1: Global sensitivity analysis using in vivo blood parameters as baseline values



Supplementary Table C-1: Affinity parameters for two FcR ODE model

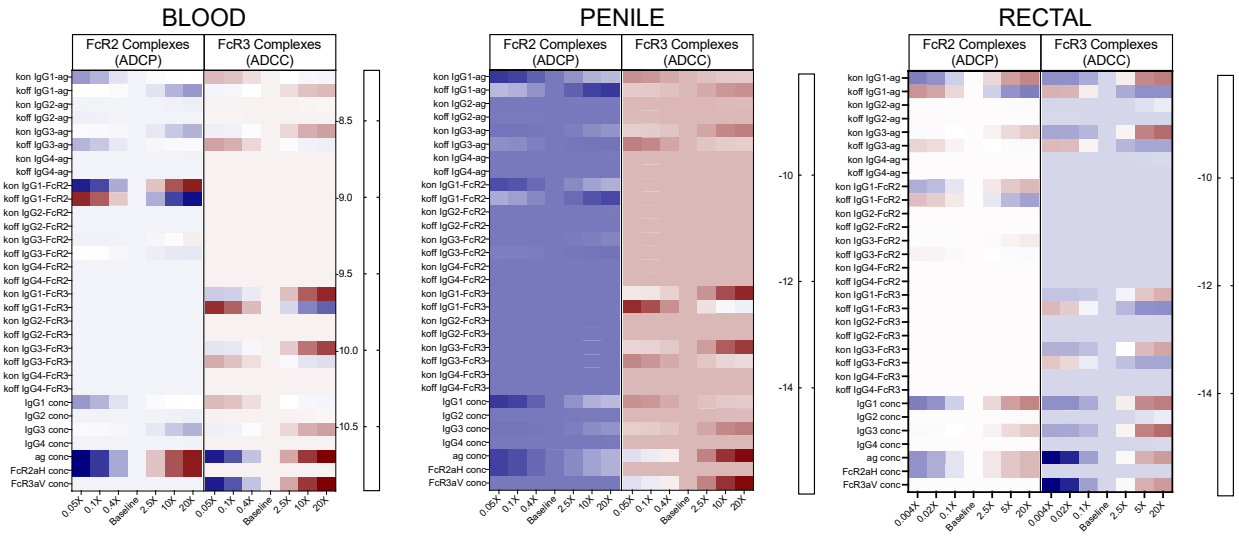
FcRII Parameters	Value	FcRIII Parameters	Value	Units	Source
$k_{on\ IgG1\text{-}FcRIIaH}$	52e-6	$k_{on\ IgG1\text{-}FcRIIIaV}$	20e-6	$nM^{-1}s^{-1}$	k_{on} and k_{off} calculated from K_a measured in Bruhns et al. (2009)[162]
$k_{on\ IgG2\text{-}FcRIIaH}$	4.5e-6	$k_{on\ IgG2\text{-}FcRIIIaV}$	0.7e-6	$nM^{-1}s^{-1}$	
$k_{on\ IgG3\text{-}FcRIIaH}$	8.9e-6	$k_{on\ IgG3\text{-}FcRIIIaV}$	98e-6	$nM^{-1}s^{-1}$	
$k_{on\ IgG4\text{-}FcRIIaH}$	1.7e-6	$k_{on\ IgG4\text{-}FcRIIIaV}$	2.5e-6	$nM^{-1}s^{-1}$	
$k_{on\ IgG1\text{-}FcRIIaR}$	35e-6	$k_{on\ IgG1\text{-}FcRIIIaF}$	11.7e-6	$nM^{-1}s^{-1}$	
$k_{on\ IgG2\text{-}FcRIIaR}$	1e-6	$k_{on\ IgG2\text{-}FcRIIIaF}$	0.3e-6	$nM^{-1}s^{-1}$	
$k_{on\ IgG3\text{-}FcRIIaR}$	9.1e-6	$k_{on\ IgG3\text{-}FcRIIIaF}$	77e-6	$nM^{-1}s^{-1}$	
$k_{on\ IgG4\text{-}FcRIIaR}$	2.1e-6	$k_{on\ IgG4\text{-}FcRIIIaF}$	2e-6	$nM^{-1}s^{-1}$	

General Parameters	Value	Units	Source
$k_{off\ IgG1\text{-}4\text{-}FcRII/III}$	0.01	s^{-1}	Average value measured in pooled RV144 plasma for FcRIIIaV
$k_{on\ IgG1\text{-}4\text{-}ag}$	10e-6	$nM^{-1}s^{-1}$	SPR measurements from pooled IgG from HIV individuals
$k_{off\ IgG1\text{-}4\text{-}ag}$	2e-4	s^{-1}	

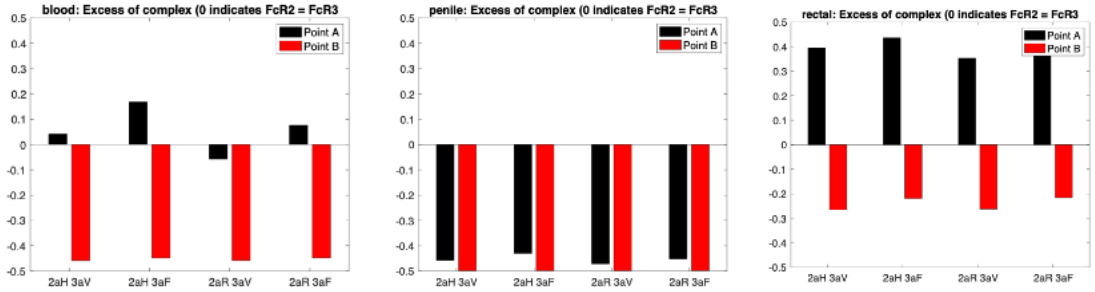
Supplementary Table C-2: Concentration parameters for two FcR ODE model

Parameter	Blood value	Penile value	Rectal value	Units	Sources
IgG1 total	581	2.32	0.277	nM	Subclass proportions/concentrations estimated from Raux et al. (2000)[167] and Pillay et al. (2019)[168]
IgG2 total	2.3	0.0093	0.0011		
IgG3 total	82.6	0.67	0.092		
IgG4 total	0.23	0.00093	0.00011		
Antigen total	2.2e-6	4.2e-7	1.1e-5		Zuckerman et al. (2004)[169]
FcRII total	2.5e-2	2.2e-3	7.3e-3		Cheeseman et al. (2016)[171]
FcRIII total	5.5e-2	1.1e-1	2.2e-3		

Supplementary Figure C-2: 1D Sensitivity analysis across blood and mucosal tissues.



Supplementary Figure C-3: Genetic polymorphisms across tissues.



Appendix D: Unpublished Data

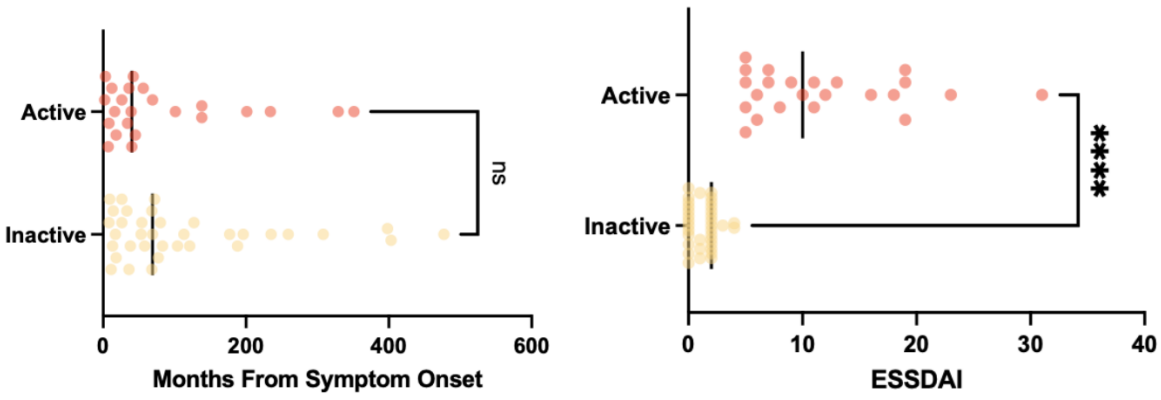
D.1 Serological signatures that explain heterogeneity in disease severity in Sjogren's syndrome

We also wanted to investigate any significant differences in autoantibody responses between inactive (less severe, EULAR's Sjogren's Syndrome Disease Activity Index or ESSDAI ≤4) versus active (more severe, ESSDAI ≥ 5) Sjogren's syndrome. Among the Sjogren's syndrome patients, EULAR's Sjogren's Syndrome Disease Activity Index (ESSDAI) scoring was based on constitutional symptoms, lymphadenopathy, glandular involvement, articular involvement, cutaneous involvement, pulmonary involvement, renal involvement, muscular involvement, peripheral nervous system involvement, central nervous system involvement, hematological findings, and biological laboratory findings. A score of 0-4 was considered inactive/low activity (n=35), 5-12 moderate disease activity (n=15), and >12 high disease activity (n=8) (**Supplementary Figure D-1**). Univariate analysis revealed differences in autoantibody responses between active or more severe disease and inactive or less severe disease (**Supplementary Figure D-2** and **Supplementary Figure D-3**). For Ro60, there are significantly higher levels of IgG, FcgR2aH, FcgR2aR, FcgR2b, and FcgR3aV in active Sjogren's vs. inactive (and seroconverted vs. non-Sjogren's). There appear to be two different populations within both inactive and active populations of seropositive and seronegative patients, with a subset of patients showing very high responses and another subset with lower responses. For the La antigen, there is significantly higher levels of IgA in active vs. inactive vs. non Sjogren's, and higher FcgR2aH, FcgR2aR, FcgR2b, FcgR3aV, and FcgR3aF in active Sjogren's

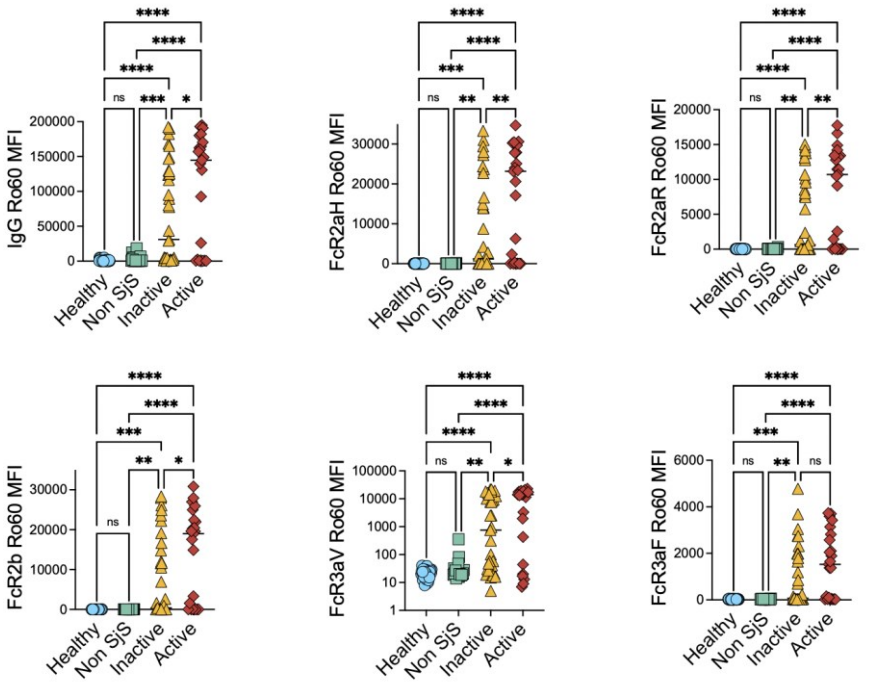
vs. inactive (and seroconverted vs. non Sjogren's). Again, there appear to be two different populations in both inactive and active populations. Lastly, for the Ro52 antigen, univariate analysis shows significantly higher FcgR2aH, FcgR2aR, FcgR2b, and FcgR3aV in active Sjogren's vs. inactive (and seroconverted vs. non Sjogren's).

To further explore the serological difference based on disease severity, we then utilized a systems serology approach with multivariate analysis. Supervised feature selection selected a set of antibody features that was able to distinguish between active and inactive Sjogren's syndrome (90.2% calibration, 79.9% cross validation accuracy) (). Active disease cases appear to have overwhelmingly higher responses of FcR engagement, particularly to the Ro52 and La antigens, in comparison to inactive disease (**Supplementary Figure D-4**). Furthermore, many of the FcR responses appear to be FcR2a, which is associated with phagocytic activity and ADCP. Thus, this led us to explore the role of glycosylation and cell-based phagocytosis in Sjogren's disease severity.

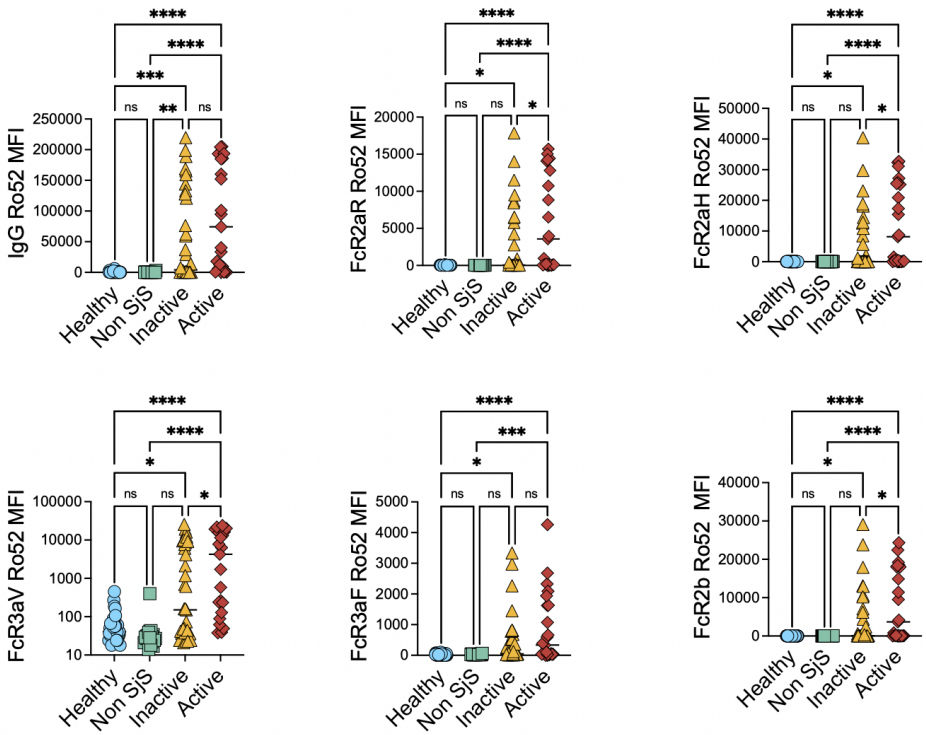
Supplementary Figure D-1: I GET DRY Cohort data months from symptom onset and ESSDAI severity index by active (moderate/severe) vs. inactive (mild) disease status. Asterisks indicate level of significance.



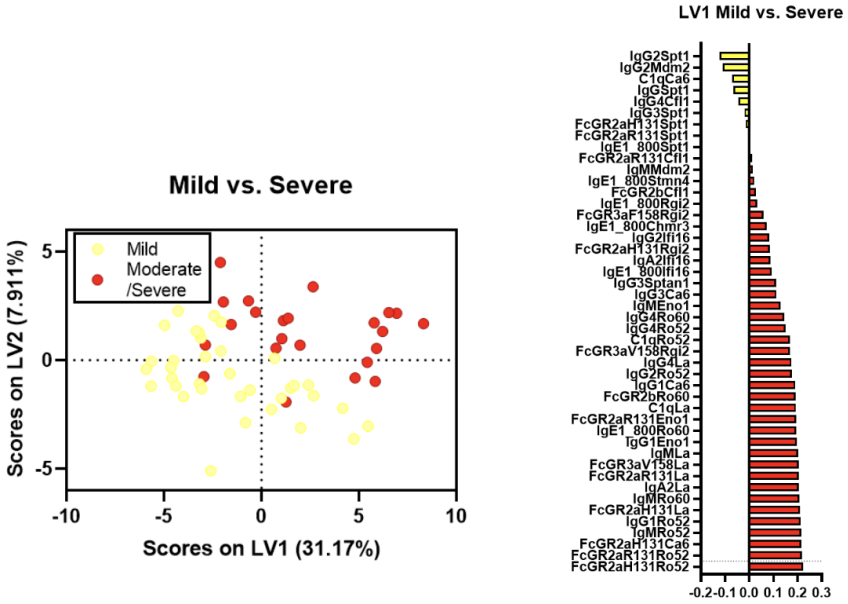
Supplementary Figure D-2: Univariate analysis of Ro60 responses across healthy donors, non-Sjogren's patients, and Sjogren's patients (inactive or mild versus active or moderate/severe disease).



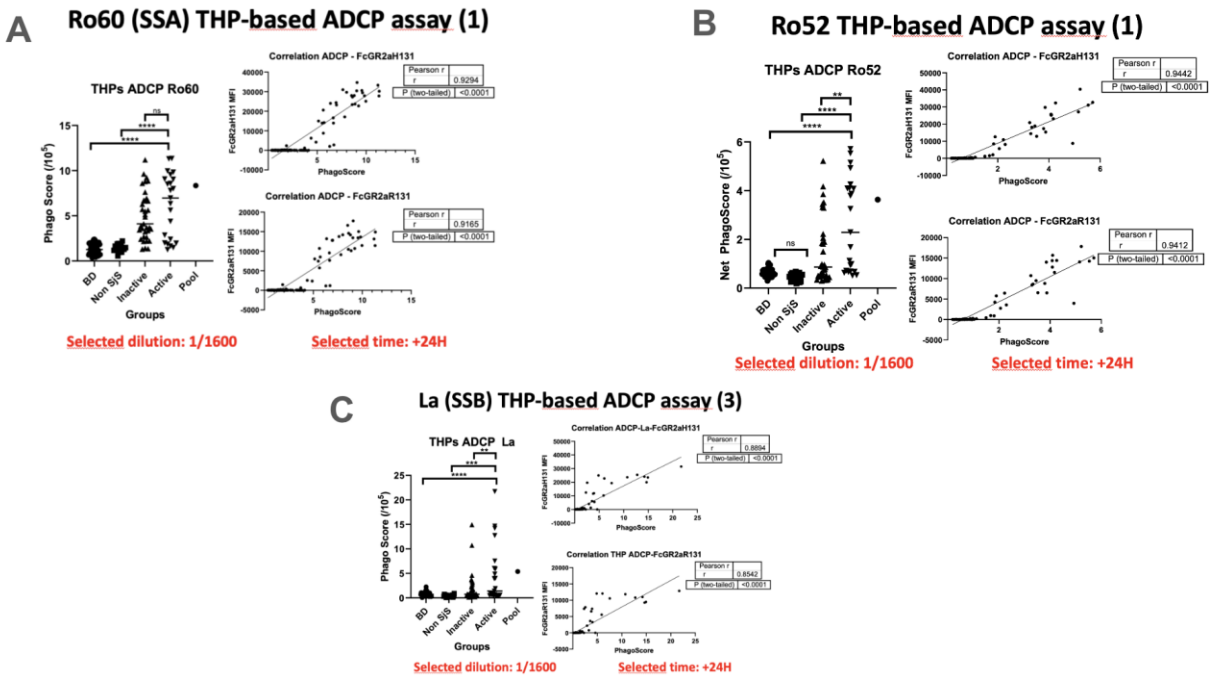
Supplementary Figure D-3: Univariate analysis of Ro52 responses across healthy donors, non-Sjogren's patients, and Sjogren's patients (inactive or mild versus active or moderate/severe disease).



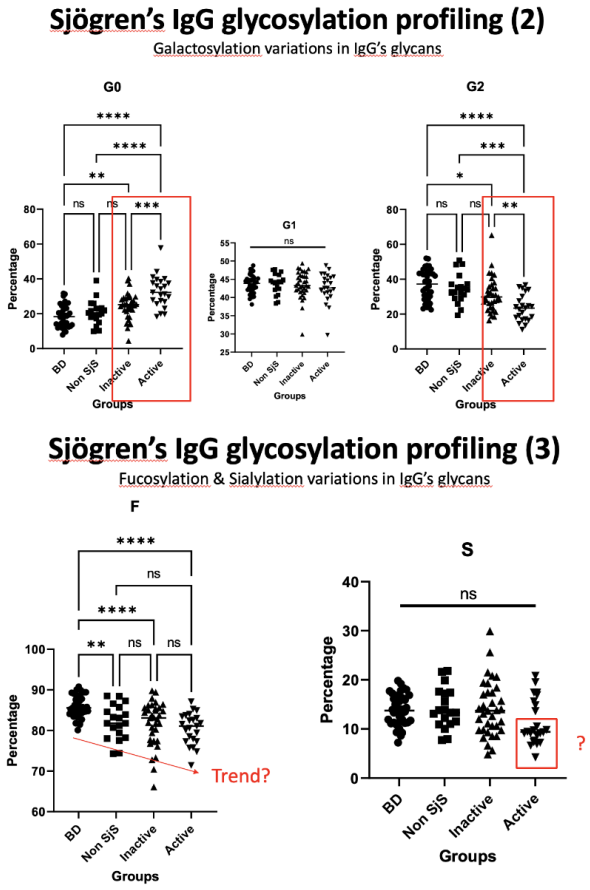
Supplementary Figure D-4: Mild Sjogren's versus moderate and severe Sjogren's PLSDA scores (a) and Elastic-net-selected LV1 loadings (b).



Supplementary Figure D-5: Cell-based phagocytosis assays based on antigen-specific disease activity for A) Ro60, B) Ro52, or C) La.



Supplementary Figure D-6: IgG glycosylation profiling by disease activity



Bibliography

1. Sinha, A. A., Lopez, M. T. & McDevitt, H. O. Autoimmune diseases: the failure of self tolerance. *Science* **248**, 1380–1388 (1990).
2. Arnold, K. B. & Chung, A. W. Prospects from systems serology research. *Immunology* **153**, 279–289 (2018).
3. Nicholson, L. B. The immune system. *Essays Biochem.* **60**, 275–301 (2016).
4. Nimmerjahn, F. & Ravetch, J. V. Fcγ receptors as regulators of immune responses. *Nat. Rev. Immunol.* **8**, 34–47 (2008).
5. Aitken, E. H. *et al.* Developing a multivariate prediction model of antibody features associated with protection of malaria-infected pregnant women from placental malaria. *eLife* **10**, e65776 (2021).
6. Arnold, K. B. & Chung, A. W. Prospects from systems serology research. *Immunology* **153**, 279–289 (2018).
7. Chung, A. W. & Alter, G. Systems serology: profiling vaccine induced humoral immunity against HIV. *Retrovirology* **14**, 57 (2017).
8. Chung, A. W. *et al.* Dissecting Polyclonal Vaccine-Induced Humoral Immunity against HIV Using Systems Serology. *Cell* **163**, 988–998 (2015).
9. Lemke, M. M. *et al.* A systems approach to elucidate personalized mechanistic complexities of antibody-Fc receptor activation post-vaccination. *Cell Rep. Med.* **2**, 100386 (2021).

10. Selva, K. J. *et al.* Systems serology detects functionally distinct coronavirus antibody features in children and elderly. *Nat. Commun.* **12**, 2037 (2021).

11. Tosif, S. *et al.* Immune responses to SARS-CoV-2 in three children of parents with symptomatic COVID-19. *Nat. Commun.* **11**, 5703 (2020).

12. Loos, C. *et al.* Systems serology-based comparison of antibody effector functions induced by adjuvanted vaccines to guide vaccine design. *Npj Vaccines* **8**, 1–15 (2023).

13. Robinett, R. A. *et al.* Dissecting FcγR Regulation through a Multivalent Binding Model. *Cell Syst.* **7**, 41-48.e5 (2018).

14. Ackerman, M. E., Barouch, D. H. & Alter, G. Systems serology for evaluation of HIV vaccine trials. *Immunol. Rev.* **275**, 262–270 (2017).

15. Pittala, S., Morrison, K. S. & Ackerman, M. E. Systems Serology for Decoding Infection and Vaccine-Induced Antibody Responses to HIV-1. *Curr. Opin. HIV AIDS* **14**, 253–264 (2019).

16. Gebru, A. A. *et al.* Global burden of COVID-19: Situational analyis and review. *Hum. Antibodies* **29**, 139–148 (2021).

17. Zimmermann, P. & Curtis, N. Why is COVID-19 less severe in children? A review of the proposed mechanisms underlying the age-related difference in severity of SARS-CoV-2 infections. *Arch. Dis. Child.* **106**, 429–439 (2021).

18. CDC. COVID Data Tracker. *Centers for Disease Control and Prevention* https://covid.cdc.gov/covid-data-tracker (2020).

19. Ramos-Casals, M., Brito-Zerón, P., Sisó-Almirall, A. & Bosch, X. Primary Sjögren syndrome. *BMJ* **344**, e3821 (2012).

20. Sandhya, P., Kurien, B. T., Danda, D. & Scofield, R. H. Update on Pathogenesis of Sjögren's syndrome. *Curr. Rheumatol. Rev.* **13**, 5–22 (2017).

21. Nocturne, G. & Mariette, X. B cells in the pathogenesis of primary Sjögren syndrome. *Nat. Rev. Rheumatol.* **14**, 133–145 (2018).

22. Reeves, W. H., Li, Y. & Zhuang, H. 130 - Autoantibodies in systemic lupus erythematosus. in *Rheumatology (Sixth Edition)* (eds. Hochberg, M. C., Silman, A. J., Smolen, J. S., Weinblatt, M. E. & Weisman, M. H.) 1074–1081 (Mosby, Philadelphia, 2015). doi:10.1016/B978-0-323-09138-1.00130-3.

23. Shiboski, C. H. *et al.* 2016 American College of Rheumatology/European League Against Rheumatism classification criteria for primary Sjögren's syndrome: A consensus and data-driven methodology involving three international patient cohorts. *Ann. Rheum. Dis.* **76**, 9–16 (2017).

24. Shiboski, C. H. *et al.* 2016 American College of Rheumatology/European League Against Rheumatism Classification Criteria for Primary Sjögren's Syndrome: A Consensus and Data-Driven Methodology Involving Three International Patient Cohorts. *Arthritis Rheumatol. Hoboken NJ* **69**, 35–45 (2017).

25. Ramos-Casals, M. *et al.* EULAR recommendations for the management of Sjögren's syndrome with topical and systemic therapies. *Ann. Rheum. Dis.* **79**, 3–18 (2020).

26. Ben Mkaddem, S., Benhamou, M. & Monteiro, R. C. Understanding Fc Receptor Involvement in Inflammatory Diseases: From Mechanisms to New Therapeutic Tools. *Front. Immunol.* **10**, (2019).

27. Jourdain, H., Gage, S. B. de, Desplas, D. & Dray-Spira, R. Real-world effectiveness of pre-exposure prophylaxis in men at high risk of HIV infection in France: a nested case-control study. *Lancet Public Health* **7**, e529–e536 (2022).

28. Rerks-Ngarm, S. *et al.* Vaccination with ALVAC and AIDSVAX to Prevent HIV-1 Infection in Thailand. *N. Engl. J. Med.* **361**, 2209–2220 (2009).

29. Shubin, Z. *et al.* Additional boosting to the RV144 vaccine regimen increased Fc-mediated effector function magnitude but not durability. *AIDS* **37**, 1519 (2023).

30. Su, B. *et al.* Update on Fc-Mediated Antibody Functions Against HIV-1 Beyond Neutralization. *Front. Immunol.* **10**, 457357 (2019).

31. Li, Q. *et al.* Early Transmission Dynamics in Wuhan, China, of Novel Coronavirus-Infected Pneumonia. *N. Engl. J. Med.* **382**, 1199–1207 (2020).

32. COVID-19 Map. *Johns Hopkins Coronavirus Resource Center* https://coronavirus.jhu.edu/map.html.

33. Wu, Z. & McGoogan, J. M. Characteristics of and Important Lessons From the Coronavirus Disease 2019 (COVID-19) Outbreak in China: Summary of a Report of 72 314 Cases From the Chinese Center for Disease Control and Prevention. *JAMA* **323**, 1239–1242 (2020).

34. CDCMMWR. Severe Outcomes Among Patients with Coronavirus Disease 2019 (COVID-19) — United States, February 12–March 16, 2020. *MMWR Morb. Mortal. Wkly. Rep.* **69**, (2020).

35. Short, K. R., Kedzierska, K. & van de Sandt, C. E. Back to the Future: Lessons Learned From the 1918 Influenza Pandemic. *Front. Cell. Infect. Microbiol.* **8**, 343 (2018).

36. Henry, C. *et al.* Influenza Virus Vaccination Elicits Poorly Adapted B Cell Responses in Elderly Individuals. *Cell Host Microbe* **25**, 357-366.e6 (2019).

37. Carsetti, R. *et al.* The immune system of children: the key to understanding SARS-CoV-2 susceptibility? *Lancet Child Adolesc. Health* **4**, 414–416 (2020).

38. Ilinykh, P. A. *et al.* Non-neutralizing Antibodies from a Marburg Infection Survivor Mediate Protection by Fc-Effector Functions and by Enhancing Efficacy of Other Antibodies. *Cell Host Microbe* **27**, 976-991.e11 (2020).

39. Henry Dunand, C. J. *et al.* Both Neutralizing and Non-Neutralizing Human H7N9 Influenza Vaccine-Induced Monoclonal Antibodies Confer Protection. *Cell Host Microbe* **19**, 800–813 (2016).

40. Yasui, F. *et al.* Phagocytic cells contribute to the antibody-mediated elimination of pulmonary-infected SARS coronavirus. *Virology* **454–455**, 157–168 (2014).

41. Yuan, F. F. *et al.* Influence of FcgammaRIIA and MBL polymorphisms on severe acute respiratory syndrome. *Tissue Antigens* **66**, 291–296 (2005).

42. Schäfer, A. *et al.* Antibody potency, effector function, and combinations in protection and therapy for SARS-CoV-2 infection in vivo. *J. Exp. Med.* **218**, e20201993 (2021).

43. Jaume, M. *et al.* Anti-severe acute respiratory syndrome coronavirus spike antibodies trigger infection of human immune cells via a pH- and cysteine protease-independent FcγR pathway. *J. Virol.* **85**, 10582–10597 (2011).

44. Liu, L. *et al.* Anti–spike IgG causes severe acute lung injury by skewing macrophage responses during acute SARS-CoV infection. *JCI Insight* **4**, e123158.

45. Katzelnick, L. C. *et al.* Antibody-dependent enhancement of severe dengue disease in humans. *Science* **358**, 929–932 (2017).

46. Tetro, J. A. Is COVID-19 receiving ADE from other coronaviruses? *Microbes Infect.* **22**, 72–73 (2020).

47. Wines, B. D., Billings, H., Mclean, M. R., Kent, S. J. & Hogarth, P. M. Antibody Functional Assays as Measures of Fc Receptor-Mediated Immunity to HIV - New Technologies and their Impact on the HIV Vaccine Field. *Curr. HIV Res.* **15**, 202–215 (2017).

48. McLean, M. R. *et al.* Dimeric Fcγ Receptor Enzyme-Linked Immunosorbent Assay To Study HIV-Specific Antibodies: A New Look into Breadth of Fcγ Receptor Antibodies Induced by the RV144 Vaccine Trial. *J. Immunol. Baltim. Md 1950* **199**, 816–826 (2017).

49. Edridge, A. W. D. *et al.* Seasonal coronavirus protective immunity is short-lasting. *Nat. Med.* **26**, 1691–1693 (2020).

50. Le Bert, N. *et al.* SARS-CoV-2-specific T cell immunity in cases of COVID-19 and SARS, and uninfected controls. *Nature* **584**, 457–462 (2020).

51. Ravichandran, S. *et al.* Antibody signature induced by SARS-CoV-2 spike protein immunogens in rabbits. *Sci. Transl. Med.* **12**, eabc3539 (2020).

52. Koutsakos, M. *et al.* Circulating TFH cells, serological memory, and tissue compartmentalization shape human influenza-specific B cell immunity. *Sci. Transl. Med.* **10**, eaan8405 (2018).

53. Thursz, M. R. *et al.* Association between an MHC class II allele and clearance of hepatitis B virus in the Gambia. *N. Engl. J. Med.* **332**, 1065–1069 (1995).

54. Hajeer, A. H., Balkhy, H., Johani, S., Yousef, M. Z. & Arabi, Y. Association of human leukocyte antigen class II alleles with severe Middle East respiratory syndrome-coronavirus infection. *Ann. Thorac. Med.* **11**, 211–213 (2016).

55. Ovsyannikova, I. G., Pankratz, V. S., Vierkant, R. A., Jacobson, R. M. & Poland, G. A. Human leukocyte antigen haplotypes in the genetic control of immune response to measles-mumps-rubella vaccine. *J. Infect. Dis.* **193**, 655–663 (2006).

56. Vanderven, H. A. *et al.* Antibody-Dependent Cellular Cytotoxicity Responses to Seasonal Influenza Vaccination in Older Adults. *J. Infect. Dis.* **217**, 12–23 (2017).

57. Rowntree, L. C. *et al.* Robust correlations across six SARS-CoV-2 serology assays detecting distinct antibody features. *Clin. Transl. Immunol.* **10**, e1258 (2021).

58. Wrapp, D. *et al.* Cryo-EM structure of the 2019-nCoV spike in the prefusion conformation. *Science* **367**, 1260–1263 (2020).

59. Damelang, T., Rogerson, S. J., Kent, S. J. & Chung, A. W. Role of IgG3 in Infectious Diseases. *Trends Immunol.* **40**, 197–211 (2019).

60. Jiang, S., Hillyer, C. & Du, L. Neutralizing Antibodies against SARS-CoV-2 and Other Human Coronaviruses. *Trends Immunol.* **41**, 355–359 (2020).

61. Juno, J. A. *et al.* Humoral and circulating follicular helper T cell responses in recovered patients with COVID-19. *Nat. Med.* **26**, 1428–1434 (2020).

62. Amanat, F. *et al.* A serological assay to detect SARS-CoV-2 seroconversion in humans. *MedRxiv Prepr. Serv. Health Sci.* 2020.03.17.20037713 (2020) doi:10.1101/2020.03.17.20037713.

63. Fleit, H. B. & Kobasiuk, C. D. The human monocyte-like cell line THP-1 expresses Fc gamma RI and Fc gamma RII. *J. Leukoc. Biol.* **49**, 556–565 (1991).

64. Muenchhoff, M. *et al.* Nonprogressing HIV-infected children share fundamental immunological features of nonpathogenic SIV infection. *Sci. Transl. Med.* **8**, 358ra125 (2016).

65. Wec, A. Z. *et al.* Broad neutralization of SARS-related viruses by human monoclonal antibodies. *Science* **369**, 731–736 (2020).

66. Prévost, J. *et al.* Cross-Sectional Evaluation of Humoral Responses against SARS-CoV-2 Spike. *Cell Rep. Med.* **1**, 100126 (2020).

67. Westerhuis, B. M. *et al.* Severe COVID-19 patients display a back boost of seasonal coronavirus-specific antibodies. 2020.10.10.20210070 Preprint at https://doi.org/10.1101/2020.10.10.20210070 (2020).

68. Aydillo, T. *et al.* Antibody Immunological Imprinting on COVID-19 Patients. 2020.10.14.20212662 Preprint at https://doi.org/10.1101/2020.10.14.20212662 (2020).

69. Wines, B. D. *et al.* Dimeric FcγR Ectodomains as Probes of the Fc Receptor Function of Anti-Influenza Virus IgG. *J. Immunol. Baltim. Md 1950* **197**, 1507–1516 (2016).

70. Parsons, M. S. *et al.* Partial efficacy of a broadly neutralizing antibody against cell-associated SHIV infection. *Sci. Transl. Med.* **9**, eaaf1483 (2017).

71. Anand, S. P. *et al.* Two Families of Env Antibodies Efficiently Engage Fc-Gamma Receptors and Eliminate HIV-1-Infected Cells. *J. Virol.* **93**, e01823-18 (2019).

72. Vanderven, H. A. *et al.* Fc functional antibodies in humans with severe H7N9 and seasonal influenza. *JCI Insight* **2**, e92750.

73. Kristensen, A. B. *et al.* Antibody Responses with Fc-Mediated Functions after Vaccination of HIV-Infected Subjects with Trivalent Influenza Vaccine. *J. Virol.* **90**, 5724–5734 (2016).

74. Kurtovic, L. *et al.* Multifunctional Antibodies Are Induced by the RTS,S Malaria Vaccine and Associated With Protection in a Phase 1/2a Trial. *J. Infect. Dis.* **224**, 1128–1138 (2021).

75. Ackerman, M. E. *et al.* Polyfunctional HIV-Specific Antibody Responses Are Associated with Spontaneous HIV Control. *PLoS Pathog.* **12**, e1005315 (2016).

76. Lofano, G. *et al.* Antigen-specific antibody Fc glycosylation enhances humoral immunity via the recruitment of complement. *Sci. Immunol.* **3**, eaat7796 (2018).

77. Saphire, E. O. *et al.* Systematic Analysis of Monoclonal Antibodies against Ebola Virus GP Defines Features that Contribute to Protection. *Cell* **174**, 938-952.e13 (2018).

78. Suscovich, T. J. *et al.* Mapping functional humoral correlates of protection against malaria challenge following RTS,S/AS01 vaccination. *Sci. Transl. Med.* **12**, eabb4757 (2020).

79. Chenoweth, A. M., Wines, B. D., Anania, J. C. & Mark Hogarth, P. Harnessing the immune system via FcγR function in immune therapy: a pathway to next-gen mAbs. *Immunol. Cell Biol.* **98**, 287–304 (2020).

80. Chung, A. W. *et al.* Identification of antibody glycosylation structures that predict monoclonal antibody Fc-effector function. *AIDS Lond. Engl.* **28**, 2523–2530 (2014).

81. Chung, A. W. *et al.* Polyfunctional Fc-Effector Profiles Mediated by IgG Subclass Selection Distinguish RV144 and VAX003 Vaccines. *Sci. Transl. Med.* **6**, 228ra38-228ra38 (2014).

82. Lu, L. L. *et al.* A Functional Role for Antibodies in Tuberculosis. *Cell* **167**, 433-443.e14 (2016).

83. Wang, T. T. *et al.* IgG antibodies to dengue enhanced for FcγRIIIA binding determine disease severity. *Science* **355**, 395–398 (2017).

84. McLean, M. R., Lu, L. L., Kent, S. J. & Chung, A. W. An Inflammatory Story: Antibodies in Tuberculosis Comorbidities. *Front. Immunol.* **10**, 2846 (2019).

85. Chakraborty, S. *et al.* Proinflammatory IgG Fc structures in patients with severe COVID-19. *Nat. Immunol.* **22**, 67–73 (2021).

86. Larsen, M. D. *et al.* Afucosylated IgG characterizes enveloped viral responses and correlates with COVID-19 severity. *Science* **371**, eabc8378 (2021).

87. Genomewide Association Study of Severe Covid-19 with Respiratory Failure. *N. Engl. J. Med.* **383**, 1522–1534 (2020).

88. Brown, E. P. *et al.* High-throughput, multiplexed IgG subclassing of antigen-specific antibodies from clinical samples. *J. Immunol. Methods* **386**, 117–123 (2012).

89. Stadlbauer, D. *et al.* SARS-CoV-2 Seroconversion in Humans: A Detailed Protocol for a Serological Assay, Antigen Production, and Test Setup. *Curr. Protoc. Microbiol.* **57**, e100 (2020).

90. Caly, L. *et al.* Isolation and rapid sharing of the 2019 novel coronavirus (SARS-CoV-2) from the first patient diagnosed with COVID-19 in Australia. *Med. J. Aust.* **212**, 459–462 (2020).

91. Houser, K. V. *et al.* Prophylaxis With a Middle East Respiratory Syndrome Coronavirus (MERS-CoV)-Specific Human Monoclonal Antibody Protects Rabbits From MERS-CoV Infection. *J. Infect. Dis.* **213**, 1557–1561 (2016).

92. Subbarao, K. *et al.* Prior infection and passive transfer of neutralizing antibody prevent replication of severe acute respiratory syndrome coronavirus in the respiratory tract of mice. *J. Virol.* **78**, 3572–3577 (2004).

93. Ackerman, M. E. *et al.* A robust, high-throughput assay to determine the phagocytic activity of clinical antibody samples. *J. Immunol. Methods* **366**, 8–19 (2011).

94. Atyeo, C. *et al.* Distinct Early Serological Signatures Track with SARS-CoV-2 Survival. *Immunity* **53**, 524-532.e4 (2020).

95. Lee, W. S. *et al.* Decay of Fc-dependent antibody functions after mild to moderate COVID-19. *Cell Rep. Med.* **2**, 100296 (2021).

96. Darrah, P. A. *et al.* Multifunctional TH1 cells define a correlate of vaccine-mediated protection against Leishmania major. *Nat. Med.* **13**, 843–850 (2007).

97. Ho, S. Y., Wong, L. & Goh, W. W. B. Avoid Oversimplifications in Machine Learning: Going beyond the Class-Prediction Accuracy. *Patterns* **1**, 100025 (2020).

98. Gunn, B. *et al.* Enhanced binding of antibodies generated during chronic HIV infection to mucus component MUC16. *Mucosal Immunol.* **9**, 1549–1558 (2016).

99. Gunn, B. M. *et al.* A Role for Fc Function in Therapeutic Monoclonal Antibody-Mediated Protection against Ebola Virus. *Cell Host Microbe* **24**, 221-233.e5 (2018).

100. Worley, B., Halouska, S. & Powers, R. Utilities for quantifying separation in PCA/PLS-DA scores plots. *Anal. Biochem.* **433**, 102–104 (2013).

101. Mariette, X. & Criswell, L. A. Primary Sjögren's Syndrome. *N. Engl. J. Med.* **378**, 931–939 (2018).

102. Ramos-Casals, M. *et al.* Systemic involvement in primary Sjögren's syndrome evaluated by the EULAR-SS disease activity index: analysis of 921 Spanish patients (GEAS-SS Registry). *Rheumatology* **53**, 321–331 (2014).

103. Brito-Zerón, P. *et al.* Sjögren syndrome. *Nat. Rev. Dis. Primer* **2**, 16047 (2016).

104. Reichlin, M. Antibodies to Ro and La. *Ann. Med. Interne (Paris)* **149**, 34–41 (1998).

105. Vílchez-Oya, F., Balastegui Martin, H., García-Martínez, E. & Corominas, H. Not all autoantibodies are clinically relevant. Classic and novel autoantibodies in Sjögren's syndrome: A critical review. *Front. Immunol.* **13**, 1003054 (2022).

106. Hung, T. *et al.* The Ro60 autoantigen binds endogenous retroelements and regulates inflammatory gene expression. *Science* **350**, 455–459 (2015).

107. Jones, E. L., Laidlaw, S. M. & Dustin, L. B. TRIM21/Ro52 - Roles in Innate Immunity and Autoimmune Disease. *Front. Immunol.* **12**, 738473 (2021).

108. Decker, P. *et al.* An updated review of anti-Ro52 (TRIM21) antibodies impact in connective tissue diseases clinical management. *Autoimmun. Rev.* **21**, 103013 (2022).

109. Trzeciak, M., Bagavant, H., Papinska, J. & Deshmukh, U. S. Immune Response Targeting Sjögren's Syndrome Antigen Ro52 Suppresses Tear Production in Female Mice. *Int. J. Mol. Sci.* **19**, 2935 (2018).

110. Szczerba, B. M. *et al.* Interaction between innate immunity and Ro52-induced antibody causes Sjögren's syndrome-like disorder in mice. *Ann. Rheum. Dis.* **75**, 617–622 (2016).

111. Fayyaz, A., Kurien, B. T. & Scofield, H. Autoantibodies in Sjögren's Syndrome. *Rheum. Dis. Clin. North Am.* **42**, 419–434 (2016).

112. Shiboski, C. H. *et al.* 2016 American College of Rheumatology/European League Against Rheumatism classification criteria for primary Sjögren's syndrome: A consensus and data-driven methodology involving three international patient cohorts. *Ann. Rheum. Dis.* **76**, 9–16 (2017).

113. Vitali, C. *et al.* Classification criteria for Sjögren's syndrome: a revised version of the European criteria proposed by the American-European Consensus Group. *Ann. Rheum. Dis.* **61**, 554–558 (2002).

114. Chalayer, E. *et al.* Fc receptors gone wrong: A comprehensive review of their roles in autoimmune and inflammatory diseases. *Autoimmun. Rev.* **21**, 103016 (2022).

115. Richards, J. O. *et al.* Optimization of antibody binding to FcγRIIa enhances macrophage phagocytosis of tumor cells. *Mol. Cancer Ther.* **7**, 2517–2527 (2008).

116. Takai, T. Roles of Fc receptors in autoimmunity. *Nat. Rev. Immunol.* **2**, 580–592 (2002).

117. Su, K. *et al.* Expression profile of FcgammaRIIb on leukocytes and its dysregulation in systemic lupus erythematosus. *J. Immunol. Baltim. Md 1950* **178**, 3272–3280 (2007).

118. Chen, H. *et al.* High-dose methylprednisolone pulse therapy upregulated FcγRIIb expression on B cells in primary Sjögren's syndrome patients with thrombocytopenia. *Clin. Rheumatol.* **32**, 1783–1790 (2013).

119. Tsang-A-Sjoe, M. W. P. *et al.* Fc-gamma receptor polymorphisms differentially influence susceptibility to systemic lupus erythematosus and lupus nephritis. *Rheumatol. Oxf. Engl.* **55**, 939–948 (2016).

120. Koene, H. R. *et al.* The Fc gammaRIIIA-158F allele is a risk factor for systemic lupus erythematosus. *Arthritis Rheum.* **41**, 1813–1818 (1998).

121. Hamburger, M. I., Moutsopoulos, H. M., Lawley, T. J. & Frank, M. M. Sjögren's syndrome: a defect in reticuloendothelial system Fc-receptor-specific clearance. *Ann. Intern. Med.* **91**, 534–538 (1979).

122. Haldorsen, K. *et al.* No association of primary Sjögren's syndrome with Fcγ receptor gene variants. *Genes Immun.* **14**, 234–237 (2013).

123. Chung, A. W. *et al.* Dissecting Polyclonal Vaccine-Induced Humoral Immunity against HIV Using Systems Serology. *Cell* **163**, 988–998 (2015).

124. Lu, L. L. *et al.* A Functional Role for Antibodies in Tuberculosis. *Cell* **167**, 433-443.e14 (2016).

125. Arnold, K. B. & Chung, A. W. Prospects from systems serology research. *Immunology* **153**, 279–289 (2018).

126. Chung, A. W. *et al.* Systems immunology reveals a linked IgG3-C4 response in patients with acute rheumatic fever. *Immunol. Cell Biol.* **98**, 12–21 (2020).

127. Selva, K. J. *et al.* Systems serology detects functionally distinct coronavirus antibody features in children and elderly. *Nat. Commun.* **12**, 2037 (2021).

128. McLean, M. R. *et al.* Serological and cellular inflammatory signatures in end-stage kidney disease and latent tuberculosis. *Clin. Transl. Immunol.* **10**, e1355 (2021).

129. Multiparametric autoantibody analysis: a new paradigm for the diagnosis of connective tissue diseases - PubMed. https://pubmed-ncbi-nlm-nih-gov.proxy.lib.umich.edu/36564813/.

130. Longobardi, S. *et al.* Autoantibodies identify primary Sjögren's syndrome in patients lacking serum IgG specific for Ro/SS-A and La/SS-B. *Ann. Rheum. Dis.* **82**, 1181–1190 (2023).

131. Chung, A. W. *et al.* Identification of antibody glycosylation structures that predict monoclonal antibody Fc-effector function. *AIDS Lond. Engl.* **28**, 2523–2530 (2014).

132. Youinou, P. *et al.* Galactose terminating oligosaccharides of IgG in patients with primary Sjögren's syndrome. *J. Autoimmun.* **5**, 393–400 (1992).

133. Seeling, M., Brückner, C. & Nimmerjahn, F. Differential antibody glycosylation in autoimmunity: sweet biomarker or modulator of disease activity? *Nat. Rev. Rheumatol.* **13**, 621–630 (2017).

134. Flevaris, K. & Kontoravdi, C. Immunoglobulin G N-glycan Biomarkers for Autoimmune Diseases: Current State and a Glycoinformatics Perspective. *Int. J. Mol. Sci.* **23**, 5180 (2022).

135. Novel Concepts of Altered Immunoglobulin G Galactosylation in Autoimmune Diseases - PubMed. https://pubmed-ncbi-nlm-nih-gov.proxy.lib.umich.edu/29616041/.

136. Burbelo, P. D., Iadarola, M. J., Keller, J. M. & Warner, B. M. Autoantibodies Targeting Intracellular and Extracellular Proteins in Autoimmunity. *Front. Immunol.* **12**, 548469 (2021).

137. Seror, R. *et al.* Defining disease activity states and clinically meaningful improvement in primary Sjögren's syndrome with EULAR primary Sjögren's syndrome disease activity (ESSDAI) and patient-reported indexes (ESSPRI). *Ann. Rheum. Dis.* **75**, 382–389 (2016).

138. Tosif, S. *et al.* Immune responses to SARS-CoV-2 in three children of parents with symptomatic COVID-19. *Nat. Commun.* **11**, 5703 (2020).

139. Wuji Zhang *et al.* Immune responses in the respiratory tract and blood of COVID-19 patients reveal mechanisms of disease severity. *Submitted*.

140. McLean, M. R. *et al.* Dimeric Fcγ Receptor Enzyme-Linked Immunosorbent Assay To Study HIV-Specific Antibodies: A New Look into Breadth of Fcγ Receptor Antibodies Induced by the RV144 Vaccine Trial. *J. Immunol. Baltim. Md 1950* **199**, 816–826 (2017).

141. Lee, W. S. *et al.* Decay of Fc-dependent antibody functions after mild to moderate COVID-19. *Cell Rep. Med.* **2**, 100296 (2021).

142. Lopez, E. *et al.* Simultaneous evaluation of antibodies that inhibit SARS-CoV-2 variants via multiplex assay. *JCI Insight* **6**, e150012 (2021).

143. Haycroft, E. R. *et al.* Antibody glycosylation correlates with disease progression in SIV-Mycobacterium tuberculosis coinfected cynomolgus macaques. *Clin. Transl. Immunol.* **12**, e1474 (2023).

144. Ackerman, M. E. *et al.* A robust, high-throughput assay to determine the phagocytic activity of clinical antibody samples. *J. Immunol. Methods* **366**, 8–19 (2011).

145. Gunn, B. M. *et al.* Enhanced binding of antibodies generated during chronic HIV infection to mucus component MUC16. *Mucosal Immunol.* **9**, 1549–1558 (2016).

146. McCoy, L. E. & Burton, D. R. Identification and specificity of broadly neutralizing antibodies against HIV. *Immunol. Rev.* **275**, 11–20 (2017).

147. Escolano, A., Dosenovic, P. & Nussenzweig, M. C. Progress toward active or passive HIV-1 vaccination. *J. Exp. Med.* **214**, 3–16 (2017).

148. Burton, D. R. & Hangartner, L. Broadly Neutralizing Antibodies to HIV and Their Role in Vaccine Design. *Annu. Rev. Immunol.* **34**, 635–659 (2016).

149. Pegu, A., Hessell, A. J., Mascola, J. R. & Haigwood, N. L. Use of broadly neutralizing antibodies for HIV-1 prevention. *Immunol. Rev.* **275**, 296–312 (2017).

150. Sok, D. & Burton, D. R. Recent progress in broadly neutralizing antibodies to HIV. *Nat. Immunol.* **19**, 1179–1188 (2018).

151. Moldt, B. *et al.* Neutralizing antibody affords comparable protection against vaginal and rectal simian/human immunodeficiency virus challenge in macaques. *AIDS Lond. Engl.* **30**, 1543–1551 (2016).

152. Fischinger, S. *et al.* IgG3 collaborates with IgG1 and IgA to recruit effector function in RV144 vaccinees. *JCI Insight* **5**, e140925.

153. Chung, A. W. *et al.* Polyfunctional Fc-effector profiles mediated by IgG subclass selection distinguish RV144 and VAX003 vaccines. *Sci. Transl. Med.* **6**, (2014).

154. Yates, N. L. *et al.* Vaccine-Induced Env V1–V2 IgG3 Correlates with Lower HIV-1 Infection Risk and Declines Soon After Vaccination. *Sci. Transl. Med.* **6**, 228ra39 (2014).

155. Skowronski, D. M. *et al.* Serial Vaccination and the Antigenic Distance Hypothesis: Effects on Influenza Vaccine Effectiveness During A(H3N2) Epidemics in Canada, 2010–2011 to 2014–2015. *J. Infect. Dis.* **215**, 1059–1099 (2017).

156. Smith, D. J., Forrest, S., Ackley, D. H. & Perelson, A. S. Variable efficacy of repeated annual influenza vaccination. *Proc. Natl. Acad. Sci. U. S. A.* **96**, 14001–14006 (1999).

157. Forthal, D. N. *et al.* IgG2 inhibits HIV-1 internalization by monocytes, and IgG subclass binding is affected by gp120 glycosylation. *AIDS* **25**, 2099–2104 (2011).

158. Patel, P. *et al.* Estimating per-act HIV transmission risk: a systematic review. *AIDS Lond. Engl.* **28**, 1509–1519 (2014).

159. John, G. C. & Kreiss, J. Mother-to-child transmission of human immunodeficiency virus type 1. *Epidemiol. Rev.* **18**, 149–157 (1996).

160. Baggaley, R. F., Boily, M.-C., White, R. G. & Alary, M. Risk of HIV-1 transmission for parenteral exposure and blood transfusion: a systematic review and meta-analysis. *AIDS Lond. Engl.* **20**, 805–812 (2006).

161. Chenine, A. L. *et al.* Relative Transmissibility of an R5 Clade C Simian- Human Immunodeficiency Virus Across Different Mucosae in Macaques Parallels the Relative Risks of Sexual HIV-1 Transmission in Humans via Different Routes. *J. Infect. Dis.* **201**, 1155–1163 (2010).

162. Bruhns, P. *et al.* Specificity and affinity of human Fcγ receptors and their polymorphic variants for human IgG subclasses. *Blood* **113**, 3716–3725 (2009).

163. Cottignies-Calamarte, A., Tudor, D. & Bomsel, M. Antibody Fc-chimerism and effector functions: When IgG takes advantage of IgA. *Front. Immunol.* **14**, (2023).

164. Smalls-Mantey, A. *et al.* Antibody-Dependent Cellular Cytotoxicity against Primary HIV-Infected CD4+ T Cells Is Directly Associated with the Magnitude of Surface IgG Binding. *J. Virol.* **86**, 8672–8680 (2012).

165. Forthal, D. N. & Finzi, A. Antibody-Dependent Cellular Cytotoxicity (ADCC) in HIV Infection. *AIDS Lond. Engl.* **32**, 2439–2451 (2018).

166. Chung, A., Rollman, E., Johansson, S., Kent, S. J. & Stratov, I. The utility of ADCC responses in HIV infection. *Curr. HIV Res.* **6**, 515–519 (2008).

167. Raux, M. *et al.* IgG subclass distribution in serum and various mucosal fluids of HIV type 1-infected subjects. *AIDS Res. Hum. Retroviruses* **16**, 583–594 (2000).

168. Pillay, T. *et al.* Semen IgM, IgG1, and IgG3 Differentially Associate With Pro-Inflammatory Cytokines in HIV-Infected Men. *Front. Immunol.* **9**, 3141 (2019).

169. Zuckerman, R. A. *et al.* Higher concentration of HIV RNA in rectal mucosa secretions than in blood and seminal plasma, among men who have sex with men, independent of antiretroviral therapy. *J. Infect. Dis.* **190**, 156–161 (2004).

170. Zhu, P. *et al.* Distribution and three-dimensional structure of AIDS virus envelope spikes. *Nature* **441**, 847–852 (2006).

171. Cheeseman, H. M. *et al.* Expression Profile of Human Fc Receptors in Mucosal Tissue: Implications for Antibody-Dependent Cellular Effector Functions Targeting HIV-1 Transmission. *PloS One* **11**, e0154656 (2016).

172. Raedler, M. D. *et al.* Serologic assay to quantify human immunoglobulin G antibodies to the Staphylococcus aureus iron surface determinant B antigen. *Clin. Vaccine Immunol.* **16**, 739–748 (2009).

173. Marino, S., Hogue, I. B., Ray, C. J. & Kirschner, D. E. A methodology for performing global uncertainty and sensitivity analysis in systems biology. *J. Theor. Biol.* **254**, 178–196 (2008).

174. Rerks-Ngarm, S. *et al.* Randomized, Double-Blind Evaluation of Late Boost Strategies for HIV-Uninfected Vaccine Recipients in the RV144 HIV Vaccine Efficacy Trial. *J. Infect. Dis.* **215**, 1255–1263 (2017).

175. Madhavi, V. *et al.* HIV-1 Env- and Vpu-Specific Antibody-Dependent Cellular Cytotoxicity Responses Associated with Elite Control of HIV. *J. Virol.* **91**, 10.1128/jvi.00700-17 (2017).

176. Zhang, W. *et al.* SARS-CoV-2 infection results in immune responses in the respiratory tract and peripheral blood that suggest mechanisms of disease severity. *Nat. Commun.* **13**, 2774 (2022).

177. Augusto, D. G. *et al.* A common allele of HLA is associated with asymptomatic SARS-CoV-2 infection. *Nature* **620**, 128–136 (2023).

178. Tay, G. K. *et al.* HLA class I associations with the severity of COVID-19 disease in the United Arab Emirates. *PLOS ONE* **18**, e0285712 (2023).

179. Mentzer, A. J. *et al.* Human leukocyte antigen alleles associate with COVID-19 vaccine immunogenicity and risk of breakthrough infection. *Nat. Med.* **29**, 147–157 (2023).

180. Weiner, J. *et al.* Increased risk of severe clinical course of COVID-19 in carriers of HLA-C*04:01. *eClinicalMedicine* **40**, (2021).

181. Shah, A. & Coiado, O. C. COVID-19 vaccine and booster hesitation around the world: A literature review. *Front. Med.* **9**, 1054557 (2023).

182. Kip, K. E. *et al.* Evolving Real-World Effectiveness of Monoclonal Antibodies for Treatment of COVID-19. *Ann. Intern. Med.* M22-1286 (2023) doi:10.7326/M22-1286.

183. Miner, M. D., Corey, L. & Montefiori, D. Broadly neutralizing monoclonal antibodies for HIV prevention. *J. Int. AIDS Soc.* **24**, (2021).

184. Vílchez-Oya, F., Balastegui Martin, H., García-Martínez, E. & Corominas, H. Not all autoantibodies are clinically relevant. Classic and novel autoantibodies in Sjögren's syndrome: A critical review. *Front. Immunol.* **13**, (2022).

185. Shen, L. *et al.* Novel autoantibodies in Sjogren's syndrome. *Clin. Immunol. Orlando Fla* **145**, 251–255 (2012).

186. Cui, L. *et al.* Investigation of three potential autoantibodies in Sjogren's syndrome and associated MALT lymphoma. *Oncotarget* **8**, 30039–30049 (2017).

187. Mona, M. *et al.* Clinical usefulness of anti-muscarinic type 3 receptor autoantibodies in patients with primary Sjögren's syndrome. *Clin. Exp. Rheumatol.* **39**, 795–803 (2021).

188. Baer, A. N., Petri, M., Sohn, J., Rosen, A. & Casciola-Rosen, L. Association of Antibodies to Interferon-Inducible Protein-16 With Markers of More Severe Disease in Primary Sjögren's Syndrome. *Arthritis Care Res.* **68**, 254–260 (2016).

189. Deroo, L. *et al.* The value of separate detection of anti-Ro52, anti-Ro60 and anti-SSB/La reactivities in relation to diagnosis and phenotypes in primary Sjögren's syndrome. *Clin. Exp. Rheumatol.* **40**, 2310–1317 (2022).

190. Liu, Y. *et al.* Autoantibody to MDM2: A potential serological marker of primary Sjogren's syndrome. *Oncotarget* **8**, 14306–14313 (2017).

191. Ulbricht, K. U., Schmidt, R. E. & Witte, T. Antibodies against alpha-fodrin in Sjögren's syndrome. *Autoimmun. Rev.* **2**, 109–113 (2003).

192. Zheng, J. *et al.* Characteristics of primary Sjögren's syndrome-associated peripheral nervous system lesions. *J. Neurol.* **270**, 5527–5535 (2023).

193. Lawrence, E. J., Arpag, G., Arnaiz, C. & Zanic, M. SSNA1 stabilizes dynamic microtubules and detects microtubule damage. *eLife* **10**, e67282 (2021).

194. Duda, S. *et al.* Autoantibodies binding to stathmin-4: new marker for polyneuropathy in primary Sjögren's syndrome. *Immunol. Res.* **65**, 1099–1102 (2017).

195. Davis, S. K. *et al.* Heterologous SARS-CoV-2 IgA neutralising antibody responses in convalescent plasma. *Clin. Transl. Immunol.* **11**, e1424 (2022).

196. Darrah, P. A. *et al.* Multifunctional TH1 cells define a correlate of vaccine-mediated protection against Leishmania major. *Nat. Med.* **13**, 843–850 (2007).

197. Gunn, B. M. *et al.* A Role for Fc Function in Therapeutic Monoclonal Antibody-Mediated Protection against Ebola Virus. *Cell Host Microbe* **24**, 221-233.e5 (2018).